Physics – Uspekhi **64** (9) 890 – 922 (2021)

REVIEWS OF TOPICAL PROBLEMS PACS numbers: 74.20.Mn, **74.25.–q**, 74.25.Jb, **74.72.–h**

Pseudogap problem in high-temperature superconductors

S I Vedeneev

DOI: https://doi.org/10.3367/UFNe.2020.12.038896

Contents

1. Introduction **890**
2. Superconducting energy gap in cuprates **891**
3. Studies of the pseudogap in high-temperature superconducting cuprates **892**
3.1 Brief history; 3.2 Tunnel studies; 3.3 Photoemission spectroscopy with high angular resolution; 3.4 Nernst effect in cuprates; 3.5 Optical studies; 3.6 Orders inside the pseudogap region; 3.7 Quantum critical point in the pseudogap region
4. High-temperature electron-doped superconducting materials **915**
4.1 Superconducting gap in electron-doped cuprates; 4.2 Pseudogap in electron-doped cuprates
5. Iron-based high-temperature superconducting systems **917**
6. Conclusions **918**
References **919**

Abstract. It has been more than 30 years since the discovery of high-temperature superconductors (HTSCs). The number of articles published on the subject is huge, but the cause of the high superconducting transition temperature T_c is still an open question. The so-called 'pseudogap' HTSC phase — an anomalous 'normal' state — turned out to be as complicated a problem as high-temperature superconductivity itself. Its role remains unexplained. We discuss here only key experimental results with the aim to demonstrate the complexity and intricacy arising in the explanation of problems related to the nature of this unique phenomenon.

Keywords: pseudogap, superconducting gap, tunneling spectroscopy, photoemission, Nernst effect, orders

1. Introduction

The discovery of high-temperature superconductivity (HTSC) in the copper oxide BaLaCuO (a cuprate with quasi-two-dimensional copper–oxygen planes) [1] and the rapid increase in the superconducting transition temperature T_c in cuprates to values appreciably above the boiling temperature of liquid nitrogen (77.4 K) [2] are among the major scientific breakthroughs of the 20th century. The discovery of HTSC gave rise to numerous innovative investigations. In the course of the almost three decades that have passed since then, much has become known about new forms of quantum matter exhibited by these strongly correlated electron systems. Although a qualitative understanding of the nature of the superconducting state itself has been achieved, the causes of the high T_c in HTSCs remain an unsolved problem. Among the issues to be resolved are the remarkable complexity of the phase diagram, the uniquely high importance of different forms of collective fluctuations, and the simplicity and insensitivity to the details of the material in the normal state [3]. A circumstance of no little importance is the existence of a 'pseudogap' in cuprates. Being present in superconductors with a record high atmospheric-pressure T_c, the pseudogap in cuprates has become the most enigmatic phase in the physics of condensed matter. Its origin and relation to superconductivity have not yet been understood.

It was established in recent years that, in strongly correlated electron materials, which, besides the cuprates, include 'peculiar' superconductors (including ferrous chemical compounds, chalcogenides, organic superconductors, and some C_{60} compounds doped with alkali metal ions), depending on their composition, pressure, and the magnetic field, several different broken-symmetry phases can emerge. For example, it has become common to consider superconductivity and antiferromagnetism as competing orders, because the microscopic coexistence of two broken symmetries is a relatively rare phenomenon, and, wherever they coexist, one order suppresses the other. This competition often leads to quantum phase transitions, whose nature and role in superconductivity of cuprates are still under discussion. In these compounds, a number of effects have been revealed that show a dramatic dependence on the level of doping of the carriers.

This seems to add even more complexity to the understanding of the nature of the pseudogap, because it can be related to orders associated with charge density waves (CDWs) and spin density waves (SDWs) [4], quadrupole density waves [5], pair density waves (PDWs) [6, 7], stripe order [8], short-range antiferromagnetism [9], orbital magnetism or loop currents [10], electronic nematicity [7, 11], crystal lattice [12] and Fermi surface [13] reconstructions, and the state regarded as a precursor of superconductivity [14, 15].

S I Vedeneev
Lebedev Physical Institute, Russian Academy of Sciences,
Leninskii prosp. 53, 119991 Moscow, Russian Federation
E-mail: vedeneev@sci.lebedev.ru, vedeneevsi@lebedev.ru

Received 27 July 2020, revised 11 November 2020
Uspekhi Fizicheskikh Nauk **191** (9) 937 – 972 (2021)
Translated by S Alekseev

Other orders may also exist that violate symmetry at comparable initial temperatures in a wide range of parameters of the material. Some of these phenomena are discussed in more detail in what follows.

The pseudogap in correlated electron systems remains one of the most discussed phenomena in theoretical studies. Theoretical explanations of the pseudogap phase, including orders of the types mentioned above, are equally numerous. Two key pseudogap scenarios are the most frequent ones in theoretical studies, each of which is substantiated by a number of experiments [16]. According to the first, the pseudogap is a special state of matter with the order parameter that is either bilinear fermionic (for example, the loop current order type [17]) or compound four-fermionic (for example, spin nematic [7, 18, 19]). In the framework of this scenario, the pseudogap opening temperature T^* is a phase transition temperature. The other scenario is that the pseudogap is a precursor of an ordered state, the magnetism caused by SDWs [1] [20–23], superconductivity [24–27], or both these orders (the SDW order dominates at a low level of doping, whereas the superconductivity precursor is prevalent at a high level of doping).

The purpose of this review is not so much to single out certain studies of the pseudogap and its relation to superconductivity, but rather to discuss the results of most insightful experimental methods for studying HTSC with the aim to outline the achievements and new problems. We mainly discuss the data from experiments on the tunnel effect, photoemission spectroscopy with high angular resolution, the Nernst effect, optical investigations, and the results of studies of electron-doped materials and iron-based superconductors. But the discussion extends to excursions into results obtained by other methods. The reader will hopefully find the information in this review useful and might conceive ideas that would help clarify the difficult pseudogap problem.

For those wishing to take a broader look at these problems, we recommend a number of reviews devoted to ground states in cuprates [28, 29], their optical investigations [30–33], quantum criticality [34, 35], the two-gap problem [36], the electrodynamics of correlated electronic materials [33], studies of electron-doped superconductors [37–39], and recent papers [40–44]. Some ideas on the variety of the theoretical models proposed to explain the pseudogap phenomenon can be gleaned from [7, 45–52].

The author in no way aspires to offer even a short review of experimental work devoted to the pseudogap in copper oxides. The literature on the subject is so vast that embracing all studies is a hopeless task. Significant omissions are regrettable, but inevitable.

2. Superconducting energy gap in cuprates

Although reviews are available that contain data on the superconducting gap in cuprates, it is apparently useful to begin the discussion of pseudogap studies with a review of the main features of the superconducting gap in HTSCs.

As is known, the superconducting state in 'normal' superconductors is characterized by zero resistance, anomalous diamagnetism with a strong dependence on temperature, anomalous thermal properties, the existence of a superconducting energy gap, etc. In the normal state at temperatures above T_c, these features are absent, except for some superconducting fluctuations near T_c.

But the first experimental studies of cuprates already showed how strongly their properties differ from those of normal superconductors. In the normal state, the conductance of these compounds turns out to be almost two orders of magnitude less than that of simple metals, and its frequency and temperature dependences were incompatible with the commonly accepted theory of metals. This was the reason why cuprates at temperatures above T_c were called strange metals. A similar behavior, which has been revealed in many materials of interest for electronics [53], suggests that this is not only a property of high-temperature superconductors but also a general property of strongly correlated electron systems.[2]

From the standpoint of the theory of normal superconductors, copper oxides seemed to be the least promising compounds for searching for new high-T_c materials. For some time after the discovery of HTSC, doubts were even expressed as regards the presence of superconducting pairs in them.[3] In normal superconductors, superconductivity starts being destroyed with a decay of electron pairs, but as the temperature increases in cuprates, thermal excitations deprive the pairs of the ability to carry superconducting current, while the pairs may continue to exist [56, 57].

Although several hundred high-temperature cuprates exist, all of them have a layered structure, and, along the [001] crystallographic direction, their elementary cells are made of one or several superconducting CuO_2 planes separated by insulating layers (Fig. 1a, b). Because the crystal structure is quasi-two-dimensional, their electron and superconducting properties are highly anisotropic. For example, the temperature dependence of their resistance across the CuO_2 plane (along the *c*-axis) demonstrates an expressly 'semiconducting' behavior, in contrast to the temperature dependence of their resistance along the CuO_2 plane (the *ab* plane), which has a 'metallic' character. The properties of the normal and superconducting states of cuprates are highly dependent on the doping level — the concentration of charge carriers in the CuO_2 layers. Undoped cuprates are good insulators and antiferromagnets.

In normal superconductors, one of the main characteristics of the superconducting state is the energy gap 2Δ, which is proportional to T_c, with its reduced value $2\Delta/(k_B T_c)$ lying in the range 3.5–4.3 (k_B is the Boltzmann constant). At the same time, the first tunneling spectroscopy studies and angle-resolved photoemission spectroscopy (ARPES),[4] conducted with high-quality single crystals of the two main HTSC compounds, $Bi_2Sr_2CaCu_2O_{8+\delta}$ (Bi2212) [5] and $YBa_2Cu_3O_7$ (YBCO), revealed a very large

[1] This is a thermodynamically equilibrium state of matter with a spatially inhomogeneous periodic distribution of the local magnetic moment density.

[2] The existence of magnetism and a Mott transition in cuprates at a low level of doping assumes the existence of strong electron correlations [54].

[3] The first proof of the existence of standard Cooper pairs with the charge $2e$ in HTSCs was obtained from observations of the ac Josephson effect between an HTSC single crystal and a normal superconductor [55].

[4] ARPES measures the filled part of the one-particle spectral function, which describes energies admissible for one-particle excitations with a given momentum. This method is used to study Fermi surfaces, quasiparticle lifetimes, the superconducting gap and its symmetries, and surface states in topological materials.

[5] In single crystals of the Bi2212 system, the energy gap and its temperature dependence were first measured by the tunnel effect method in [60, 61].

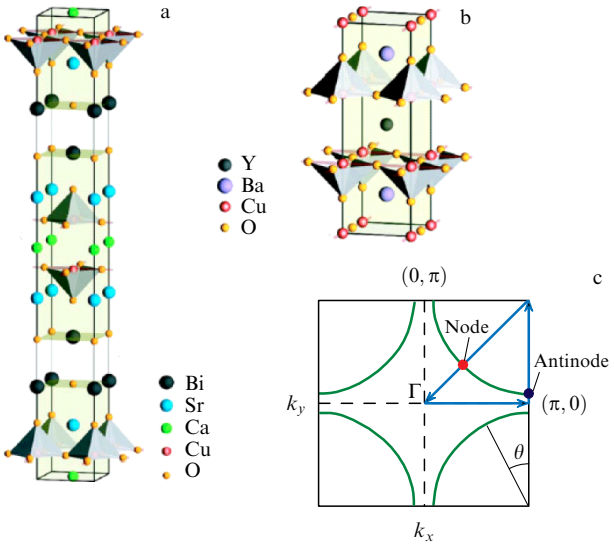

Figure 1. (Color online.) Crystal structures of the most frequently studied cuprates. (a) Tetragonal elementary cell of $Bi_2Sr_2CaCu_2O_{8+\delta}$ with $a = b = 5.4$ Å. (b) Orthorhombic elementary cell of YBCO ($YBa_2Cu_3O_{6+x}$) with $a_0 = 3.82$ Å and $b_0 = 3.89$ Å [58]. (c) Fermi surface of cuprates with the nodal and antinodal momenta and the Fermi angle indicated [59].

superconducting gap, with $2\Delta/(k_B T_c) \sim 6$–11 for Bi2212 [60, 62–70] and 3.6–7.6 for YBCO [71–76]. Moreover, at high concentrations of charge carriers in Bi2212, the gap decreased with decreasing T_c, as in normal superconductors. But at a low concentration of carriers, the gap in Bi2212 increases with a decrease in T_c [77, 78], which contradicts the theory of normal superconductors. In [78], the $2\Delta/(k_B T_c)$ ratio ranged up to 14.

In hole-doped cuprates, the wave function of a superconducting pair has the $d_{x^2-y^2}$-wave symmetry, i.e., the superconducting energy gap on the Fermi surface in k-space obeys the law $\Delta_d(\mathbf{k}) = \Delta_0(\cos k_x - \cos k_y)$ (where $\mathbf{k}$ is the wave vector) and has four zeros on the diagonal of the square in the first Brillouin zone (BZ), where it changes sign under the wave vector rotation through $\pi/2$ (Fig. 1c), whereas in normal superconductors the gap has an isotropic s-wave symmetry $\Delta_s(\mathbf{k}) = \Delta_0$ and is independent of either the position in real space or the momentum in k-space along the Fermi surface. On the Fermi surface in HTSCs, the superconducting gap is the largest in the direction of the antinodal Fermi momentum (k_F) on the BZ boundary near the $(\pi, 0)$ point. Its size gradually decreases along the Fermi surface toward the nodal momentum and vanishes at the nodal momentum k_F directed along the BZ diagonal [59].

The d-wave symmetry of the superconducting gap was first observed in cuprates in ARPES experiments [69, 79] and has been confirmed many times afterwards by the results of numerous other experiments on heat conductance [80] and heat capacity [81, 82] measurements, neutron scattering [83, 84], Raman scattering [85], etc. Vast information on the superconducting gap symmetry in cuprates is obtained by scanning tunneling microscopy (STM) [6] [86–89].

[6] In contrast to ARPES experiments, where the obtained information is averaged over a considerable area of the surface, STM is capable of mapping microscopic changes in the states.

To conclude this section, we discuss the recent paper [90] devoted to tunneling studies of the highest-temperature cuprate in the Bi-family,[7] $Bi_2Sr_2Ca_2Cu_3O_{10+\delta}$ (Bi2223), with three CuO_2 planes and $T_c = 110$–113 K. This compound is interesting, because its CuO_2 inner plane (IP) is located between two outer planes (OPs), and it is therefore assumed to have an electronic structure different from the structure of those planes, together with a lower density of carriers [92, 93]. The debate is still ongoing as to whether the coupling between the OP and IP layers in CuO_2 is single-particle [94] or Josephson [95] in nature. ARPES studies of Bi2223 have revealed the existence of two IP and OP zones [96, 97]. The authors of [90] used STM to study a periodic variation in the superconducting gap magnitude with a structural 'supermodulation,' which had previously been observed in two-layer Bi2212 [98]. The topography of a clean BiO surface exhibited supermodulation of the atomic lattice. A strong periodic change was observed in the tunnel contact conductance $dI/dV(V)$ with supermodulation (here, I is the current running through the contact and V is the bias on it): spectra in the valleys had sharper maxima of the gap and lower magnitudes of the gap compared with spectra on the crests. In an underdoped sample, periodic variations in the spectra were stronger than in a sample with optimal doping. The average superconducting gap magnitude in an optimally doped sample was about 45 meV, whereas for an underdoped sample it reached $\simeq 67$ meV, thereby confirming a higher density of holes.[8]

Another new feature, according to the authors of [90], is the existence of two superconducting gaps in the tunneling spectra of the optimally doped Bi2223 sample, which are rarely observed in underdoped samples. It was assumed in [90] that the two-gap feature is related to two Fermi surfaces of the CuO_2 IP and OP, revealed in ARPES experiments [96, 97] and in tunnel measurements with the help of point contacts [100].[9] The authors discussed a number of theories regarding the effect of supermodulation on superconductivity in Bi-based cuprates, but they believe that none of them can explain why structural supermodulation has a stronger effect in the optimally doped sample. Another issue that is still unclarified is how the CuO_2 IP affects the high T_c of three-layer cuprates. The authors assume that studying the response of superconducting pairs to lattice deformations and investigating the coupling between CuO_2 planes would provide useful information on the nature of superconductivity.

3. Studies of the pseudogap in high-temperature superconducting cuprates

3.1 Brief history

The most unexpected and remarkable revelation has been the existence in cuprates at temperatures much higher than T_c of a second, incomplete, energy gap at low energies, character-

[7] Although the superconductivity mechanism in cuprates is still elusive, there is an empirical rule that, for every family of cuprates, the maximal T_c increases as the number of CuO_2 planes in the elementary cell increases within the three-layer limit [91].

[8] The first measurements of the superconducting gap in Bi2223 single crystals were made in [99].

[9] Similar double maxima at the bias $2\Delta_{p-p}/e$ were observed in some tunneling spectra of Bi2212 single crystals, which was suggestive of two nanosize superconducting patches in the tunnel contact region [101].

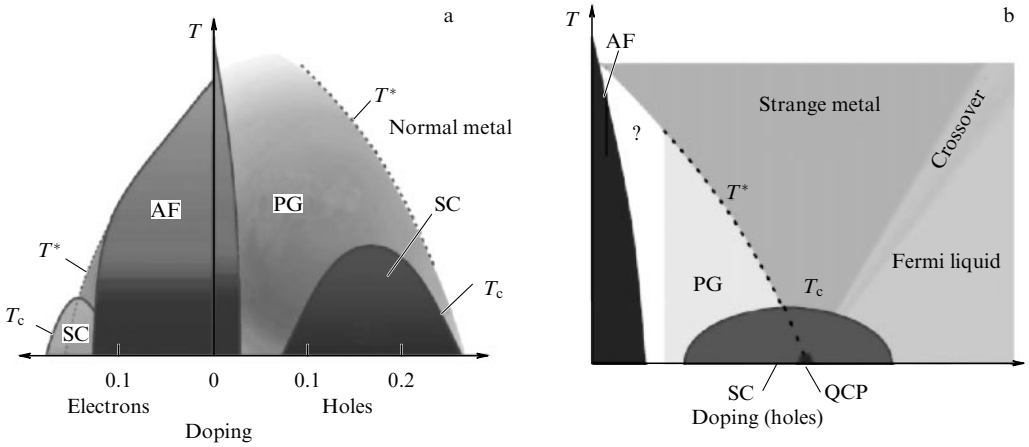

Figure 2. Two scenarios for phase diagrams of electron- and hole-doped cuprates, showing superconducting (SC), antiferromagnetic (AF), and pseudogap (PG) phases. (a) Pseudogap T^* line is tangent to the superconducting dome on the side of the high level of doping [58]. (b) T^* line intersects the superconducting dome and terminates at a quantum critical point (QCP), where temperature T^* tends to zero. Exact boundary of the pseudogap region at a low level of doping is unknown. Transition between the Fermi-liquid phase and the strange-metal phase occurs gradually (via a crossover) [107].

ized by a strong suppression of the density of states; it was called the pseudogap.[10] In some cuprates, the pseudogap was observed up to relatively high temperatures T^*, depending on the doping level. At the same time, the conductivity of the samples remained finite at $T < T^*$. Arguably, no other problem in the physics of cuprates has received greater attention than the nature and origin of the pseudogap.

As we have noted, all cuprates consist of one or several superconducting CuO_2 planes separated by nonsuperconducting layers that serve as "charge carrier reservoirs" when the material is doped. When electrons are eliminated from the CuO_2 planes, we speak of a hole-doped HTSC, and when electrons are added to the CuO_2 planes, of an electron-doped HTSC [103]. Overdoping or a low level of doping can be achieved in cuprates by cation substitution in their composition or by changing the oxygen content in the CuO_2 planes [104].

Although most HTSCs are hole-doped compounds, there are a few electron-doped materials. The majority of these materials have the chemical formula $R_{2-x}M_xCuO_4$, where R is the rare earth element Pr, Nd, Sm, or Eu and M is Ce or Th [105, 106]. The most significant difference between these systems is exhibited in their phase diagrams. There is only an approximate symmetry with respect to the zero doping level between p and n types, because the antiferromagnetic (AF) phase is much more stable in an electron-doped material.

The 'parent' HTSC compound is an AF Mott insulator.[11] Despite the similar roles played by charge carriers in cuprate HTSCs, there is a difference between phase diagrams of hole- and electron-doped materials.

In Fig. 2a, we show the phase diagram of electron- and hole-doped cuprates that was generally accepted in the early 2000s. The superconducting region (SC) of hole-doped cuprates is surrounded by three different regions: the fully developed AF order (AF), the region of the highest doping with the properties characteristic of a Fermi liquid (denoted as 'normal metal'), and the pseudogap region (PG), in which the concept of the Fermi surface itself loses meaning [108]. It has been established since then that hole-doped cuprates have a distinct phase separation between the AF order (or AF spin fluctuations) and the superconducting state (see, e.g., [109, 110]), and we therefore first discuss the best-studied hole-doped HTSC systems.

Doping with holes rapidly suppresses the AF order. After the addition of holes, cuprates become superconducting at $p_{min} \approx 0.05$ (where p is the charge carrier concentration per copper atom). As the carrier concentration increases, T_c increases, reaches a maximum at the optimum value $p_{opt} \approx 0.15$–0.17, and then decreases, tending to zero at $p_{max} \approx 0.25$–0.27.

The first indication of the existence of a pseudogap in cuprates was obtained when the Knight shift[12] K was observed to decrease in nuclear magnetic resonance (NMR) measurements with the $YBa_2Cu_3O_{6+x}$ compound in the range 300–77 K [111]; for normal metals, spin susceptibility and hence K are almost independent of the temperature. This result has received numerous confirmations in other NMR studies (see, e.g., [112–114] and the references therein). In particular, Curro et al. [113] reliably demonstrated that, as the temperature decreases and reaches $T_c \approx 80$ K, the $YBa_2Cu_4O_8$ system loses 80% of its spin susceptibility.

Later, Kawasaki at al. [115] measured the Knight shift in the $Bi_2Sr_{2-x}La_xCuO_{6+\delta}$ [Bi(La)2201] cuprate with one CuO_2 layer for $0.0 \leqslant x \leqslant 0.9$ with $T_c^{max} \sim 32$ K in magnetic fields up to 44 T. The relatively low T_c value in this compound allowed suppressing superconductivity by moderate magnetic fields. As an example, Fig. 3 shows the temperature dependence of K for a sample with $x = 0.40$, measured in fields of 7, 30, and 44 T. It can be seen that, in the region of high T, the Knight shift is independent of the temperature, which corresponds to the complete Fermi surface at temperatures above T^* [116]. At $T < T^* \sim 160$ K, K considerably decreases. Because the Knight shift is directly proportional to the density of states, these results indicate some loss in the

[10] The term 'pseudogap' was introduced by Mott to denote a minimum in the density of states on the Fermi surface in a disordered material, occurring as a result of Coulomb repulsion in the forbidden band [102].

[11] The notion of a Mott insulator was introduced many years ago to describe the situation where the material must be a metal in accordance with the band theory but is an insulator due to strong electron–electron repulsion [45].

[12] An increase in the nuclear magnetic resonance frequency due to the superfine coupling of the nuclei to conductance electrons.

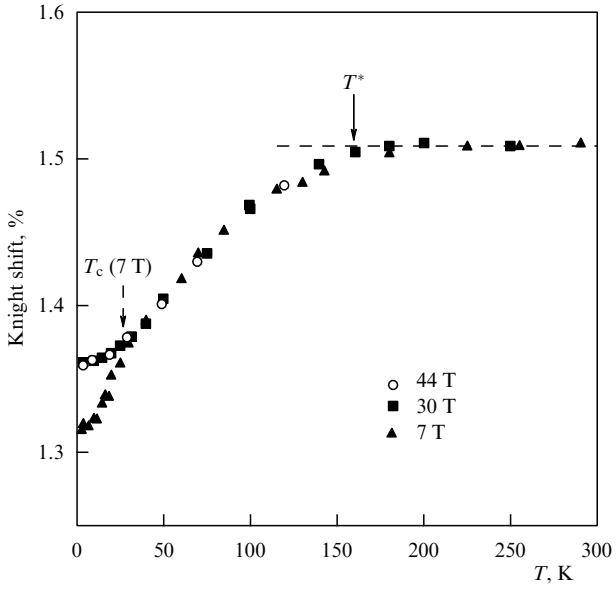

Figure 3. Dependence of the Knight shift on the ^{63}Cu nucleus at $x = 0.40$, measured in different magnetic fields ($B \parallel c$). Respective solid and dashed arrows show the pseudogap opening temperature T^* and T_c ($B = 7$ T). Dashed line is drawn by eye [115].

density of states on the Fermi surface at temperatures below T^*, thereby suggesting a pseudogap opening. We see in the figure that, for the field $B = 7$ T, K sharply decreases at $T < T_c(B) \sim 30$ K due to a decrease in the spin susceptibility as a result of the formation of Cooper pairs. In fields of 30 and 40 T and at $T < 30$ K, superconductivity is entirely suppressed, the sample is in the normal state, and K is independent of the magnetic field. This reflects the property of the pseudogap ground state and appears to be an argument against the scenario where the pseudogap is considered a precursor of superconductivity, because the strong magnetic field can be expected to exert much less influence on superconducting fluctuations due to quantization of orbital motions. The authors of [115] also studied the dependence of the Knight shift in the pseudogap state on the doping level. The analysis of the results allowed them to conclude that the pseudogap ground state is a metallic state with a finite density of states, which decreases as the doping level decreases (the La content increases), but remains sufficiently high even in the vicinity of a magnetically ordered phase, which is very close to the Mott state. This involves the assumption that the pseudogap abruptly vanishes as the phase corresponding to the Mott insulator is reached.

Soon after the first information on the existence of a pseudogap in cuprates was extracted from NMR data, direct experimental methods for measuring electron excitation spectra, such as ARPES [79] and tunneling spectroscopy [78], provided proof of the existence of a pseudogap in the normal state of cuprates at $T < T^*$. Subsequently, the pseudogap was measured in different cuprates with the help of the Nernst effect (see, e.g., [117]), polarization neutronography [118–120], ultrasonic methods [121], terahertz polarimetry [122], and optical methods [123]. It has been shown in ARPES experiments [79, 104] and with the help of scanning tunneling spectroscopy [77] that the normal-state gap, just like the superconducting gap, has the d-wave symmetry. In striving to understand the nature of HTSC, the debates mainly centered around the pseudogap, which has become center stage in the phenomenology of cuprates. But although studies of the enigmatic pseudogap state of cuprates are of great interest, the problem of its nature is still debatable. This is arguably one of the remaining problems in the theory of superconductivity. The authors of [124] called the pseudogap region of the phase diagram the unresolved puzzle within the HTSC problem. For a long time after the general acceptance of the existence of the pseudogap in cuprates, its discussion in experimental and theoretical papers was centered around the question of whether the pseudogap is related to or is distinct from superconductivity.

As noted above, two pseudogap scenarios are still in existence. Some groups of researchers assume that the pseudogap in the normal state can be considered a precursor of superconductivity, with superconducting phase coherence in the pre-formed Cooper pairs being suppressed by thermal or quantum fluctuations at $T > T_c$ and subsequently setting in at $T < T_c$ (see, e.g., [108, 125, 126]). Alternatively, superconducting fluctuations were proposed as a possible origin of the pseudogap [127]. In some experiments, the diamagnetic response that they induce was observed at temperatures up to 120 K [117], and interlayer pair coherence was observed at temperatures up to 180 K [128]. This suggests that strong pair fluctuations can be related to the pseudogap, but other experiments show that pair fluctuations are limited to the temperature of 20 K, or somewhat greater than T_c [129], and even have a Gaussian nature [130]. Relatively recently, Lee [131] suggested that the pseudogap could be understood as a competing phase, which is a fluctuating superconductor with finite momentum, i.e., a PDW-type order.[13]

In the tunneling experiments in [77, 78], a pseudogap was also observed in Bi2212 samples with both low and high doping levels, and was found to be in a scaling relation with the superconducting gap. This allowed the authors to consider the pseudogap in the normal state to be a precursor of superconductivity. Among the later papers substantiating this scenario, we mention the ARPES experiments in [134–137]. On the other hand, ARPES studies of the HTSC cuprate $La_{2-x}Sr_xCuO_4$ (LSCO) in [138] revealed that the pseudogap is practically the same at different doping levels, whereas the superconducting gap is proportional to T_c. By comparing their results with data from studies of other cuprates, the authors concluded that the pseudogap is practically independent of the HTSC material, which is evidence in favor of different natures of the superconducting gap and the pseudogap.

The discovery of a high Nernst signal at temperatures above T_c was indicative of a vortex scenario of pseudogap formation and the existence of a significant temperature range above T_c hosting superconducting fluctuations [56, 139, 140]. This was confirmed theoretically [141] and by subsequent experiments [130, 142]. Later, however, the original interpretation of the Nernst effect in HTSCs was called into question, and a much narrower temperature range of fluctuations was proposed [143]. Therefore, the question of the range of superconducting fluctuations and of their relation to the pseudogap opening in cuprates remains controversial. On the other hand, the authors of [144], by measuring the angular dependence of magnetoresistance along and across the CuO_2 planes in the temperature range 30 mK–1 K and magnetic fields up to 28 T in a high-quality

[13] PDW — pair density wave — is a state with a spatial modulation of the coupling amplitude, first introduced in [132] and in [133].

single crystal of the monolayer HTSC $Bi_{2+x}Sr_{2-x}CuO_{6+\delta}$ (Bi2201), which remains nonsuperconducting at temperatures down to 20 mK, provided proof of the existence of vortex excitations even in a nonsuperconducting cuprate. Among the papers arriving at the conclusion that the pseudogap is unrelated to superconductivity, we also note [145–152].

Finally, the observed semiconducting behavior of the temperature dependence of resistance and the negative magnetoresistance of cuprates across CuO_2 planes in the normal state were discussed from the standpoint of various models, in particular, those with a pseudogap and with its suppression by the magnetic field [56, 153]. Intense studies of the anisotropy of transport in Bi2212 and YBCO systems [154] have shown that the pseudogap opening temperature coincides with the onset of the semiconducting behavior of the resistance across the CuO_2 planes. Generally speaking, one-particle conductance along the c-axis in cuprates and its dependence on the magnetic field are of some interest, because they serve as a measure of the quasiparticle density of states in the CuO_2 planes. In [155], for example, magnetotransport was measured in Bi2201 single crystals in a wide range of doping at different temperatures, down to 25 mK, and in fields up to 55 T. It was found that, in a magnetic field, in the region of semiconducting behavior of the temperature dependence of resistance along the c-axis, the conductance σ_c is well described by a functional of the form $\sigma_c = \sigma_0 \exp(-\Delta_0/(g\mu_B B))$, where Δ_0 is the pseudogap, independent of the magnetic field B accessible in experiments, g is the electron g-factor, and μ_B is Bohr's magneton. The value of Δ_0 was quite close to the magnitude of the superconducting gap, and its dependence on the doping level was similar to the dependence of the latter. Interpretations of these findings were based on regarding the microscopically inhomogeneous distribution of singlet formations as the nature of the pseudogap.

Because the properties of copper oxides were under constant study with increased accuracy and sensitivity, it has become clear that the well understood quantum theory of solids, which has been successful in describing the electron properties of normal metals and superconductors, cannot fully reflect the features of copper oxides and, in a broader sense, of the entire family of highly correlated electron systems, among which copper oxides are the most studied. HTSC phase diagrams have been changed and updated many times. Not infrequently, different methods for measuring the same material led to inconsistent results. This is especially true of YBCO, especially as regards neutron scattering experiments and muon spin relaxation measurements in this cuprate [124]. It is therefore useful to discuss the key, i.e., the most conclusive, studies.

3.2 Tunnel studies

It is well known that tunneling spectroscopy is one of the most informative methods for studying the electron properties of solids, and its was successfully used in investigating simple superconductors. Because the conductance of a tunnel structure (planar junction or tunneling contact) is directly proportional to the quasiparticle density of states, tunneling spectroscopy has played an important role in verifying the Bardeen–Cooper–Schriffer (BCS) superconductivity theory. In particular, the energy positions of singularities in tunneling spectra at energies above the superconducting gap energy were coincident with the positions of maxima in phonon spectra in the investigated superconductors, which unambiguously proved the importance of the electron-phonon coupling in the superconductivity mechanism of normal superconductors. This raised hopes that tunnel studies would also allow collecting information on the superconductivity mechanism in HTSCs. However, the tunneling spectroscopy method was faced there with substantial hurdles, and some authors of experimental studies arrived at erroneous interpretations of the results, which did have some effect on the theoretical understanding of the pseudogap problem. To see the underlying reasons, it is worth discussing the results of tunnel studies of the HTSC pseudogap in greater detail.

Because of the extremely short coherence length and the high inhomogeneity of the investigated samples, the results obtained in different laboratories within the first years of studies were poorly reproducible. Generally speaking, tunnel studies of superconductors were a complicated task, but with the advent of high-vacuum tunnel microscopes operating at liquid helium temperatures, tunnel experiments have become more accessible. However, the interpretation of their results can still be ambiguous. Three main methods were typically used in tunnel studies of HTSC single crystals: in order of appearance, they are a point tunnel contact of the superconductor–insulator–normal metal or superconductor–insulator–superconductor (SIS) type, which later found applications in scanning tunneling microscopy (STM) and scanning tunneling spectroscopy (STS); an SIS tunnel junction on a microcrack in a single crystal (tunnel break-junction); and a mesastructure with inner interlayer tunnel junctions (intrinsic tunneling spectroscopy, or interlayer tunneling spectroscopy).

The first attempts to measure the pseudogap in cuprates by the tunneling method are already mentioned in review [58]. In addition, we note studies [156–159], where the STM method and the break-junction method were also used to measure the temperature dependences of tunneling spectra in Bi2212 samples. In all measurements, as the temperature increases and passes through T_c, a continuous change in the superconducting gap tunneling conductances was observed, until smooth normal-state quasiparticle spectra with a deep minimum at the zero bias formed, which the authors attributed to the pseudogap, drawing an analogy with ARPES experiments [79, 160]. These results, in the opinion of their authors, indicated the same nature of the superconducting gap and the pseudogap. Kugler at al. [161] also used STM to study the temperature dependence of tunneling spectra, but now in samples of a monolayer cuprate Bi2201. For single crystals of this compound, T_c^{max} is almost an order of magnitude less than that for Bi2212, and therefore Bi2201 samples must be a suitable material for verifying the relations between the pseudogap and the superconducting gap.[14] A comparison of the obtained results with the data cited above has shown that the pseudogap and the superconducting gap are related, just as in the case of Bi2212, which once again was convincing evidence of their common nature.

Work with point tunnel contacts and break junctions often encounters problems with maintaining the required stability under changes in temperature, and experimentalists very soon started using inner interlayer tunneling junctions.

[14] Unfortunately, the quality of the Bi2201 samples used in these experiments was not very high, because they had $T_c = 10$ K, while, according to references [162, 163], given by the authors, T_c is equal to 13 K in Bi2201 single crystals.

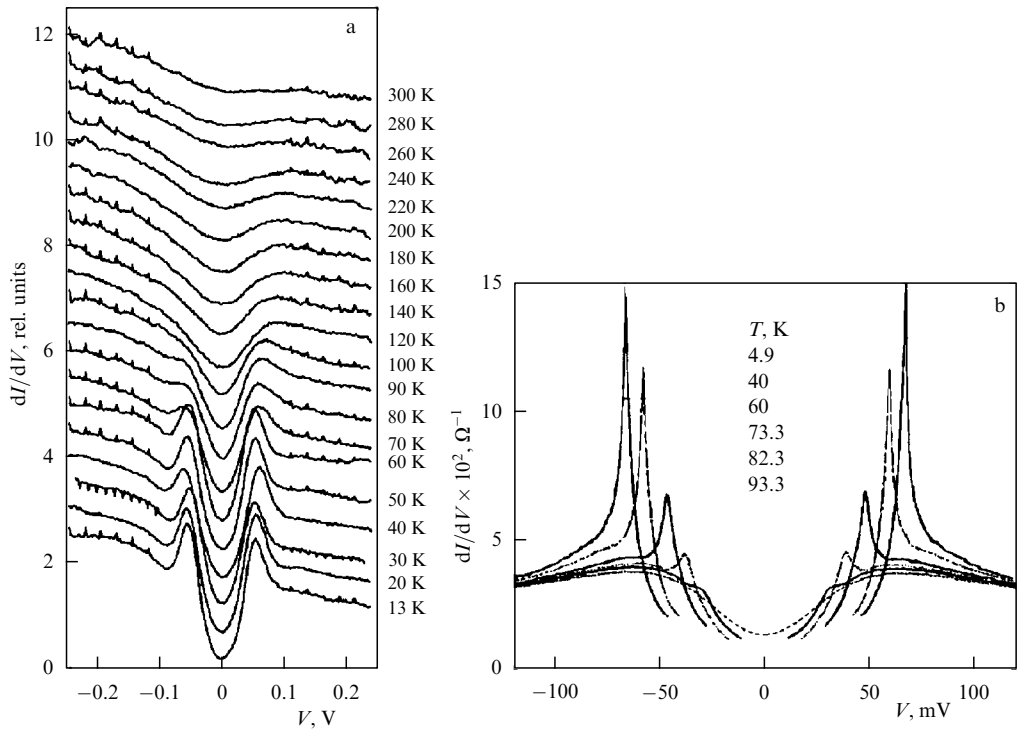

Figure 4. (a) Tunneling spectra $dI/dV(V)$ proportional to the one-electron density of states at different temperatures for an optimally doped Bi2212 sample with $T_c \sim 90$ K. Data obtained using STM with the tips, made of Pt–Ir or W, pressed against the *ab* plane of the sample. Curves are shifted with respect to the lower curve for visual clarity. The gap can be clearly seen even at $T = 300$ K. At $T = T_c$, there are some characteristic changes in the spectra [157]. (b) Tunneling spectra $dI/dV(V)$ of a mesastructure made of optimally doped Bi2212 with $T_c = 93$ K at different temperatures. The mesastructure 3.5×7.5 μm^2 in area consisted of 10 inner tunneling junctions [168].

The crystal structure of, e.g., Bi2212 along the *c*-axis is given by a system of identical stable inner Josephson junctions, in which each pair of neighboring CuO_2 layers is separated by $Bi_2Sr_2O_4$ (BiO/SrO) layers acting as an insulating tunneling barrier. Preparing such a structure using photolithography was straightforward, and it was first used for studying inner Josephson effects in Bi2212 [164].

Papers soon appeared where inner tunneling junctions based on Bi2212 2–30 μm^2 in size were now used to measure temperature dependences of the superconducting gap and the pseudogap at equal doping levels of the samples and to gain insight into the nature of the pseudogap [165–171]. Because the spectra of inner tunneling junctions are superficially of a higher quality than those obtained with the help of break-junctions or point contacts with STM, these papers were very widely cited, including in various reviews (see, e.g., [172]), despite the opinion held by the authors of [173], who called for care in accepting the results of such experiments. Subsequently, many papers were published devoted to tunneling studies of mesastructures made of Bi-based cuprates. In contrast to the spectra obtained in STM, STS, break-junction (Fig. 4a), and ARPES experiments, tunneling spectra of mesastructures (Fig. 4b) had very narrow maxima, which the authors believed were related to the superconducting gaps [167–170, 174], although the d-wave superconducting gap does not lead to narrow peaks in the density of states, as often is the case in simple superconductors. In view of the high resistance of mesastructures along the *c*-axis (which is just the direction for recording spectra of inner tunnel junctions) and poor heat conductance of the cuprate material, mesastructures are spontaneously heated by the measuring current (self-heating) [173, 175, 176], and, as a result, the measured spectra of inner tunneling junctions can be strongly distorted.

Subsequently, various measures started to be taken to exclude mesastructure heating in experiments. It was shown that the spontaneous heating of the structure decreases as its area decreases, and it is only for a submicrometer size that the spectra are close to the STM and break-junction spectra [177]. Different mesastructure geometries were also used (see, e.g., [178]). In some studies, e.g., [179–181], tunneling characteristics were measured using very short current pulses.

Still, despite the risk of spontaneous heating, HTSC studies with mesastructures went on. For example, some conclusions were arrived at in [182–186] regarding the magnitude and the temperature dependence of the superconducting gap, together with conjectures on its relation to the pseudogap or the absence of such a relation. This led to a paper by Kurter at al. [187], where the spontaneous heating of Bi2212 mesastructures with different numbers N of internal tunnel transitions was studied in great detail. The author showed that, as N increases, the heating of the structure also increases, the positions of gap peaks on tunneling spectra are shifted toward a lower bias, and, for $N \geqslant 12$, the width of the peaks decreases and the peaks themselves increase and strongly sharpen (see Fig. 4b or Fig. 2 in [187]). Sharp peaks represent mesastructure transitions to the normal state. Because the width of the peak and its position on the bias axis for the thinnest ($N = 6$) among the investigated mesastructures agree with the data obtained with a break-junction, the authors of [187] suggest using the break-junction spectra as indicators of the Bi2212-mesastructure quality. In their conclusions, they emphasize that an important advantage of the STM and STS methods is the considerable decrease in the

heating of the tunneling contact due to its small area and enhanced heat removal.

Papers [188, 189] are of some interest. In the first one, tunnel studies of the superconducting gap and the pseudogap in mesastructures made of a nearly optimally doped Bi(La)2201 were performed. As claimed by the authors, this is the first study where spontaneous heating of tunneling structures was eliminated due to their submicrometer size. It was found that the pseudogap opens at $T^* = 165 \pm 15$ K, whereas the superconducting gap started forming at $T_{c0} = 40$ K, which is considerably higher than the superconducting transition temperature $T_c = 30$ K. This should explain numerous odd features observed in a number of previous experiments [115, 145, 146, 150, 152, 190–192].

In [189], the superconducting gap and the pseudogap were also studied in mesastructures less than 1 μm in size, but made of Bi2212. According to the obtained dependence of the gap on the temperature and doping level, the superconducting gap starts opening in Bi2212, as in Bi(La)2201, at a temperature much greater than T_c, but much lower than T^*. Depending on the doping level, the samples had $T_c = 71$–89 K, $T_{c0} = 100$–150 K, and $T^* = 140$–310 K. As in [188], superconducting pairs formed in Bi2212 in the temperature range between T_{c0} and T_c. These findings seem to be substantiated by ARPES experiments [149, 152], although, according to some other ARPES data [148], the superconducting gap closed, as usual, at T_c. Despite the novelty of the tunneling results, the authors of the papers cited above see the following unresolved problems: what is the nature of the pseudogap and does the same physics underlie the superconducting phase and the pseudogap phase? The different dependences of the pseudogap and the superconducting gap on the temperature and doping level obtained in [189] for Bi2212 are an indication in favor of their common microscopic origin.

These problems could be clarified somewhat by tunneling experiments in strong magnetic fields (so-called magnetotunneling), which allows obtaining tunneling spectra at very low temperatures in the superconducting and normal (after suppression of superconductivity by the magnetic field) states of the sample. In that case, it would be possible to unambiguously differentiate between the superconducting and nonsuperconducting contributions to the pseudogap.[15]

Jacobs et al. [194] studied tunneling spectra of mesastructures made of Bi2212 with different doping levels ($T_c = 80$–92 K) in a magnetic field of 10 T at different temperatures. In fabricating the mesastructures, measures were taken to eliminate the possibility of their spontaneous heating. Tunneling spectra were measured in parallel and perpendicular magnetic fields. The experiments showed the existence of superconducting correlations in underdoped samples at a temperature much higher than T_c, up to $1.5T_c$, in the form of fluctuations of both the phase and the amplitude of the superconducting order parameter. This distinguishes the gap formed as a result of superconducting fluctuations from the pseudogap that is a precursor of superconductivity, a scenario that typically assumes the formation of superconducting pairs with macroscopic phase coherence breaking due to fluctuations of the phase but not the amplitude of the order parameter [108]. In [194], amplitude fluctuations of the order parameter were limited by T_c, rather than the higher temperature T_{c0} mentioned above. In addition, only a small part of the tunneling density of states in the pseudogap region was found to be caused by superconducting correlations. As the temperature increased, it vanished rapidly. The existence of superconducting correlations at temperatures several ten kelvin above T_c qualitatively agrees with the Nernst effect data (see Section 3.4). But we note that direct phase-sensitive experiments (for example, the Josephson effect) have not revealed a significant concentration of Cooper pairs at temperatures much greater than T_c [195]. Therefore, the question of superconducting correlations at $T > T_c$ remains open.

To continue with the subject, we note recent paper [196], reporting tunneling studies of mesastructures made of Bi2212 single crystals with $T_c = 86$–78 K and carrier concentrations 0.16–0.19 in a wide range of temperatures and for magnetic fields up to 13 T. In these experiments, the energy gap persisted at temperatures $T > T_c$, up to 150 K. Special attention was given to a mesastructure 0.81 μm^2 in area in an overdoped sample with $T_c = 80$ K and the hole concentration $p = 0.19$. As regards the superconducting fluctuations at $T > T_c$ and their relation to the pseudogap, the authors arrived at a conclusion coincident to that in earlier study [194], where moderate and insufficiently doped Bi2212 crystals, in which the pseudogap is typically observed, were studied. The authors of [196] made a more precise numerical comparison of experimental data with the result of the theory of superconducting fluctuations [197] based on the Ginzburg–Landau theory and showed that, in an overdoped sample, for which no proof of the pseudogap existence is available, the existence of the gap at temperatures above T_c also agrees well with the theory of superconducting fluctuations.

In Fig. 5, taken from [196], we show the tunneling conductances $dI/dV(V)$ and their dip–hump structure[16] above the superconducting gap at different temperatures, depending on the bias. We note a deep minimum in the structure in Fig. 5a, which is suggestive of a strong coupling of electrons participating in superconductivity to the narrow bosonic mode that was observed, e.g., in ARPES experiments [199, 200] and in optical conductance measurements [201]. In Fig. 5a, we can clearly see a strong temperature dependence of the dip–hump structure and the vanishing of the minimum at $T = 50$ K, although the superconducting gap is almost unchanged compared with its low-temperature magnitude. The decay of the maximum of the structure is much weaker, but the maximum also disappears at temperatures between 50 and 60 K. The authors believe that, due to the strong temperature dependence of the structure and especially due to its shift with changes in the temperature, it cannot be a manifestation of the usual phonon mechanism of superconductivity.

As can be seen from Fig. 5b, the minimum is partially suppressed by the magnetic field but is not shifted, as is the case when the temperature increases. Next, at a temperature above T_c, the gap feature on the tunneling conductances

[15] A magnetic field was first used for this purpose in [193], where tunneling experiments were performed with single crystals of the monolayer cuprate Bi2201.

[16] The additional structure frequently observed in reproducible tunneling spectra at energies above the superconducting gap in the form of a small minimum with a subsequent wide maximum was called the dip–hump structure. Zasadzinski et al. [198] were among the first to report the existence of such a structure in the tunneling break-junction spectra of Bi2212 single crystals. It was assumed in that paper and in their subsequent work that the dip–hump structure arises due to the coupling of quasiparticles to some type of collective excitations that are important for superconductivity.

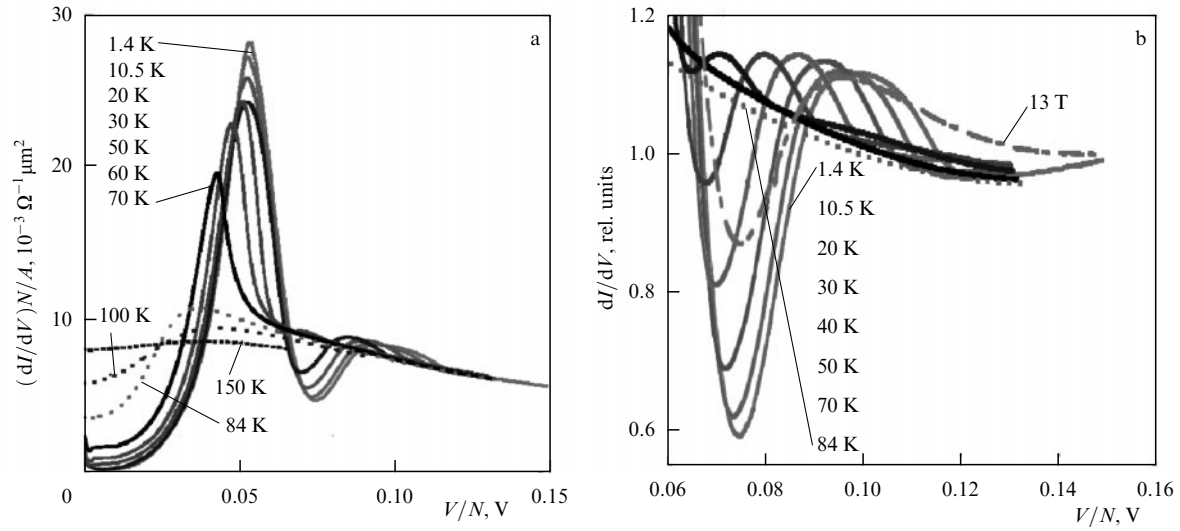

Figure 5. (a) Tunneling conductance dI/dV of a mesastructure made of optimally doped Bi2212 with $T_c \approx 86.5$ K as a function of the bias on one V/N tunneling junction at different temperatures. Mesastructure 0.81 μm^2 in area consisted of $N = 10$ inner tunneling junctions. (b) Zoom of the dip–hump structure in Fig. a. For visual clarity, the data are normalized. Part of the dI/dV curve at $T = 1.4$ K is also shown, measured in magnetic field of 13 T in the $B \parallel c$ geometry [196].

dI/dV becomes a smeared maximum, whose width increases as the temperature increases (Fig. 5a). The existence of this wide maximum in a sample with the concentration $p = 0.19$ agrees with the data of laser ARPES studies of Bi2212 [202], where the pseudogap was observed above T_c at concentrations up to $p = 0.22$. Nonetheless, the authors believe that their data contradict the conclusions in [202], and at temperatures above T_c the pseudogap can be explained by superconducting fluctuations [197].

We note that the same opinion was expressed in earlier papers devoted to ARPES experiments [203, 204] and in recent study [205], whose author made a detailed comparison of ARPES data with the results of studies of some bulk properties of HTSCs. Indeed, the ARPES [152, 206], tunneling [207], and terahertz spectroscopy [208] data can be explained by superconducting fluctuations revealed at temperatures 10 to 20 K higher than T_c. But this temperature range increases as the sensitivity of experiments increases. The Nernst effect (see Section 3.4) and torsional magnetometry used to measure diamagnetism fluctuations [142] extend this range considerably.

In [196], tunneling data were analyzed in the framework of a simple model of a semiconductor for SIS tunneling transitions [209] with the use of the Dynes formula [210] for the tunneling density of states with d-wave superconductivity taken into account. Previously, this formula was widely used to determine the broadening of tunneling spectra due to the finite lifetime of excited quasiparticles in usual superconductors with strong coupling.[17] In the opinion of the authors, electron–electron scattering can be the reason for spectrum broadening for d-wave superconductors. This may not be the sole reason, however, because there are unpopulated quasiparticle states with arbitrarily low energies in d-wave superconductors, and the broadening of tunneling spectra can occur as a result of inelastic scattering of quasiparticles by bosons participating in the coupling of electrons. Here, we also note studies attempting to apply Eliashberg's theory, developed for usual superconductors with a strong coupling, to HTSCs [211–213].

[17] In the HTSC case, the Dynes formula was first used in [70] to extract the density of states from the tunneling spectra obtained on Bi2212 single crystals. The first attempt to relate the structure later called the dip–hump structure to the phonon spectrum was also made there.

3.3 Photoemission spectroscopy with high angular resolution

In the initial studies of high-temperature cuprates, the ARPES method played an important role in establishing the anisotropy and structure of both the superconducting gap and the pseudogap. Most frequently, ARPES experiments were performed with Bi2212 samples, because the options for obtaining a clean fresh surface, sharp spectral lines, and high T_c meant this compound was selected from the range of other cuprates as an ideal material for surface-sensitive spectroscopy. According to ARPES results, the pseudogap opens at a temperature T^* in the antinodal region of the momentum space, located at a boundary of the BZ, where it is maximal, together with the superconducting gap, which, following the d-wave symmetry, is absent in the nodal region of the Fermi surface, whereas the pseudogap remains constant over the entire antinodal region, with gapless patches of the Fermi surface preserved around the nodal regions (for optimally doped Bi2212) [46], which were called 'Fermi arcs' in [116]. The different phenomenology on different parts of the same Fermi surface is interpreted as being due to dominating gaps of two different sources [77, 116, 160]. In Fig. 6, we show a diagram of the nodal–antinodal splitting on 1/4 of the BZ with the Fermi surface.

In the early 2000s, the techniques and methods of ARPES experiments were considerably improved, and recently the energy resolution in ARPES experiments has become better than 10 meV, which allows investigating smaller gaps near nodal regions with improved accuracy. To increase the luminosity of photoemission sources, lasers, synchrotrons, and gasdischarge lamps came into use. Experiments started being performed with more extensive statistics collected, the measurements were made in broader ranges of temperature, momentum, and doping, and they were completed sooner than the samples started aging. This has led to an improved

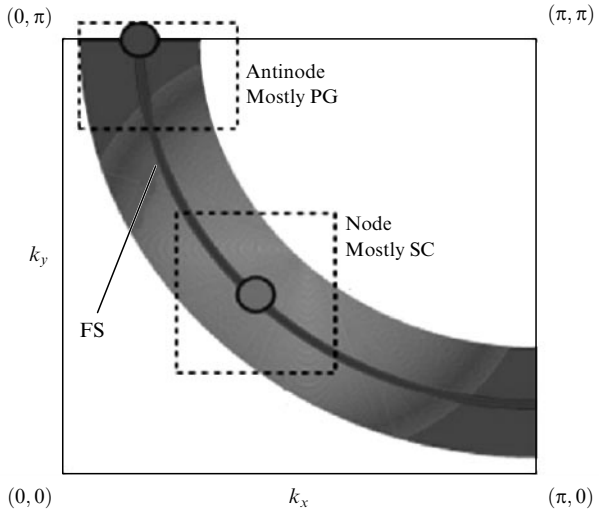

Figure 6. Nodal–antinodal dichotomy (splitting) on 1/4 of the BZ with a Fermi surface. Various phenomenologies on different parts of the same Fermi surface are interpreted as the dominance of the gap or of two different sources. (From [214].)

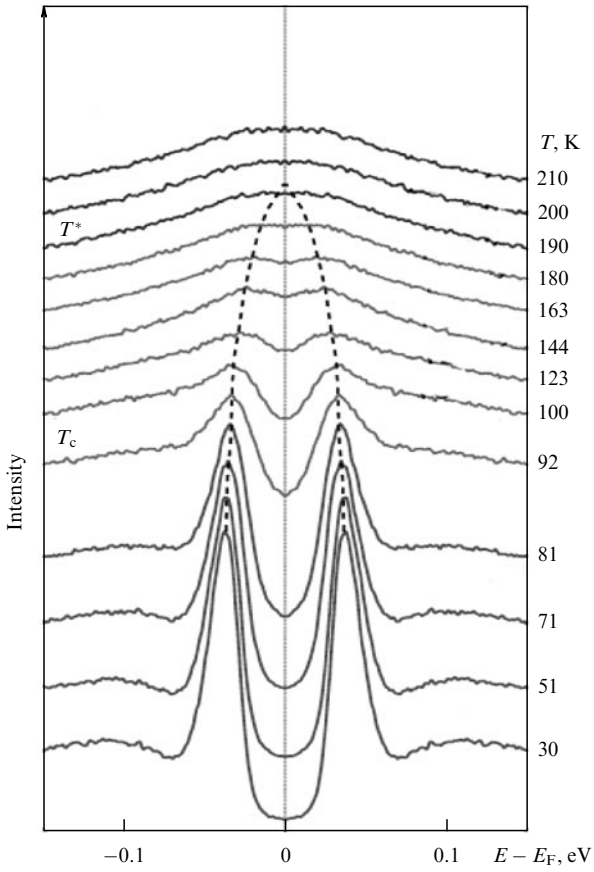

Figure 7. Typical symmetric ARPES spectra of Bi2212 at different temperatures in the nodal region of the Fermi surface. T^* is standardly identified in the data as the temperature at which spectra merge into a single peak (dashed curve). An underdoped sample with $T_c = 92$ K at $p \approx 0.14$ [59].

understanding of the pseudogap problem by many research groups.

In Fig. 7, we show typical symmetric ARPES spectra of Bi2212 at different temperatures in the nodal region of the Fermi surface. The temperature T^* is typically identified as the one at which the spectra merge into one maximum (dashed line) [59].

But studies supporting alternative pseudogap scenarios have not ceased appearing. For example, in [136], the momentum and temperature dependences of the superconducting gap and the pseudogap were investigated in detail for a low-temperature representative of the Bi family, optimally doped Bi(La)2201, with the help of laser ARPES with superhigh resolution. In the superconducting state of the sample, the spectra revealed an anisotropic superconducting gap with the standard d-wave symmetry. In the normal state, the opening of the pseudogap was observed on a small Fermi arc near the nodal region. In the normal state, except in the Fermi arc, the pseudogap was similar in magnitude and momentum dependence to the superconducting gap. The pseudogap changed insignificantly with temperature and did not change under the transition through T_c. In the opinion of the authors, these results indicate a close relation between the pseudogap and the superconducting gap and support the single-gap scenario, in which the pseudogap is a precursor of superconductivity.

Two years earlier, ARPES experiments with a similar cuprate Bi(La,Pb)2201 delivered the very opposite results [215]. The ARPES spectra showed that the gap in the superconducting state has two components corresponding to the superconducting gap and the pseudogap. The observation of different momentum and temperature dependences of these allowed assuming that these gaps represent two separate energy scales. Near the nodal region, the spectra at temperatures below T_c have a sharp peak corresponding to a small gap, which closed at T_c. Near the antinodal region, the spectra are broad, with a large energy gap at temperatures both above and below T_c. The shape of these spectra and the magnitude of the gap remain practically constant under the transition through T_c, which is suggestive of the coexistence of superconducting and pseudogap states at temperatures below T_c and of the dominance of the latter in spectra near the antinodal region. The author hypothesized that the pseudogap state is competing with superconductivity and attenuates it in the antinodal region.

More recently, the BZ region between the nodal and antinodal directions was discussed in the language of a 'two-gap' pattern, according to which the superconducting gap and the electron pseudogap phase coexist at temperatures below T_c, but the pseudogap is unrelated to superconductivity. In the superconducting state, the pseudogap dominates near the antinodal region, whereas the superconducting gap plays a major role near the nodal region, although the superconducting features do exist across the entire Fermi surface (see Fig. 6). The difference between the natures of the pseudogap and the superconducting gap is substantiated by numerous data from ARPES experiments, including different levels of doping, the dependence of the gap on temperature and momentum on the Fermi surface [216, 217], electron–hole symmetry breaking in the antinodal region at $T < T^*$ [218], and direct X-ray spectroscopy proof of competition between the pseudogap phase and the superconducting order parameter in Bi2212 [219].

There are numerous proofs of the existence of the pseudogap phase inside the superconducting dome on the phase diagram of cuprates in the region of slight overdoping at $p \approx 18$–20%. These include the measurement of quantum

oscillations, which revealed a divergence of the effective mass in approaching the above level of doping [220], the discovery of the interference of quasiparticles, entailing the appearance of a 'large' Fermi surface [221], the observation of a maximum in the superfluid density [222], and a change in the carrier density [223]. But we must note that not all experiments support the existence of a boundary of the pseudogap phase inside the superconducting dome on the overdoped side. In particular, the results of recent measurements of the superfluid density in ultra-clean LSCO films failed to reproduce the previously observed anomalies at 19% doping [224].

The question about the terminal point of the pseudogap phase at $T > T_c$ is more controversial. According to one version of the phase diagram, T^* is under the superconducting dome near the region of optimal doping, whereas, according to another, it intersects the superconducting dome in the region of overdoping. This question is quite difficult to resolve, because both versions of the phase diagram are based on results obtained with different compounds, which could be synthesized in different doping regions and with different experimental methods. This is why, on the phase diagram shown in Fig. 8 (taken from [214]), the data for two cuprates, Bi2212 and YBCO, are separated, despite the two systems frequently being compared because both are two-layered and have close values of T_c. The phase diagram in which the pseudogap is absent on the overdoped side at $T > T_c$ is confirmed by data on YBCO, the preferable compound for scattering and transport experiments but that is at a disadvantage as regards ARPES studies because of the self-doping of the sample surface and contamination of the spectra with contributions from chains [225].

The last phase diagram in which the pseudogap is present on the overdoped side at doping levels of at least $p \approx 0.22$ is the so-called "spectroscopist's phase diagram," because ARPES, STM, and Raman scattering[18] all show that the normal state of overdoped Bi2212 has a gap qualitatively similar to the one observed on the underdoped side of the diagram [73, 202]. In ARPES experiments, T^* is usually determined by the mirror-symmetric spectrum at k_F near the Fermi energy E_F. The corresponding procedure, invoking the Fermi–Dirac distribution function, is described in [116].

To estimate T^* quantitatively, other methods of processing symmetric spectra can also be used [226, 227]; they typically yield T^* values scattered in a range of 30 K. An alternative explanation of this uncertainty may be provided by experiments on neutron scattering in Bi2212, in which the pseudogap was identified via magnetic order inside the elementary cell [228]. Some results of that study may be indicative of the existence of underdoped or optimally doped parts inside the sample, which affect the spectroscopic determination of the pseudogap in overdoped samples. Another hypothesis is that, in the normal state, the gap in the temperature region above T_c is different on the underdoped and overdoped sides of the phase diagram, the latter being explained by superconducting fluctuations [229, 230]. But this interpretation is inconsistent with data from other ARPES experiments with Bi2212, in which the same pseudogap is observed, corresponding to the phase-diagram region located on both sides of the optimum doping level [226]. The existence of a pseudogap of the same nature and with the same properties in both the slightly underdoped and

[18] Raman, or combinational, inelastic scattering of optical radiation in gases, liquids, and crystal attended by a change in its frequency.

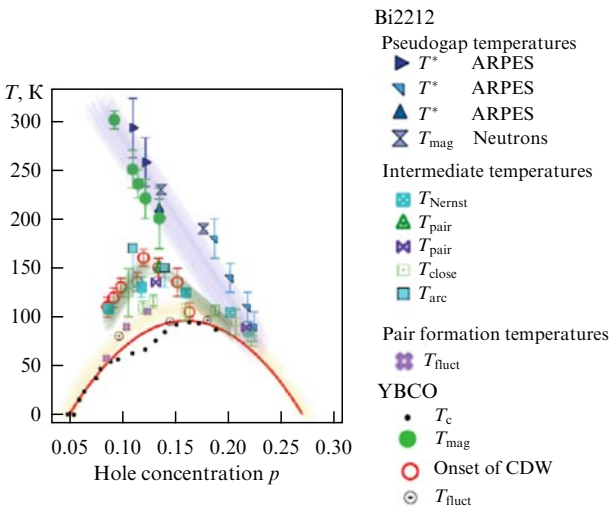

Figure 8. (Color online.) Schematic T–p phase diagram for Bi2212 and YBCO cuprates with hole doping, whose level was determined by the value of T_c with the use of the known empirical 'universal curve.' T_{mag} is the temperature of the appearance of magnetic order inside elementary cells, T_{Nernst} is the temperature of the appearance of a vortex Nernst signal, T_{pair} is the temperature of the onset of the formation of superconducting pairs, T_{close} is the temperature of the start of destruction of superconducting pairs, T_{arc} is the temperature of the appearance of Fermi arcs, and T_{fluct} is the temperature of the onset of superconducting fluctuations. The data relate to different studies and were obtained by different methods (see [214]).

weakly overdoped Bi2212 allows assuming that different T^* can occur in phase diagrams, because the materials of YBCO and Bi2212 are not identical, the more reliable data on the pseudogap therefore being those obtained in overdoped Bi2212.

Chemical variations are a source of additional complications in establishing and interpreting the phase diagram of cuprates. In many studies with overdoped Bi2212, samples doped with Pb are used, which typically ensure more stable doping. The substitution of Bi with lead considerably reduces umklapp processes and makes some methods of data interpretation more straightforward. Although the effect of this chemical substitution on the pseudogap has not been examined quantitatively, it can be helpful in finding the features of the pseudogap on the overdoped side of the phase diagram at $T > T_c$. In the case of YBCO, strong doping is hampered, because total saturation of chains with oxygen corresponds to $p = 0.194$ [231], and therefore the comparison of these two-layer cuprates beyond the presumed low-temperature terminal point of the pseudogap becomes meaningless. In a strongly underdoped regime, chemical stability is usually achieved by using cation substitution of Ca, although the procedure is not indisputable [232]. Still, at different levels of doping, with chemical alignment, ARPES spectra look consistent and their behavior evolves smoothly in approaching the doping level at which samples with the cation substitution become preferable.

In a broader sense, a universal distinctive property of cuprates, depending on the composition, is the long-standing problem that hinders understanding of the pseudogap, that the doping level (in this case, x) is not known precisely for many cuprates, including Bi2212. In the Bi family of cuprates, it is determined from the value of T_c using the known empirical 'universal curve' (parabola)

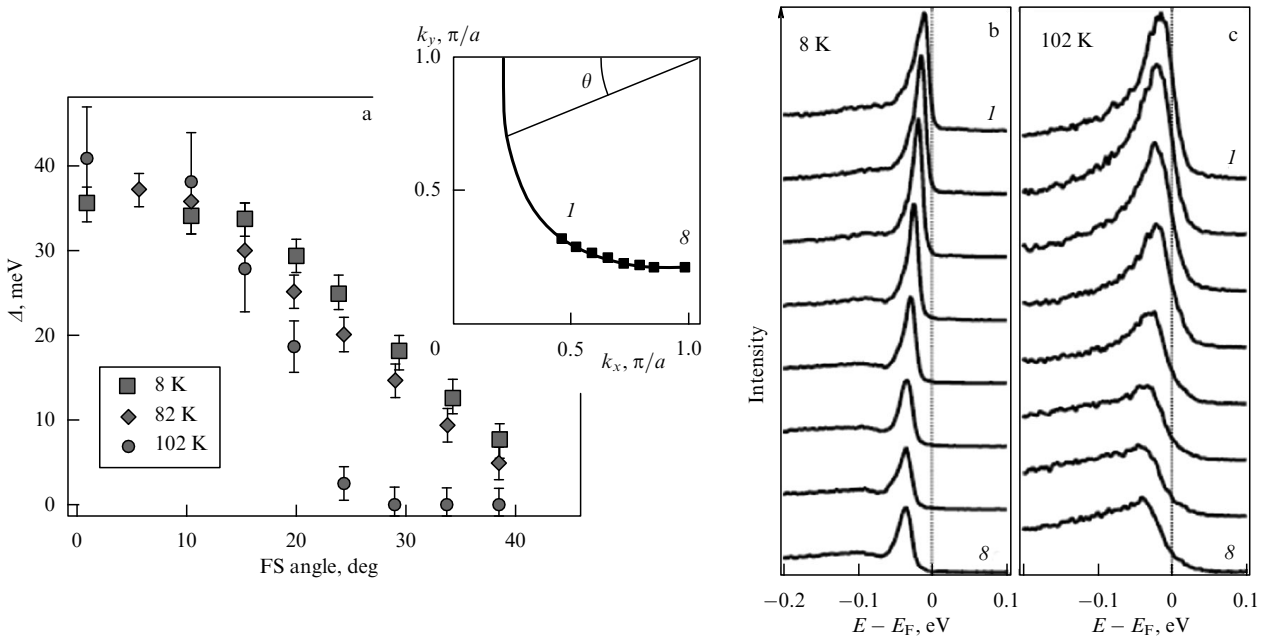

Figure 9. (a) Pseudogap as a function of angles on the Fermi surface defined in the inset, at temperatures below and above T_c. (b, c) Mirror-symmetric ARPES spectra at k_F at different points of the Fermi surface, shown in the inset, at temperatures of 8 K (below T_c) and 102 K (above T_c). Gap manifests itself in shifts of the spectral maxima with respect to the Fermi energy. Bi2212 sample with $T_c = 92$ K [216].

$T_c(x) = T_{c,\max}[1-82.6(x-0.16)^2]$ [233] and its modifications for YBCO [231]. A detailed discussion of this problem, together with phase diagrams for other cuprates and a comparison of their families, can be found in [124, 152, 234–236].

As regards the underdoped edge of the pseudogap, it seems to smoothly pass into its parent AF phase. Measurements of neutron scattering in YBCO showed a sharp decrease in T_{mag} at a doping level below $p \approx 0.085$, which coincides with the doping level at which slowly fluctuating short-range SDW correlations start. In ARPES experiments, the low-temperature boundary of the pseudogap phase is observed at a similar level of doping, with the gap opening in the nodal region of the momentum space, which is present at temperatures both below and above T_c [237, 238]. In LSCO, this gap was directly related to the incommensurate SDW order [239]. ARPES measurements did not confirm the effect of that order on the antinodal pseudogap; in particular, T^* is very high at this doping level (the doping in several upper elementary cells has a tendency to instability at high temperature [240]), while Bi2212 spectra become progressively broader, such that it is difficult to determine the features and energy of the spectra [202].

The pseudogap measured in ARPES experiments is typically characterized by a single number, the magnitude of the gap for each momentum around the Fermi surface. In Fig. 9, we show the total magnitude of the pseudogap in Bi2212 [216]. We can see that the pseudogap exists in the antinodal region for $T > T_c$, changes inconsiderably compared with its magnitude in the superconducting state (at least near the optimal doping), and vanishes near Fermi arcs in the nodal region. This simplification, even if convenient in many cases, obscures some subtleties that may be significant for relating experiment to theory. Among them, we note features that are often hidden when the data are described only by the gap value: the dependence of spectral line shapes on the doping level and their changes as the temperature passes through T_c, and also the finite density of states at the Fermi level.

The observed shape evolution of ARPES spectra of normal-state samples with variations in the level of doping was previously regarded as the onset of quasiparticle coherence on the overdoped side of the phase diagram [241]. In other versions, the possibility of a different nature of the gap in the normal state was considered. For example, this could be superconducting fluctuations in the case of overdoped samples [230]. The authors of [230] analyzed the role of nanosize inhomogeneities that can be present in cuprates with a high doping level and suggested drawing a clearer distinction between the pseudogap and the superconducting gap in them. They revised the phase diagram structure usually extracted from ARPES experiments, such as the one shown in Fig. 2a. In that diagram, the pseudogap line is tangential to the superconducting dome from the side of the high doping level. But such a diagram, as the authors believe, is difficult to reconcile with other experiments and models, which may be indicative of the possibility of a critical point being present inside the superconducting dome, as can be seen in Fig. 2b, which shows the phase diagram of cuprates accepted in the last decade. In that case, within the mean-field description, a pseudogap dependent on the level of doping can be related to the formation of spin singlets.[19]

The high degree of inhomogeneity of the sample can also lead to an extension of the ARPES spectra in the case of insufficient doping. This is confirmed by STM experiments whose results demonstrate a wider distribution of local gaps for a low level of doping [242]. Changes in the shape of ARPES spectra in cuprates as the sample temperature passes through T_c is another important factor in considering their dependence on momentum. This effect is pronounced in the antinodal region of momentum space.

[19] The question of singlet formations as the nature of the pseudogap was discussed previously in [155].

Finally, as is known, the pseudogap is characterized by a finite density of states inside the gap, which is maximal for states with the Fermi momentum close to the nodal direction $(0,0)$–(π,π) of the BZ and strongly decreases near the antinodal region $(\pi,0)$, in which the pseudogap magnitude is small (see, e.g., [243]). Moreover, two different states coexist in the pseudogap region: one is due to the formation of superconducting pairs and persists up to an intermediate temperature $T_{\rm pair} < T^*$, and the other, extending to T^*, is the real pseudogap characterized by the suppression of the spectral weight of quasiparticle excitations and anomalies in the transport properties.[20] The temperature $T_{\rm pair}$ can be about 120–150 K even for materials with very different $T_{\rm c}$, and this may set a restriction on the maximum attainable $T_{\rm c}$ in cuprates [152].

The pseudogap state at temperatures above $T_{\rm c}$ is represented in momentum space by four disconnected Fermi arcs centered around the momenta where the nodal points of the d-wave superconducting gap existed at $T < T_{\rm c}$ [116]. An interesting interpretation of the Fermi arcs is that they constitute only a part of the assumed large Fermi surface that maintains superconductivity in cuprates [244]. On the other hand, the existence of Fermi arcs, once they are regarded literally as disconnected segments of gapless excitations, is anomalous, because the Fermi surface shape is assumed to be closed.

The results of two ARPES experiments with Bi2212 [202, 245] are worthy of note here. In [245], it was shown that, at temperatures somewhat higher than $T_{\rm c}$, the Fermi arc length increases linearly as the temperature increases, whereas in [202], where samples with two different doping levels were investigated, the linear growth of the Fermi arc length saturated at a temperature close to $T_{\rm pair}$, which was reported in [152, 227]. At T^*, the full Fermi surface was reconstructed, which means that T^* sets the upper temperature bound for Fermi arcs. Also studied in [152, 227] were the properties of apparently disconnected Fermi arcs, with the result that the normal-state Fermi surface is strongly 'flattened' into Fermi arcs at pseudogap temperature T^*. It came as a surprise to the authors that the length of Fermi arcs remained constant in the temperature range between T^* and $T_{\rm pair}$, which is consistent with the existence of an ordered state at a temperature below T^*. At $T_{\rm pair}$ (below which the gap closes near the nodal region and superconducting pairs form), these arcs turned into either a point or a very short arc whose length was limited by the resolution of the experiment.

The first thing to note about the experimental phase diagram in Fig. 8 is that charge ordering must apparently be different from the pseudogap. The pseudogap, according to spectroscopic data, at least as understood until very recently, is a gap on part of the Fermi surface with a finite density of states inside the gap. This imposes certain restrictions on CDWs[21] with a short correlation length [246, 247]. This is why the main objections arose when short-order CDWs were discovered in YBCO with the wave vector $q \approx 0.3$, consistent with antinodal nesting[22] [143, 248]. But further analysis showed that charge ordering and the pseudogap had different dependences on the doping level: the former was dome-shaped with a maximum at a doping $\approx 1/8$ [4, 249], and the latter increased monotonically as the doping level decreased.

In all of this reasoning, it is assumed at the very least that the pseudogap and CDWs are of different natures in cuprates. But a conclusion following from the foregoing is that cuprates can have three characteristic temperatures in the normal state: the temperature of the onset of superconducting fluctuations, approximately 10 to 20 K above $T_{\rm c}$; a somewhat higher temperature of the onset of charge correlations, which is maximal at a doping level close to 1/8; and, finally, the pseudogap opening temperature T^*. Moreover, the most recent ARPES data cast doubt on the appearance of Fermi arcs at $T > T_{\rm c}$ and substantiate the scenario according to which point nodes are preserved at higher temperatures, similarly to the temperature of the onset of charge correlations [214].

In view of these doubts and the conjecture that the Fermi surface in cuprates must be closed (see above), while a number of calculations for the doped AF phase have shown that the Fermi surface must consist of small pockets, which at high doping levels undergo a transition to an entirely closed Fermi surface characteristic of a metallic system [250, 251], Fermi surface structures were investigated in recent ARPES experiments [252] in Bi2212 single crystals with optimum and low levels of doping. Study [252] is of independent interest because, instead of the usual chemical doping, the method of laser pumping (photodoping) with a femtosecond laser was used to effect changes in the concentration of holes in the sample. By pumping additional holes into the samples and tracing the changes in momentum-dependent Fermi wave vectors around the Fermi arcs on femtosecond time scales, the authors of [252] confirmed the existence of small hole pockets in the pseudogap region, characteristic of a doped Mott insulator. There are a number of papers devoted to this problem (see, e.g., [253–255]), but discussing them goes outside the scope of this review.

3.4 Nernst effect in cuprates

In attempting to understand the pseudogap state, the authors of [117] addressed the question about the nature of the superconducting transition in cuprates at $T_{\rm c}$: whether it follows the standard (BCS) scenario with the closure of the superconducting gap or the scenario violating phase coherence at long distances by thermally generated vortices at a zero magnetic field [108]. The first case would mean that the pseudogap state, by its nature, is antagonistic to d-wave superconductivity and competes with it. In the second case, on the contrary, the condensate of pairs lacking phase coherence exists in the pseudogap state at temperatures much higher than $T_{\rm c}$. These two states are closely related, are hardly distinguishable, and are fundamental for the superconductivity mechanism in cuprates.

Direct proof that the superconducting transition in cuprates occurs according to the scenario with phase

[20] In quantum mechanics, the spectral weight is given by the spectral function, which in this case is determined by the retarded Green's function for electrons in a crystal. Roughly speaking, the spectral function (ignoring the temperature) gives the probability distribution that an electron with a vector **k** has a frequency (or energy) ω. Alternatively, the spectral function can be regarded as a kind of density of states for a given **k**.

[21] Periodic spatial displacements of ions and the electron density in a metal (standing electron density waves).

[22] The Kohn anomaly. The existence of two parts of the Fermi surface (in particular, almost parallel ones) that can be superimposed by translation by some vector of the reciprocal lattice implies instability of the Fermi-liquid state. This, in turn, leads to the appearance of additional order parameters, for example, SDW.

coherence violation (in the pseudogap state) was obtained in experiments studying the Nernst effect on LSCO single crystals [56]. A large Nernst signal was also detected in many hole-doped cuprates, and it was observed in a wide temperature range both below and considerably above T_c. The results were interpreted as proof of the existence of vortices at a temperature above T_c, supporting the scenario with phase coherence violation. Among the pioneering studies by Wang and Ong and collaborators [117, 139, 140, 142, 256–258] on measurements of the Nernst effect in cuprates, the most revealing one is apparently paper [117]. We describe its results in some detail.

As is known, in type-II superconductors, in a magnetic field close to the upper critical field, vortices exist in the state of a 'vortex liquid' of movable excitations. In that state, vortices easily move under the temperature gradient ∇T with a velocity $\mathbf{v}$ toward the colder edge of the sample (see, e.g., [259]). Because of the 2π-phase singularity at each core (central part) of the vortex, the motion of vortices causes a phase slip [260], which as a result of a ac Josephson effect leads to the appearance of a Josephson bias. It can be expressed as the transverse electric field $\mathbf{E} = \mathbf{B} \times \mathbf{v}$. The appearance of an electric field $\mathbf{E}$ in the presence of a temperature gradient and a magnetic field $\mathbf{B}$ is known as the Nernst effect. The Nernst signal, defined as E per unit of the temperature gradient, $e_N = E/|\nabla T|$, is much greater in ferromagnets and superconductors than in non-magnetic normal metals. In metals, where the Nernst signal is linear in the magnetic field, it is customary to measure the Nernst coefficient $\nu = e_N/B$. In type-II superconductors, the e_N signal is strongly nonlinear, and therefore the Nernst signal $e_N(H, T)$ is more useful than ν in measuring the Nernst effect in cuprates. Because E can be measured with high accuracy, the Nernst effect can be used as a highly sensitive method for detecting vortices.

The Nernst signal measured in experiment is the sum of two contributions, from vortices and from charge carriers (quasiparticles): $e_N = e_N^s + e_N^n$. The quasiparticle Nernst signal can be expressed as $e_N^n = \rho^n \alpha_{xy}^n - \rho_{xy}^n \alpha^n$, where ρ_{xy}^n and ρ^n are the respective Hall and specific resistances, and $\alpha^n \equiv \alpha_{xx}^n$ is related to the thermal emf as $S = \rho^n \alpha^n$ [117]. Although the quasiparticle Nernst signal is very small in cuprates with hole impurities at $T < T_c$ [256], it is carefully measured via measurements of the thermal emf, Hall angle, and specific resistance.

To compile the overall picture, the Nernst signal related to the pair condensate was measured in [117] at $T > T_c$ in high-quality single crystals of Bi2212, Bi2223, LSCO, YBCO, and Bi(La)2201 cuprates with different doping levels. For brevity in this section, we use the notation UD, OP, and OV for underdoping, optimum doping, and overdoping.

3.4.1 Optimum doping. In Fig. 10, taken from [117], we show the dependence of the Nernst signal e_N on the magnetic field, measured in slightly overdoped (OV) $YBa_2Cu_3O_y$ (YBCO) with $y = 6.99$ and $T_c = 92$ K at fixed temperatures. After exceeding the field of vortex lattice melting, the number of moving vortices sharply increases and the e_N signal grows almost vertically, reaches a wide maximum, and then slowly decreases (Fig. 10a). The totality of curves represents the maximal value of the e_N signal attained in the temperature ranges indicated in the figure. When the temperature exceeds T_c, the maximum values of $e_N(T)$ significantly decrease and the curves widen (Fig. 10b). But no sharp transition is observed in the e_N signal. Instead, it preserves its nonlinearity at temperatures up to 105 K. At $T > 110$ K, e_N is linear in the field, with the slope that changes slightly with the temperature, which the authors identify with the quasiparticle contribution e_N^n. To segregate the fluctuation contribution, the authors measured the temperature dependence of e_N in the magnetic field 14 T and showed that, at a temperature exceeding $T_c = 92$ K, e_N deviates from the quasiparticle dependence by 15 K.

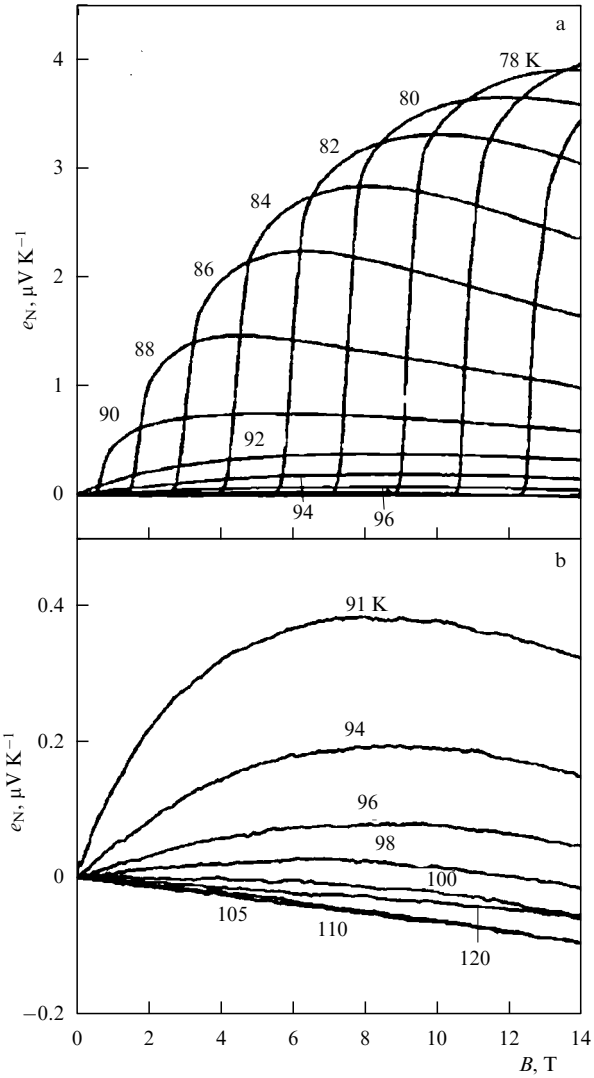

Figure 10. Dependences of the Nernst signal e_N on the magnetic field measured in slightly overdoped (OV) $YBa_2Cu_3O_y$ with $y = 6.99$ and $T_c = 92$ K at temperatures (a) below and (b) above T_c. At $T < T_c$, the e_N signal increases almost vertically after overcoming the melting field of the vortex lattice. At $T > T_c$, the negative B-linear quasiparticle contribution to e_N^n is well pronounced in Fig. b [117].

Similar measurements of the dependence of the Nernst signal e_N on the magnetic field were performed on two-layer Bi2212 with $T_c = 92$ K. The temperature T_{onset} of the onset of the vortex Nernst signal was ~ 125 K, which is 30 K higher than T_c. The wide region of the Nernst signal in Bi2212 compared with such in OP YBCO reflected its higher anisotropy. In the three-layer cuprate OP Bi2223, the Nernst signal e_N was also observed at temperatures above $T_c = 109$ K and the overall behavior of the dependence $e_N(B)$ was quite similar to that of e_N in the two-layer OP Bi2212 system. The temperature T_{onset} at which the Nernst signal starts being detected was 135 K, which is 25 K above T_c.

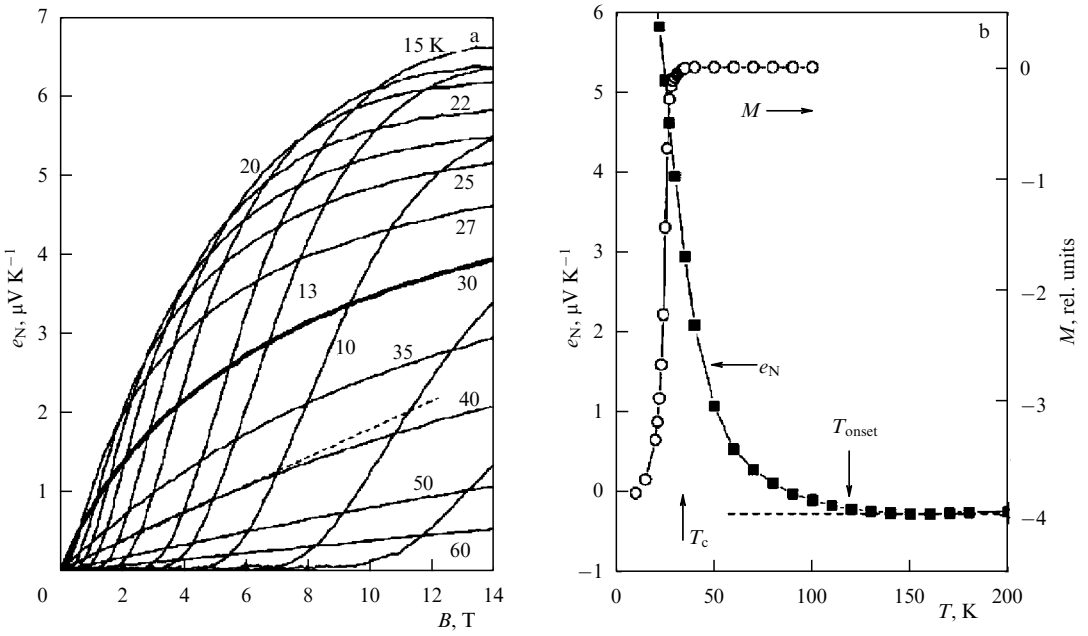

Figure 11. (a) Dependences of the Nernst signal e_N on the magnetic field for UD $La_{2-x}Sr_xCuO_4$ ($x = 0.12$, $T_c = 28.9$ K). Bold line was obtained at T_c. The dashed line at $T = 40$ K defines the initial slope used to determine ν. (b) Temperature dependence of e_N measured in a field of 14 T in UD LSCO (squares), together with the magnetization M measured in a field of 10 Oe (circles). Dashed line shows the negative quasiparticle contribution [117].

3.4.2 Underdoping. The Nernst signal at temperatures above T_c, already strong in OP cuprates, becomes even stronger in the UD regime. In Fig. 11a, we show the dependences of the Nernst signal e_N on the magnetic field for the UD $La_{2-x}Sr_xCuO_4$ (LSCO) with $x = 0.12$ and $T_c = 28.9$ K at fixed temperatures. The results look quite similar to the data for the OP YBCO (see Fig. 10). But a closer inspection of the $e_N(B)$ curves reveals an essential difference. In the OP YBCO, the maximum value of e_N at $T_c = 92$ K is approximately 0.38 μV K^{-1}, which is less than 10% of the maximum for the UD LSCO curve ($\geqslant 4$ μV K^{-1}) at temperatures below T_c. At $T > T_c$, as the temperature increases, the e_N signal rapidly decreases to a negligibly small magnitude compared with 4 μV K^{-1} (see Fig. 10). The bold line in Fig. 11a was obtained at $T = 30$ K, which is somewhat above T_c; in a magnetic field of 14 T, its magnitude ~ 4 μV K^{-1} is more than 50% of the maximum values of the $e_N(B)$ curves, and it keeps increasing as the field increases. Even at the temperature of 50 K, more than 20 K above T_c, the e_N signal constitutes a significant part of the maximum value attained by the curves. The Nernst signal decays relatively slowly as the temperature increases and becomes indistinguishable from the quasiparticle Nernst signal only for $T > 100$ K.

In Fig. 11b, we show the temperature dependence of e_N measured in a field of 14 T on the same LSCO sample, together with the magnetization M measured at 10 Oe in a superconducting quantum interference device (SQUID). The anomalous Nernst signal starts deviating from the low quasiparticle background at $T_{onset} \sim 120$ K. The temperature dependence of e_N, measured in a field of 14 T, has a long fluctuation 'tail' extending to T_{onset}.

In an LSCO with a lower $x = 0.07$ and $T_c = 11$ K, these anomalous features were enhanced. The curves obtained in the range $T = 12$–20 K in the field of 14 T are comparable with many others obtained at $T < T_c$. Similar results are also given in [261], where the Nernst effect was measured in a UD LSCO in magnetic fields up to 28 T. Therefore, from the standpoint of the Nernst effect, the borderline between the superconducting and normal states is smeared in UD cuprates. This entails a serious problem for the conventional understanding of 'fluctuations.'

The temperature dependence of the Nernst signal e_N in a strongly underdoped Bi2212 single crystal with $T_c = 50$ K and the hole concentration ~ 0.09 suggested that $T_{onset} = 118$ K, some 65 K above T_c. As in the case of LSCO with $x = 0.07$, the maxima of curves obtained at temperatures above T_c remained very large and had a high curvature characteristic of the vortex state. An important feature of Bi2212, both UD and OP, is a very small quasiparticle contribution to the Nernst signal, manifesting itself as a background. This allows unambiguously determining the initial temperature T_{onset}.

3.4.3 Phase diagrams based on the results of Nernst effect measurements. In Fig. 12, taken from [117], we present phase diagrams showing ranges of the Nernst signal observations at temperatures between T_c and T_{onset}. For LSCO (Fig. 12a), the numbers on the curves show the values of the Nernst coefficient ν in units of [nV K^{-1} T^{-1}]. The $T_{onset}(x)$ curve has finite points at $x = 0.03$ and $x = 0.26$ and attains a maximum at $x \approx 0.10$. In the case of LSCO, the Sr content x typically corresponds to the concentration of holes. In Fig. 12b, we show the results for Bi2212 (based on measurements of the Nernst signal in five crystals). The hole concentration p in Bi2212 was estimated by an empirical formula [233] with $T_{c,max} = 91$ K. We can see that the T_{onset} curves separate the superconducting and pseudogap regions. The superconducting regions lie below the T_{onset} curves, which lie below the T^* curves. The interval between T_{onset} and T_c becomes narrower toward the OV side, but remains sufficiently wide on the UD side. Interestingly, the maximum values of T_{onset} (~ 130 K) in Bi2212 and LSCO are close, despite the large difference in T_c. The maximum value of T_{onset} in YBCO is also ~ 130 K.

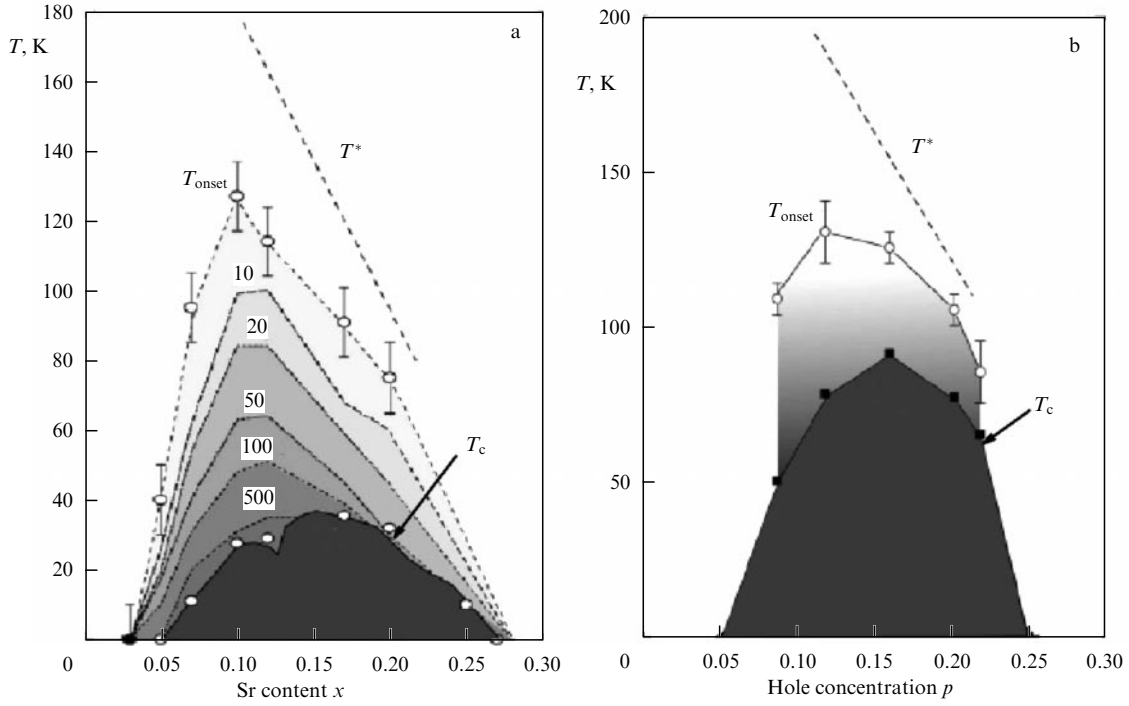

Figure 12. Phase diagrams with regions of Nernst signal observation at temperatures between T_c and T_{onset}. (a) LSCO (numbers on the curves show the values of the Nernst coefficients ν expressed in [nV K^{-1} T^{-1}]). $T_{onset}(x)$ curve has finite points at $x = 0.03$ and $x = 0.26$ and reaches a maximum at $x \approx 0.10$. (b) Bi2212 (based on measurements of the Nernst signal in five crystals). The region where the Nernst signal is present does not extend to the pseudogap temperature T^* on the OP and OV side, as this was the case in LSCO. In the UD regime, T_{onset} has a tendency to decrease as p decreases below 0.15. Dashed lines show the T^* temperatures based on heat capacity measurements. (From [117].)

In the above phase diagrams, the position of the superconducting phase under the T_{onset} curves once again emphasizes the inseparability of the superconducting region and the region where the vortex Nernst signal is observed. The high-temperature signal e_N related to vortices is observed on the x, p scales only within the superconducting region. Outside it (on the UD or OV side), the e_N signal is very small. In an LSCO with $x = 0.03$ and 0.26, the vortex signal is absent altogether. The observed correlation between the e_N and T_c dependences on x and p, and also the exact relation of the high magnetizations M at $T > T_c$ to the e_N signals measured for the same samples indicated their vortex nature. The authors of [117], based on these results and those of their previous experiments [262], concluded that the Nernst signal is produced by superconducting pairs. In the limit UD regime, where a high density of pairs cannot be maintained, or in the limit OV regime, where the pairs are absent, the vortex Nernst signal disappears, and only the standard quasiparticle contribution survives.

It was thus shown in [117] that, in the phase diagram of Bi(La)2201, Bi2212, Bi2223, LSCO, and YBCO cuprates, there is a large region above the superconducting region where vortices and hence electron pairs exist. The temperature T_c in these compounds is primarily determined by the loss of phase coherence due to spontaneous vortex–antivortex interactions by thermally generated vortices in a zero magnetic field. The upper boundary of this region is determined by the temperature T_{onset}, which is formally between T_c and T^*. Directly above the T_c curve, the phase of superconducting pairs $\theta(\mathbf{r})$ is strongly disordered by rapidly propagating vortices and antivortices, but, closer to the T_{onset} curve, fluctuations become equally important. We note that, in each of the cuprates, the edge of the vortex region does not fully extend to the pseudogap temperature T^*. This means that, in cooling a UD sample from room temperature, the pseudogap state first appears at T^*, but it is observable only in experiments that reflect spin effects. After the sample is cooled to a temperature below T_{onset}, the existing vortices give rise to the e_N signal, indicative of the presence of short-range superconducting currents. The coexistence of the pseudogap state and d-wave superconductivity in a wide temperature range $T_{onset} > T > T_c$ apparently requires that they be closely related and nearly indistinguishable. The vortex Nernst region is the one where the system smoothly evolves or oscillates between two states.

In recent study [263], the Nernst effect was measured in YBCO and three LSCO-based cuprates with the aim to clarify the boundary of the pseudogap phase in their phase diagrams. (Below, we concentrate on the additional data for YBCO because they were obtained for single crystals of a very high quality.) The authors separated the contributions to the Nernst signal made by superconducting fluctuations and by quasiparticles using the fact that only the former is suppressed by a magnetic field. They studied the region to which the superconducting fluctuations extend at temperatures above T_c depending on the doping level. The comparison of the results with the data of previous studies allowed concluding that the traditional assumption about superconducting fluctuations as the only essential contribution to the Nernst signal is not quite correct. In addition, the authors revealed that the narrower fluctuation region follows T_c rather than T^*, thereby suggesting that the pseudogap phase is not caused by fluctuations of the phase

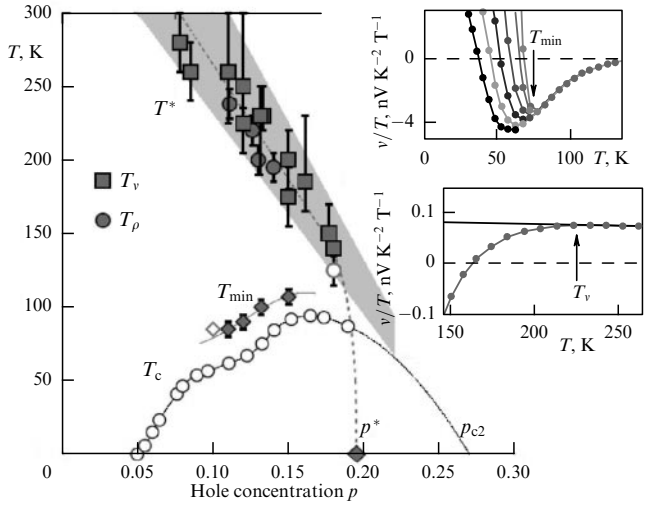

Figure 13. T–p diagram of YBCO with three characteristic temperatures: T_c (circles [231]) marks the onset of superconductivity in a zero magnetic field, below which the electric resistance is equal to zero. The solid curve is drawn over the T_c data by eye. Dashed curve is a smooth continuation of that curve under the assumption that the superconducting phase terminates at the critical doping level $p_{c2} = 0.27$. Dark diamonds show the temperatures T_{min}: at $T < T_{min}$, superconducting fluctuations become significant [265]. Light diamond shows T_{min} for a previously measured sample with $p = 0.1$ [266]. The curve is drawn over the diamonds by eye. Dark dots show the temperatures T_ρ: at $T < T_\rho$, the specific resistance $\rho(T)$ deviates from its high-temperature linear dependence (data in [234]), which is the standard definition of the pseudogap opening temperature T^* in YBCO [267]. Circle shows the temperature T_ρ for a sample with $p = 0.18$, with a high level of disorder due to electron irradiation [268]. Squares show temperature T_v: at $T < T_v$, the quasiparticle Nernst signal deviates from its high-temperature behavior [265, 269]. It can be seen that, because $T_v \simeq T_\rho$ to within the error, both temperatures are commensurate with T^*. The dotted line is a linear fit to the T^* data. Diamond on the p axis corresponds to the critical doping level $p = p^*$ at which the pseudogap phase terminates at $T = 0$ in the absence of superconductivity. In YBCO, $p^* = 0.195 \pm 0.005$ [269]. Gray stripe is the region of T^* in Bi2212 with $p \simeq 0.22$, measured by spectral methods [202]. (This region is shown in Fig. 8.) Insets show parts of the temperature dependences of the reduced Nernst coefficient v/T for YBCO with $p = 0.12$ in magnetic fields in the range from 1 to 15 T [265]. Upper inset: definition of T_{min}, the temperature near T_c at which the Nernst signal in a field of 1 T reaches a minimum, at the foot of a large positive maximum associated with superconductivity. Lower inset: definition of the temperature T_v such that at $T < T_v$ the v/T coefficient starts deviating downward from its high-temperature linear behavior determined only by the quasiparticle contribution to the Nernst signal. (From [263].)

and/or the amplitude of the superconducting order parameter. In other words, the pseudogap is not a precursor of superconductivity. [23]

[23] We note that, back in 2000, in [264], the results of a study of magnetotransport in monolayer Bi2201 single crystals in magnetic fields up to 28 T were reported. The authors discovered that, first, the semiconducting behavior of the transverse resistance (along the c-axis) was suppressed by the magnetic field, irrespective of its orientation (perpendicular or parallel to the CuO_2 planes) and, second, that the normal-state magnetoresistance across the CuO_2 planes, unlike that in the superconducting state, was independent of the orientation of the magnetic field. Such an isotropic response indicated the importance of spins effects for the normal-state pseudogap, because the response of the superconducting state due to orbital effects is strongly anisotropic. These results already gave grounds to highly doubt the superconducting nature of the pseudogap.

Based on the results in [265], where the temperature dependence of the reduced Nernst coefficient v/T was measured for YBCO with the doping level $p = 0.12$ in magnetic fields up to 15 T, the authors of [263] also deduced that the Nernst signal contains two separate contributions: a positive one, which depends on the magnetic field and increases at temperatures below T_{min} but close to T_c, and a field-independent signal, which is small and positive at high temperatures and becomes large and negative at temperatures below T_v: at $T < T_v$, the quasiparticle Nernst signal deviates from its high-temperature behavior. The first contribution is due to superconducting fluctuations, and the second, to quasiparticles.

In Fig. 13, the two temperatures T_{min} and T_v are shown on a T–p phase diagram of YBCO. The data for T_v at $p > 0.1$, reproduced from [265] and obtained at $\nabla T \parallel a$ and $\nabla T \parallel b$, exhibit the same values of T_v. The methods to choose those temperatures are presented in the insets to Fig. 13.

The standard definition of the pseudogap opening temperature T^* in YBCO is T_ρ: at lower temperatures, the specific resistance $\rho(T)$ deviates from the high-temperature linear dependence [267]. T_ρ at different doping levels are shown in the phase diagram in Fig. 13, whence we can see that $T_v = T_\rho$ to within the error. From the standpoint of pseudogap phase studies in YBCO, it is most useful to study manifestations of the Nernst effect rather than the behavior of specific resistance. The pseudogap and superconductivity affect the $v(T)$ signal in opposite ways: the former causes its decrease to negative values under cooling, and the latter determines its increase, whereas for the specific resistance both effects lead to a decrease in $\rho(T)$. This allows unambiguously separating the two contributions to the Nernst signal and tracing their initial temperatures.

3.5 Optical studies

3.5.1 Optical conductance. Studying the optical conductance $\sigma(\omega, T)$ has several advantages over studying the specific resistance to direct current, which is the zero-frequency limit. First of all, this eliminates experimental problems with electric contacts, and the absolute values of the parameters to be measured can then be extracted without making precise measurements of the geometry of submillimeter-size samples.

Optical spectroscopy of metals and semiconductors has allowed obtaining information on their electronic band structure and elementary excitations. Spectroscopy data taken together with the results obtained by other methods offer a detailed experimental picture of excitations as functions of frequency and momentum. Traditional infrared (IR) and optical spectroscopy, which relates to the process of first-order light scattering, studies excitations and collective modes in the energy range 20–50000 cm^{-1}. In that range, the far-IR region is of special interest for superconductivity, because it includes both the superconducting gap and the excitation energies that are believed to be related to the formation of the superconducting state.

Measurements of the reflection coefficient allow investigating the complex dielectric function $\varepsilon(\omega) = \varepsilon_1(\omega) + i\varepsilon_2(\omega)$, from which the complex dynamical conductance $\sigma(\omega) = \sigma_1(\omega) + i\sigma_2(\omega)$ can be obtained. The real part of the conductance $\sigma_1(\omega)$ is proportional to the total density of states and determines the absorption of radiation at a frequency ω. The real part of the inverse conductance $\sigma^{-1}(\omega)$ is proportional to the quasiparticle scattering rate τ^{-1}, and its imaginary part is proportional to the renorma-

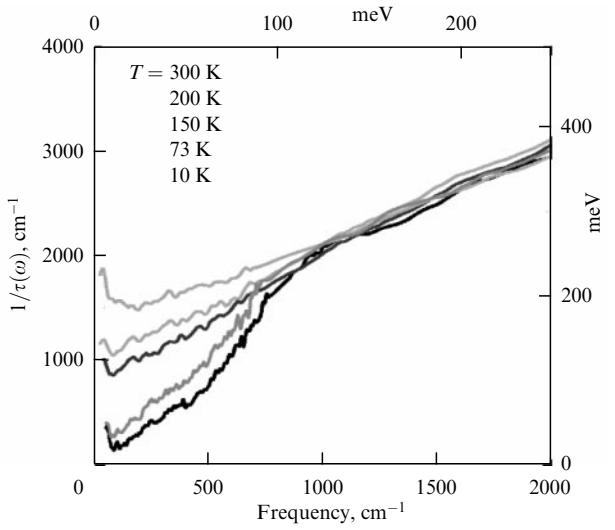

Figure 14. Dependence of the scattering rate τ^{-1} on frequency in a Bi2212 sample with a low level of doping at different temperatures. Linear dependence of the scattering rate at high frequencies terminates at a temperature of about 150 K, where a sharp decrease in the rate is observed due to the formation of the pseudogap. In the superconducting state, the frequency of this gap increases by only an inconsiderable amount [272].

lized mass $m^*/m = 1 + \lambda(\omega)$, where λ is the penetration depth. As a result, using the Kramers–Kronig [24] transformation of experimental data, any one of the optical constants can be obtained [270].

The earliest studies of the optical properties of cuprates already made it clear that their IR reflection spectra in the *ab* plane are different from the spectra of simple metals, which are mainly flat between the zero and plasma frequencies.[25] Instead, in the range of 500 cm^{-1}, the onset of strong absorption was observed in the spectra of all cuprates in the normal state. For example, in [271], the IR properties of Bi2212, BiPb2212, and Tl2201 crystals were studied in a wide range of doping levels. The authors found convincing proof of the existence of the pseudogap in samples with low and moderately high doping levels. In Fig. 14, we show the frequency-dependent scattering rate τ^{-1} in Bi2212 at different temperatures. At high frequencies $\omega > 700$ cm^{-1}, the scattering rate is approximately linear and shows no temperature dependence. At low frequencies $\omega < 700$ cm^{-1}, a pronounced temperature dependence is observed in the form of a gap feature starting at a temperature below 150 K, much greater than $T_c = 67$ K. Very similar results were obtained for BiPb2212 and Tl2201.

Because the principal features of the τ^{-1} spectra in cuprates are related to the pseudogap problem, they were summarized in [272] with small differences between different materials observed at the time disregarded. First, all the hole-doped cuprates at high temperatures or high frequency at all temperatures have a linear dependence of scattering, which is suppressed at low frequencies. Second, there are similarities in the spectra obtained in samples with a low doping level to those of optimally doped samples in the superconducting state. This was suggestive of the idea that the normal-state pseudogap and the superconducting gap are closely related.

As regards interplane optical conductance along the *c*-axis, the first experiments already showed a very low conductance of cuprates in that direction. The electron background in the original conductance σ_c turned out to be strongly suppressed, and the spectra were dominated by sharp peaks of optical phonons. After subtracting the effect of phonons, the conductance reflected the normal-state pseudogap. The actual value of the gap frequency was dependent on the assumptions made when subtracting the phonon effect. In samples with a high doping level, the $\sigma_c(\omega)$ data were the same as for a dirty metal. At a below-optimum doping, the samples exhibited nonmetallic frequency and temperature dependences of the interlayer conductance.

In [273], the reflection coefficient along the *c*-axis was measured in high-quality $YBa_2Cu_3O_{6+x}$ single crystals in wide ranges of temperature and frequency. A sample with $x = 0.70$ and $T_c = 67$ K at room temperature exhibited a pseudogap in conductance at the frequency of 200 cm^{-1}. The gap gradually increased as the temperature decreased to 10 K in the absence of a feature at T_c. On the other hand, the gap was not observed in normal-state samples with $x = 0.95$. These results, as the authors believe, are consistent with the phase diagrams proposed for the explanation of NMR data and neutron scattering.

We also mention studies [274–278], where another method, ellipsometry, was used to explore the optical conductance $\sigma_c(\omega)$. This is a polarization-optical method for directly measuring the complex conductance $\sigma(\omega)$ without having to invoke the Kramers–Kronig analysis. Access to high-luminosity sources has made it more practical compared with traditional reflection spectroscopy.

3.5.2 Raman scattering of light. Raman scattering of light is a second-order process (inelastic scattering of optical radiation), in which the absorbed photons are reemitted with a significant change in frequency, which is determined by the structure of the material. This process is much weaker than dipole absorption, which is responsible for optical conductance. In metals, Raman scattering is difficult to observe because of the low penetration depth of electromagnetic radiation (several thousand angstroms). In addition, in accordance with the momentum conservation law for free carriers, only carriers with energies up to ≈ 50 cm^{-1} can be excited in cuprates.

In normal superconductors, excitations across the energy gap are possible for Raman scattering. A Cooper pair then splits into two quasiparticles obeying the momentum conservation, which leads to the appearance of a scattering threshold at 2Δ. But early experiments did not reveal a clear scattering onset signal at 2Δ in cuprates. Instead, intense scattering was observed down to the lowest frequencies, as in the case of optical conductance.

It soon turned out, however, that, unlike optical conductance in the *ab* plane, Raman scattering allows obtaining two spectra, B_{1g} and B_{2g}, each of which is an averaged spectrum over different parts of the Fermi surface. The B_{1g} spectra project excitations around the antinodal direction $(\pi, 0)$, where the superconducting gap is maximal, whereas the B_{2g} spectra involve states near the nodal region in the diagonal direction (π, π) of the BZ. Consequently, the Raman

[24] In classical electrodynamics, the Kramers–Kronig relations link the real and imaginary parts of the dielectric permittivity.

[25] The frequency of longitudinal eigenoscillations of charged particles in the absence a magnetic field, which largely determines the optical properties of the investigated materials. Electromagnetic radiation with a frequency below the plasma frequency of the sample is well reflected from it, whereas at a frequency higher than the above plasma frequency, radiation passes through the sample or is absorbed by it.

response has a maximum at $2\Delta_{\max}$ for B_{1g} and a maximum for a somewhat lower energy for B_{2g} [279].

In [280], Raman scattering of light in Bi2212 was used to study the evolution of the pseudogap with the temperature and the doping level in the region of a superconducting dome on the T–p phase diagram. For all temperatures, the pseudogap was preserved at high doping levels, before it suddenly disappeared at $0.222 < p^* < 0.226$. This range exactly corresponds to the doping region where the normal-state pseudogap closes under the Lifshitz[26] transition in Bi2212 [73], which shows that the edge of the superconducting pseudogap is a vertical line in the T–p phase diagram (see below). Combining the results of experiments on Raman scattering of light in cuprates, the authors observed their qualitative consistency with the mean field 'cellular' dynamical theory.[27] This was proof of the existence of a pseudogap in the superconducting state, a universal property of hole-doped cuprates. In the opinion of the authors, the pseudogap in the superconducting phase is sensitive to the topology of the Fermi surface, in contrast to the superconducting gap, which seems to not change at a high doping level, thus significantly restricting the possible relation between the pseudogap and HTSC.

In Fig. 15a, borrowed from [73], we show the Raman responses $\chi''_{B_{1g}}(\omega, T)$ at different temperatures. We can see that the maximum of $2\Delta_0$ at the frequency of 408 cm^{-1}, associated with the breakup of superconducting pairs, decreases as the temperature increases, and this maximum disappears at T_c. Accordingly, the integrated intensity $I_{B_{1g}}(T) = \int \chi''_{B_{1g}}(\omega, T)\, d\omega$, shown in Fig. 15b, monotonically decreases, with a sharp decrease at T_c. Just at $T > T_c$ does the low-energy spectral weight (below 408 cm^{-1}) increase with an increase in temperature.[28] The intensity $I_{B_{1g}}(T)$ monotonically increases until it reaches a maximum at the pseudogap opening temperature T^*. At temperatures above T^*, the dependence $I_{B_{1g}}(T)$ is the same as for a normal metal. The obtained value of T^* agrees well with the previous transport and spectroscopy measurements. As the doping level increases, the difference between T_c and T^* decreases and vanishes at the concentration $p = 0.22$, indicating pseudogap closure in the normal state. For $p > 0.22$, the slope of $I_{B_{1g}}(T)$ is negative, which means the absence of the pseudogap.

The authors of [73] studied the dependence of the ratio of integrated intensities $I_{B_{1g}}/I_{B_{2g}}$ on the doping level of samples in the superconducting and normal states. It turns out that this ratio changes nonmonotonically with p and has a sharp maximum at $p = 0.22$, where the pseudogap closes. That the position of the maximum is independent of the temperature points to its relation to the increased density of states around the antinodal region of the BZ. This invariably leads to the possibility of Lifshitz's quantum phase transition induced by doping, where the Van Hove singularity intersects the Fermi level and the open disconnected hole Fermi surface closes around the $(\pm\pi, 0)$ and $(0, \pm\pi)$ points and becomes an

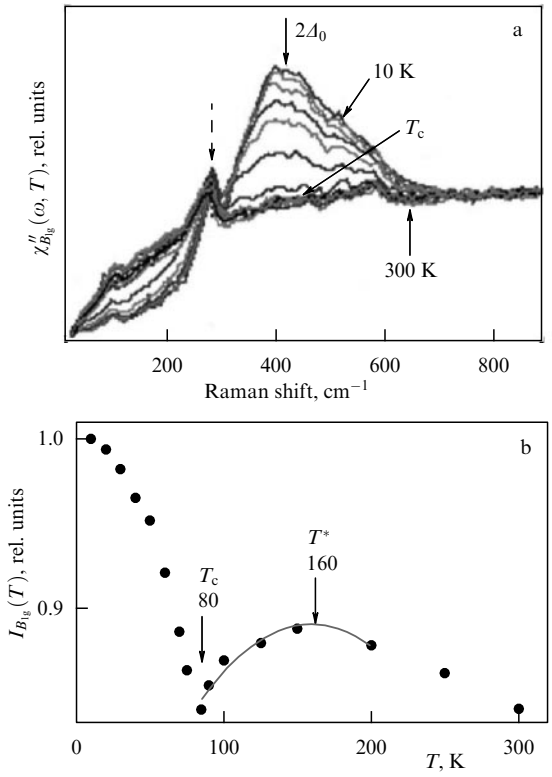

Figure 15. (a) Raman responses $\chi''_{B_{1g}}$ at different temperatures in a Bi2212 sample with a high level of doping. The value of $2\Delta_0$ was determined from the position of the maximum of B_{1g}. The arrow at the frequency of 300 cm^{-1} shows the phonon maximum. (b) Integrated Raman intensity $I_{B_{1g}}$ normalized to the intensity at 10 K. (From [280].)

electronic one. The authors adduce theoretical calculations to substantiate this assumption and conclude that the microscopic cause of the pseudogap is sensitive to the topology of the Fermi surface, and T_c is independent of this transition, demonstrating that the pseudogap and the superconducting gap have different origins in highly doped cuprates.

3.6 Orders inside the pseudogap region

Before discussing orders in the pseudogap region, it is worth recalling that the pseudogap is a particle gap in the density of electron states, which opens in superconducting cuprates in the normal state and whose origin is a long-standing mystery and a subject of intense debate in the physics of correlated electrons. Its relation to the Mott insulator phase at a low level of doping remains ambiguous, and its relation to CDW-type order [248, 281, 282], which reconstructs the Fermi surface at an intermediate level of doping [283, 284], is still unclear [220, 221, 285].

3.6.1 Spin density wave. The long-range commensurate AF order rapidly disappears as the doping level p increases: the Néel[29] temperature T_N becomes equal to zero at the critical doping level $p_N = 0.05$ in YBCO (Fig. 16) and $p_N \simeq 0.02$ in LSCO. For $p > p_N$ at low temperatures, incommensurate SDW order is observed, with the correlation lengths varying from one cuprate to another from quite small to substantially

[26] A quantum phase transition of the order $2\frac{1}{2}$.

[27] The method to determine the electronic structure of strongly correlated materials. In this case, it can describe the phase transition between a metal and a Mott insulator as the electron correlation strength increases.

[28] We recall that, in studies of HTSC spectra, the pseudogap manifests itself as a loss of the spectral weight by quasiparticles. In optical studies, instead of the spectral weight $N(\omega) \sim \int_0^\omega \sigma(\omega')\, d\omega'$, the dimensionless measure of the spectral weight $N_{\text{eff}}(\omega, T)$ is typically used as a spectral function. At $m_0/m = 1$ (where m is the electron mass), it is just equal to the number of free carriers in the elementary cell [270].

[29] The Néel temperature is the AF Curie temperature, above which an antiferromagnet turns into a paramagnet (via a second-order phase transition).

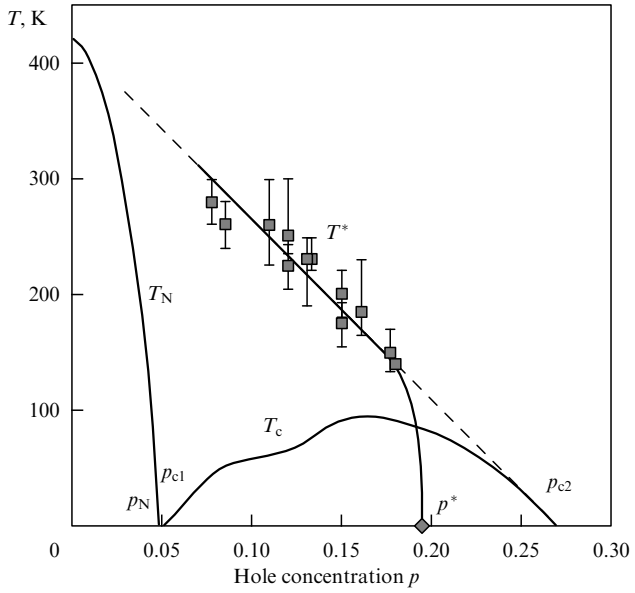

Figure 16. T–p phase diagram of YBCO: pseudogap temperatures T^* (squares), the Néel temperatures T_N (line on the left), and T_c (line at the bottom). Dashed line, drawn by eye, shows that T^* can be extrapolated to T_N at $p = 0$, but is connected to T_c on the overdoped side of the diagram, where superconductivity disappears [263].

large. In YBCO in a zero magnetic field, the short-range SDW order was observed at doping levels up to $p_{SDW} \simeq 0.07$ and disappeared with the onset of the CDW-type order with $p_1^{CDW} \simeq 0.08$. This proves that these two orders are competing (possibly because their periods are not coordinated [286]).

In LSCO, the SDW order in a zero field is preserved at doping levels up to $p_{SDW} \simeq 0.13$ and coexists with a CDW-type order, which proves the absence of competition between them (possibly because their periods are coordinated [286]). The magnetic field suppressing superconductivity enhances the SDW order in both YBCO and LSCO [287]. In LSCO, a field of 15 T shifts the SDW critical point to $p_{SDW} \simeq 0.15$ [288]. Extrapolating to higher fields can yield the value $p_{SDW} \simeq p^* = 0.18$ at $B = B_{c2} \simeq 60$ T. In other words, when the competing superconductivity is entirely suppressed by the magnetic field, the SDW order in LSCO can exist at doping levels up to p^*, which means that the nonsuperconducting ground state of the pseudogap phase can contain the SDW order. This conclusion is supported by studies of an LSCO compound with a Zn impurity (used to suppress superconductivity) by muon spin spectroscopy (μSR),[30] which revealed magnetism at doping levels up to $p = 0.19 \pm 0.01$ [289, 290].

In YBCO with superconductivity suppressed by a large magnetic field, the SDW order is not induced in the region where the CDW order exists, i.e., for p between $p_1^{CDW} = 0.08$ and $p_2^{CDW} = 0.16$ [291]. But adding a Zn impurity to suppress superconductivity, for example, for $p \simeq 0.12$, also suppresses the CDW order, and the SDW order then arises [292]. In other words, there is a three-stage competition of phases. If superconductivity is entirely suppressed, then there is a probability of the appearance of SDW order at doping levels between p_2^{CDW} and p^*, as noted above for LSCO. For YBCO, this requires a field, about 150 T, the maximum value of B_{c2} [293].

Thus, an AF or SDW order at low temperatures is ubiquitous in hole-doped cuprates, and it may well exist at all doping levels from $p = 0$ to p^* unless it is suppressed by competing superconductivity or the CDW order. This is an important property of the pseudogap phase as $T \to 0$: a second relation exists between the pseudogap and antiferromagnetism (the first being that $T^* \simeq T_N$ as $p \to 0$). Bearing this in mind, we emphasize that the pseudogap is not just the SDW-order phase, because $T_{SDW} \ll T^*$.

3.6.2 Charge density wave. The CDW order was first revealed in Nd-LSCO and $La_{2-x}Ba_xCuO_4$ cuprates at $p \simeq 0.12$ in neutron diffraction experiments [294] and then in Bi2212 with the help of STM [295, 296]. In YBCO, LSCO, Eu-LSCO, Bi(La)2201, and Hg1201, this order was found much later in various experiments with the use of ARPES, NMR, and X-ray diffraction (XRD) (for details, see, e.g., [265]). The strongest CDW order is usually observed at $p \simeq 0.12$ and is limited by a region that lies entirely within the pseudogap phase between two critical doping levels: p_1^{CDW} at low doping and p_2^{CDW} at high doping (Fig. 17). According to the authors of [265], p_2^{CDW} is much less than p^* for the four cuprates that they studied. This implies the conclusion that the pseudogap phase is neither the CDW-order phase nor a high-temperature precursor of that order. This is confirmed by the fact that the temperature of the onset of the CDW order in the same cuprates attains a maximum at $p \simeq 0.12$, whereas T^* monotonically increases with a decrease in p (see Fig. 17).

In other cuprates, the positions of p_2^{CDW} and p^* are not yet finally fixed. In STM studies of Bi2212 at $T \simeq 10$ K (below T_c), CDW modulations were detected for p up to $p = 0.17$, and a transition from Fermi arcs (with a pseudogap) at $p = 0.17$ to the full-fledged Fermi surface (without a pseudogap) was observed at $p = 0.20$. In other words, $p_2^{CDW} \simeq p^* = 0.185 \pm 0.015$. But pseudogap measurements in the normal state (with $T > T_c$) via ARPES and Raman scattering showed that $p^* = 0.22 \pm 0.01$ [73, 302]. With this uncertainty taken into account, it is possible that $p^* \simeq p_2^{CDW} + 0.03$ in Bi2212 is higher than in YBCO and LSCO. The authors hence conclude that the setting in of the CDW order is a secondary instability of the pseudogap phase.

3.6.3 Nematicity. In orthorhombic YBCO due to the presence of CuO chains along the b-axis, the specific resistance in the ab plane is anisotropic. In addition to this anisotropy, another one arises under cooling and in the case of low doping of the sample [299]. This other anisotropy, called nematicity[31] in [11], starts in the phase diagram (see Fig. 17) at temperature T_{nem}, represented by a line drawn parallel to T^*, approximately 100 K below it. Nematicity was also revealed in measurements of the Nernst coefficient [11]. Near the T_{nem} line in the region of low doping levels in Fig. 17, we give data on the anisotropy in the spectrum of spin fluctuations, which were detected via inelastic neutron scattering as a splitting of the maximum at the wave vector $\mathbf{Q} = (\pi, \pi)$ for one of the

[30] Muon spin spectroscopy studies local microfields in matter (for example, the magnetic structure of HTSCs) with the help of an elementary particle, the muon.

[31] The liquid-crystal phase that is a quantum mechanical analogue of classical liquid crystals with the ground state being intermediate between a liquid (where quantum fluctuations are large) and a crystal (where they are small). This phase is assumed to be a new state of matter, which can be a common feature of strongly correlated fermion systems (which, notably, can be high-temperature superconductors) [7].

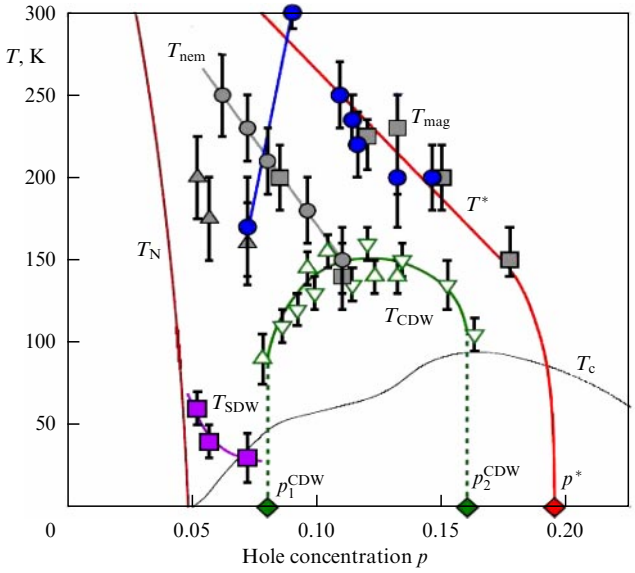

Figure 17. (Color online.) T–p phase diagram of YBCO, showing the Néel temperature T_N (brown curve), superconducting transition temperature T_c (black curve), the pseudogap opening temperature T^* (red curve), and the critical point p^* (red diamond) (all from Fig. 16). In addition, the CDW phase is shown (green), determined by the temperature T_{CDW}: at $T < T_{CDW}$, short-range CDW-type correlations were revealed with XRD (triangles pointing up [4] and triangles pointing down [249]). Two green diamonds show the critical levels of doping at which the CDW phase starts, $p_1^{CDW} = 0.08$ [297], and terminates, $p_2^{CDW} = 0.16$ [269], at $T = 0$ in the absence of superconductivity, as was discovered in Hall effect measurements in high magnetic fields. Three magenta squares on the T_{SDW} curve show the temperature below which incommensurate short-range SDW-type correlations are observed in neutron diffraction experiments [298]. Gray symbols show the temperature T_{nem} that marks the beginning of nematicity, which was discovered from the anisotropy of the specific resistance in the *ab* plane (gray dots [11, 299]), by Nernst coefficient measurements (gray squares [265, 299]), and from the spectra of spin fluctuations measured in inelastic neutron scattering experiments (gray triangles [298]). T_{mag} (blue dots) is the temperature of the onset of magnetic order inside the elementary cell, discovered using neutron diffraction [118, 300, 301]. Blue line demonstrates an abrupt decrease in T_{mag} at doping levels below $p = 0.09$. (From [263].)

directions [298]. This spin nematicity may be responsible for transport anisotropy at temperatures below T_{nem}.

Similarly, charge nematicity was observed in the CDW-order region at a higher doping level [11], starting with $T \simeq T^*$ [231]. According to the authors of [265], at a temperature above the SDW- and CDW-order temperatures, a region of enhanced nematic susceptibility exists, possibly related to a precursor of fluctuations of these two orders [303].

We note that there are three problems that preclude identifying the nematic phase with the pseudogap phase. First, $T_{nem} < T^*$ for $p < 0.11$. Second, the nematic order does not open a gap (or a pseudogap). Third, the nematic order does not induce changes to the carrier density and cannot therefore explain the principal feature of p^*. But nematicity may well be a secondary instability of the pseudogap phase, or the pseudogap can induce increased nematic susceptibility [303]. However, the relation between the charge nematicity order and superconductivity in HTSCs is still unclear [7].

More details on nematic orders in HTSCs can be found in review [7] and recent studies [304, 305], where nematicity is considered a possible candidate responsible for the origin of the pseudogap phase.

3.6.4 Magnetic order inside an elementary cell. In YBCO, Bi2212, and Hg1201 cuprates, an intra-unit-cell (IUC) magnetic order was observed via diffraction of polarized neutrons with the initial temperature T_{mag}, which was approximately the same as T^*. This order has the wave vector $Q = 0$. In Fig. 17, we show the values of T_{mag} for YBCO taken from [118, 300, 301]. It can be seen that, in the range $0.09 \leqslant p \leqslant 0.15$, $T_{mag} = T^*$ to within the uncertainty. But, at a lower doping level ($p \simeq 0.08$), the IUC magnetic order signal weakens and appears at a much lower temperature, $T_{mag} = 170 \pm 20$ K [300], whereas $T^* = 280 \pm 20$ K. It was hypothesized that the weakening of the IUC magnetic order in YBCO at low p can be caused by competition with the SDW order (or correlations), which develops below the CDW-order phase, i.e., at $p < p_1^{CDW} = 0.08$. Still, the pseudogap does not weaken at $p < p_1^{CDW}$. Indeed, T^* is higher in the $p = 0.078$ YBCO sample investigated in [265] (clearly below the CDW-phase region [297]) than T^* in a $p = 0.085$ sample, where the doping level was higher than p_1^{CDW}.

A similar disagreement was also observed in LSCO with $p = -0.085$, where $T_{mag} = 120 \pm 20$ K, whereas $T^* = 185 \pm 20$ K. This weakening at a low level of doping assumes that the IUC magnetic order is most probably a secondary instability of the pseudogap phase, rather than being its main cause. We note that, as in the case of nematic order, it is difficult to explain how another IUC order with $Q = 0$ can open the gap (or the pseudogap) and cause a change to the carrier density as the doping level passes through p^* [263].

3.6.5 Superconductivity. In contrast to the four phases discussed above, which are all bounded on the left of p^* (and below T^*), the superconducting phase extends beyond the critical points of the pseudogap. The superconductivity region in the phase diagram of cuprates is always dome-shaped, starting at p_{c1} and terminating at p_{c2} at the respective low and high doping levels (see Fig. 16). The exact values of both p_{c2} and p^* can depend on the material: in LSCO and Nd-LSCO, $p_{c2} \simeq 0.27$, whereas in $Tl_2Ba_2CuO_{6+\delta}$ (Tl2201), $p_{c2} \simeq 0.31$ [306], and in Bi2201, $p_{c2} \simeq 0.43$ [263].

In view of the large value of p, superconductivity with the $d_{x^2-y^2}$ symmetry of the order parameter results from the Fermi-liquid metallic state characterized by one large coherent hole Fermi surface [307] without a pseudogap and any form of symmetry violation. This led the authors of [265] to raise the question: what makes the electron–electron interaction in that simple state produce electron pairs? They extracted the answer from the phase diagram shown in Fig. 16. Because the linear extrapolation of the dependence $T^*(p)$ reaches $T = 0$ at $p \simeq p_{c2}$, they assumed that the interaction conducive to the formation of pairs can also be responsible for the appearance of the pseudogap.

It turns out that p_{c2} also marks the onset of a third manifestation of electron–electron coupling: the existence of a linear term in the temperature dependence of the specific resistance $\rho(T)$. Detailed studies of overdoped Tl2201 [308–310] and LSCO [311, 312] have shown that a linear term appears in $\rho(T)$ as soon as p becomes less than p_{c2}, although $\rho \propto T^2$ for $p > p_{c2}$. This empirical relation between the resistance linear in T and T_c [313] assumes that the interaction that causes anomalous inelastic scattering can also cause the formation of electron pairs. The scattering and formation

of pairs, according to the authors of [265], can be classified as AF spin fluctuations.

Thus, for $p < p_{c2}$, three main phenomena occur together in cuprates: superconductivity, the pseudogap, and anomalous scattering. (Strictly speaking, the pseudogap opens at p^*, which is somewhat lower than p_{c2}.) But the observations can also be generalized differently. The two phases of cuprates, superconductivity and the pseudogap, are both normal-state instabilities and are characterized by a resistance linear in T. Because the linear-in-T resistance is usually observed at a boundary of the AF order and is explained by scattering on AF spin fluctuations, it is tempting to relate the pseudogap and the d-wave superconductivity in cuprates to the AF correlations (possibly short-range). In this scenario, the fact that T_c decreases at the low doping level and T^* continues to increase (see Fig. 16) can be explained by the assumed competition between the superconducting phase and a sequence of other phases: first, the pseudogap phase at $p < p^*$, and then, the respective CDW-, SDW-, and AF-type orders at $p < p_2^{CDW}$, p_{SDW}, and p_N (see Fig. 17).

3.6.6 Two CDW-type orders. The discovery of various nonsuperconducting orders associated with symmetry breaking in cuprates has changed our views on the nature of HTSC, but there is still no clear answer to the question of whether these orders/phases are coupled to superconductivity. This question is especially relevant for the CDW and SDW orders universally observed in various cuprates. The phase diagram of an ideal material for studying this question must contain regions where CDW, SDW, and superconductivity orders coexist. In YBCO, one of the best studied cuprates, the CDW and SDW orders observed experimentally seem to be incommensurate, and in the phase diagram such regions are small or absent altogether [298, 314]. At the same time, in LSCO, another widely studied material, doping regions can be found where the above three orders coexist [315, 316].

The authors of recent paper [317] used resonance soft X-ray scattering to study the interaction of these orders in LSCO; in particular, they investigated the dependence of the CDW order on temperature and the doping level in detail, which proved to be significantly different from what had been assumed previously. Two CDW orders were revealed: a CDW stripe order[32] and a CDW short-range order (SRO). Although superconductivity suppresses the latter, it partially transforms it into a stripe CDW order and subsequently develops into a stripe SDW order near T_c. In addition, the behavior of the CDW order turns out to be different at different doping levels:

(1) for $x < x_{CDW} \sim 0.1$, the authors did not observe any features that could be straightforwardly identified with CDW order, although neutron scattering and NMR experiments showed the existence of CDW-order stripes [288, 318, 319];

(2) for $x_{CDW} \leqslant x \leqslant x_{SDW} \sim 0.135$, a CDW order was observed with a long correlation length, which increased even at temperatures below T_c. In the preceding studies, the concentration x_{SDW} was identified as the upper boundary of the phase diagram region where a static (quasistatic) SDW order exists at low temperatures (with the onset in the vicinity of T_c [318]). The increase in CDW correlations at temperatures below T_c was explained in [317] by their mutual commensurability with the SDW order;

[32] Stripes represent quasi-one-dimensional charge ordering in real space in the form of increased charge density.

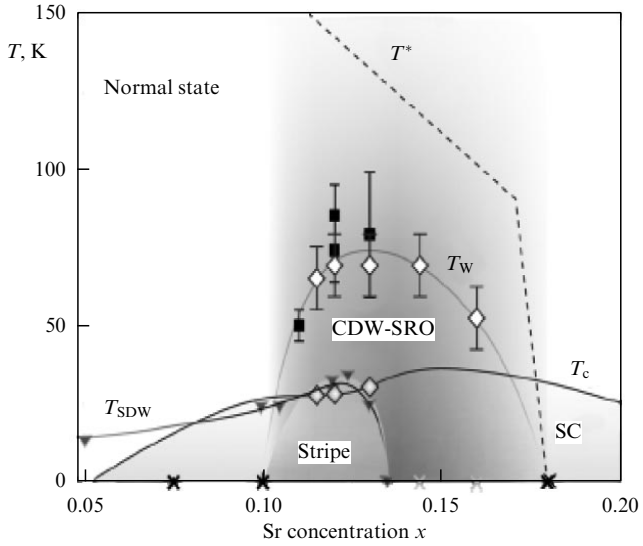

Figure 18. Schematic T–x phase diagram for LSCO. Light diamonds and dark squares, respectively, show the temperature T_W and the temperature T_{SDW} of the onset of a CDW stripe order. T_W is the temperature above which the correlation length of CDW order becomes almost independent of temperature, and in the region $T < T_W$ this length increases as the temperature decreases. The error in T_W measurements is 10 K. Squares show the temperature of the onset of CDW, measured in preliminary X-ray scattering experiments [320, 321]. T_{SDW} is the temperature of the onset of the SDW order, determined in neutron scattering measurements [318, 320], T_c and T^* are the respective temperatures of the superconducting transition [59] and pseudogap opening [263]. Dark and light crosses show doping levels at which the CDW SRO order or the CDW stripe order are not observed [317].

(3) in the region $x_{SDW} < x < x^* \sim 0.18$, where neutron scattering showed the existence of a gap in spin excitations at low temperatures and NMR studies did not reveal a quasistatic magnetic order [318, 319], clear proof was still available of the existence of well-developed short-range CDW correlations, although they were strongly suppressed at temperatures below T_c;

(4) for $x \geqslant x^*$, no clear proof of the existence of CDW or SDW orders was available. The closeness of the upper boundary of the critical doping of the CDW SRO to the critical level of the pseudogap doping $x^* = 0.18$ is puzzling [263, 320]. A similar relation was also noted in studying Bi2212 [221].

All this suggests that stripe orders and superconductivity are inhomogeneously distributed in the superconducting CuO_2 planes in LSCO. In Fig. 18, we show a schematic T–x phase diagram for LSCO, which summarizes the results in [317].

3.7 Quantum critical point in the pseudogap region

In the phase diagrams of some organic superconductors and heavy fermions, as well as iron-based superconductors, superconductivity forms a dome around a quantum critical point (QCP) where the AF phase terminates. It is believed that spin fluctuations related to the QCP cause both pairing and scattering [322]. The scattering is anomalous, which is the cause of the linear temperature dependence of the specific resistance as $T \to 0$ replacing the usual T^2 dependence for Fermi liquids [323–325]. The same features are observed in hole-doped cuprates: an anomalous linear dependence of the resistance on temperature and the formation of a superconducting dome-like region in their phase diagrams, with the exception of the critical doping level, at which the Néel

temperature T_N of the onset of a long-range AF order vanishes. Instead, these features are observed for p near the critical doping level p^*, at which the pseudogap phase terminates; the nature of that phase remains obscure, in particular, regarding whether a quantum phase transition occurs at that point [326].

The formation of superconducting pairs near a QCP and their intriguing coupling to a non-Fermi liquid (NFL) [327] remain a subject of great interest [322, 327–331]. The absence of coherence of fermions, associated with the form of the NFL eigenenergy in the normal state, hampers the pairing of electrons, whereas the pairing counteracts the incoherence due to the formation of a gap outside the low-energy states. Competition between the pairing of electrons and the NFL was analyzed analytically in [322, 329] and numerically, e.g., in [328].

Generally speaking, the question of the behavior of T^* under a T_c dome with variations in the doping level is a key missing element in the pseudogap problem [269, 332]. It was typically assumed that T^* smoothly follows its normal-state behavior and terminates ($T^* = 0$) at the QCP in the overdoped region of the phase diagram. But the phase diagram of cuprates was revised following the ARPES experiments with Bi2212 [202, 214, 333] (see above).

3.7.1 Boundary of the pseudogap phase. In the YBCO phase diagram in Fig. 13, the boundary of the pseudogap phase, shown with a dashed curve, decreases linearly as the doping level increases to $p \simeq 0.18$ and then rapidly decreases to reach the critical point $p^* = 0.195$ (marked with a diamond on the p axis). It is of interest to compare $T_v = T_\rho$ in YBCO with T^* in Bi2212, measured with different spectroscopic methods. In Fig. 13, the gray stripe shows the values of T^* depending on p for Bi2212, measured using ARPES, NMR, and tunneling [202]. We can see that the T^* line is essentially the same in both two-layer cuprates, YBCO and Bi2212. The only difference is in the values of p^* in the normal state: $p^* = 0.195 \pm 0.005$ in YBCO and $p^* = 0.22 \pm 0.1$ in Bi2212 [73].

In discussing the results, the authors of [263] also addressed several problems. The first is the question that arises after determining the boundary of the pseudogap phase $T^*(p)$: is this a phase transition or a crossover?[33] According to ARPES experiments with Bi2201 [334] and Nd-LSCO [302] at the optimum doping level, the pseudogap opens rather abruptly as the temperature decreases, suggesting a phase transition. On the other hand, the change in $\rho(T)$ upon passing through T^* occurs gradually, which is indicative of a crossover. The variation in $T_v(T)$ is also fairly gradual at high T^*, but becomes abrupt at low T^*. The pseudogap opening temperature T^* decreases monotonically with p in both cases, but $T^*_{YBCO} \simeq 1.5T^*_{LSCO}$. This is an important fact, because it can reflect the interaction strength and, possibly, the rate of formation of superconducting pairs. The smaller maximum value of T_c in LSCO (40 K) than of T_c in YBCO (93 K) may be related to the lower T^* of the former.

A linear approximation of the $T^*(p)$ dependence allows connecting the Néel temperature $T_N(0)$ at the onset of AF ordering at $p = 0$ with the boundary of the superconducting region at $T = 0$ (dashed line in Fig. 16). The slope of this line for YBCO is 1.5 times greater than for LSCO, and therefore $T_N^{YBCO} \simeq 450$ K [335] and $T_N^{LSCO} \simeq 280$ K [336] at $p = 0$. This suggests both a coupling between the pseudogap phase and the antiferromagnetism of an undoped Mott insulator and the fact that this coupling is conducive to the formation of a pseudogap and superconducting pairing.

3.7.2 Critical doping in the pseudogap region. If the linear decrease in T^* with an increasing level of doping p is a characteristic feature, then $T^*(p)$ should tend to zero at the critical doping level $p \simeq p_{c2}$, where $T_c \to 0$ at high doping (see Fig. 16). But this is not the case: the pseudogap phase terminates when $T^*(p)$ abruptly decreases to zero at the critical point p^* (see Fig. 16), much lower than than p_{c2}. At the same time, in the $La_{1.6-x}Nd_{0.4}Sr_xCuO_4$ (Nd-LSCO) cuprate, which was also investigated in [263], $T^*(p)$ extended to $p \simeq 0.23$ and only after that abruptly decreased to zero at $p^* = 0.23$ [337]. In pure LSCO, $T^*(p)$ follows the same line as in Nd-LSCO up to $p \simeq 0.16$, but then at $p = 0.17$ decreases to zero at $p \simeq 0.18$. The difference between these two materials can be seen most clearly in considering the temperature dependences of their specific normal-state resistances, measured in strong magnetic fields at different temperatures, including low ones. In Nd-LSCO, $\rho(T)$ strongly increases at $p = 0.20$ and 0.22 (see, e.g., [142]), whereas in LSCO the $\rho(T)$ dependence remains linear at temperatures extending to $T_c \to 0$ at $p = 0.18$ and 0.21 [311].

This raises the next, important and largely unexplored, question: what controls the position of p^*? Specifically, why is p^* much greater in Nd-LSCO than in LSCO, while regarding everything else the $T^*(p)$ dependence is the same? The answers to these questions will hopefully explain the fundamental nature of the pseudogap phase. A possible partial answer can be given by an interesting observation made in studying Bi2212 [73] that the end of the pseudogap phase in the normal state (at a temperature above T_c) coincides with the Lifshitz transition, which changes the topology of the Fermi surface in one of the two CuO_2 planes [338] from the level of hole doping below the critical $p_{FS} = 0.225$ to electron doping exceeding critical. The Van Hove[34] singularity then intersects the Fermi level [339]. The idea is that the pseudogap cannot form on the electron Fermi surface, and hence $p^* \leqslant p_{FS}$. This is consistent with the LSCO [340] and Nd-LSCO [302] data, and, in the opinion of the authors, encounters no contradiction in any data on cuprates. A recent study of Nd-LSCO has shown that hydrostatic pressure diminishes p^* and p_{FS} by the same amount, preserving the inequality $p^* \leqslant p_{FS}$ [341]. In numerical solutions of the Hubbard[35] model, the inequality $p^* \leqslant p_{FS}$ has also been derived [339, 342]. This nontrivial consistency between theory and experiment allows hypothesizing that the pseudogap is created by short-range AF correlations.

[33] A crossover is a radical but smooth change in the properties of a thermodynamic system under variation of the external parameters (temperature, external field strengths, etc.). A crossover, unlike a phase transition, is not attended by changes in the symmetry of the system and jumps of the thermodynamic parameters.

[34] Features of the density of quasiparticle states related to the vanishing of their group velocity at some critical points of the BZ.

[35] It is currently firmly established that electrons can form pairs even when they repel each other on the microscopic scale, but this involves nontrivial physics. A model that is frequently used as a starting point for theoretical discussions of various HTSC phenomena is the known Hubbard model, proposed in 1963 to explain metal–insulator phase transitions in transitional metals. The Hubbard model takes the hops of electrons to neighboring atoms into account in the limit of strong Coulomb repulsion. Although analytic solutions are not available even for this simplified model, there are approximate HTSC solutions, which invariably point to the d-wave superconducting state as the ground state [3].

3.7.3 Density of charge carriers in the region of a quantum critical point. As regards the question of a QCP in the phase diagram of cuprates, paper [269] is singled out, where the authors endeavored to finally clarify the relation of the pseudogap to the CDW order and the AF phase in cuprate superconductors. By measuring the Hall coefficient in YBCO in a pulsed magnetic field up to 88 T, they studied the change in carrier density in the QCP region at different temperatures, starting at 25 K. Such a high magnetic field allowed them to extend the doping range toward greater values of p and therefore to trace the normal-state properties through p^* at temperatures up to at least $T = 40$ K. They studied samples with doping levels $p = 0.16$, 0.177, 0.19, and 0.205.

It is well known that electrons in cuprate materials undergo a transition from the correlated metallic state at a high level of doping p to a Mott insulator at zero doping. But a fundamental question is how the system evolves from one state to the other. At a high level of doping, the hole Fermi surface of cuprates is a large cylinder, whose volume gives rise to the carrier density $n = 1 + p$, as has been found, for instance, by measurements of quantum oscillations [307] and calculations of the band structure. The carrier density can also be found by measuring the Hall coefficient R_H, because, in the limit $T = 0$, the Hall number n_H of a single-band metal is equal to n [269]. Indeed, in the Tl2201 cuprate with $p \approx 0.3$, the Hall coefficient measured as $T \to 0$ in magnetic fields sufficiently high for suppressing superconductivity can be expressed as $n_H = V/(eR_H) \approx 1 + p$, where e is the electron charge and V is the volume per Cu atom in the CuO_2 planes [309, 343].

On the contrary, at a low doping level, measuring the Hall coefficient R_H in LSCO [344] and YBCO [345] gives $n_H \approx p$. The equality of the carrier density and the hole concentration, $n = p$, is an experimental signature of weakly doped cuprates. The question arises: at what doping level does the transition between these two limit regimes occur? Does it occur from $n = 1 + p$ to $n = p$ at p^*, the critical doping level for the onset of the pseudogap phase, which is less than $p^* \approx 0.19$ [346]?

As a result of the measurements noted above, it was found that the critical doping level, exceeding which precludes Fermi surface reconstruction (FSR) under the action of the CDW order in normal-state YBCO at $T = 0$, is given by $p_{FSR} = 0.16 \pm 0.005$. This value agrees well with the maximum doping level at which short-range CDW modulations were discovered with the help of XRD, namely, $p_{XRD} = 0.16 \pm 0.005$ [4, 249], which corresponds to the observed CDW-order region according to the NMR data in [291]. The authors concluded that the critical doping level at which the CDW order terminates in YBCO is $p_{CDW} = 0.16 \pm 0.005$. The onset of CDW order is much lower than the pseudogap opening. Indeed, an analysis of the properties of the YBCO normal state at temperatures above T_c gives $p^* = 0.19 \pm 0.01$ [346].

Hence, the first and main conclusion in [269] is that the pseudogap and CDW order appear at two different and well separated critical levels of doping. Along with $T_{XRD} < T^*$ (and $T_{NMR} < T^*$), it now follows that $p_{CDW} < p^*$ in the normal state of YBCO. This contrasts with the simultaneous appearance of the pseudogap and short-range CDW modulations observed in Bi2212 in the superconducting state and a zero field [221].

Figure 19 shows the measured dependence of n_H on p, whence it follows that, in normal-state YBCO, the transition from a normal metal at high values of p (where $n_H = 1 + p$) to the weakly doped regime at small p (where $n_H = p$) starts abruptly at $p = p^*$ at the pseudogap opening. This is the second main conclusion in [269].

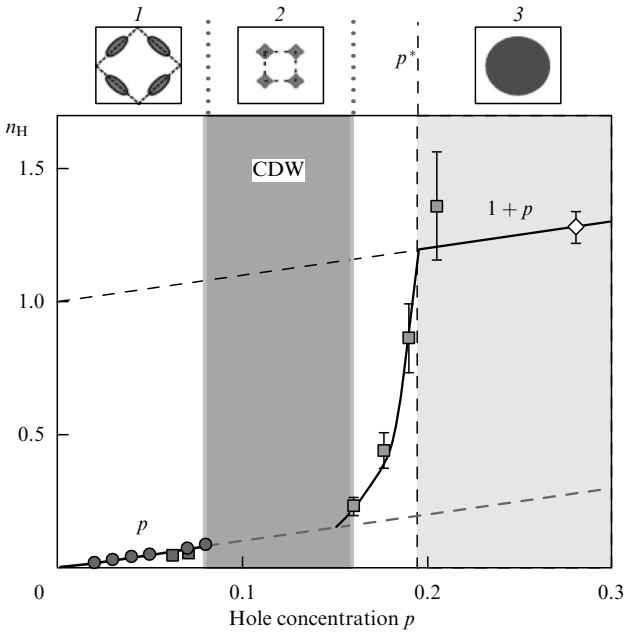

Figure 19. Dependence of the Hall number $n_H = V/(eR_H)$ on the level of doping in hole-doped cuprates, measured in the normal state at $T = 50$ K for LSCO [344] (dots) and YBCO at $p < 0.08$ [53] (two squares below). Other four squares correspond to the values of R_H measured in four YBCO samples at $p > 0.15$ in a magnetic field of 80 T. White diamond is obtained from the $R_H(T)$ dependence in the limit $T = 0$ for strongly overdoped Tl2201 [12]. Solid curve is drawn by eye. Lower line corresponds to $n_H = p$ and upper line, to $n_H = 1 + p$. The region in which the CDW order results in reconstruction of the Fermi surface in YBCO is shown as a dark gray stripe; there, $R_H < 0$ as $T \to 0$. In YBCO, carrier density is given by $n = n_H/(\rho_a/\rho_b)$, where ρ_a/ρ_b is the ratio of specific resistances in the ab plane [345]. For the sample studied, $\rho_a/\rho_b \approx 1.5$, and hence $n \approx p$ at $p = 0.16$. As can be seen, with a decrease in p, the carrier density rapidly decreases from $1 + p$ to p at $p^* = 0.19 \pm 0.01$, the critical level of doping for the emergence of the pseudogap in YBCO [346] (vertical dashed line). Upper part of the figure shows sketches of normal-state Fermi surfaces in three of the four doping regions. *1* — small nodal hole pockets at $p < 0.08$, where magnetic order is dominant at low temperatures; *2* — small electron pockets in the range $p = 0.08$–0.16, where CDW order prevails at low temperatures; *3* — one large hole Fermi surface at $p > p^*$, where the nonsuperconducting ground state is a correlated metal (light gray) [269].

The Fermi surface topology in the pseudogap phase at $T = 0$ in the absence of superconductivity and CDW order is unknown. But because the pseudogap opens at the reciprocal space points $\mathbf{k} = (0, \pm\pi)$ and $(\pm\pi, 0)$, electron states on the Fermi level must be located near $\mathbf{k} = (\pm\pi/2, \pm\pi/2)$, where the four zeros of the d-wave superconducting gap are localized. This is what was observed as nodal Fermi arcs in [221, 347] in Bi2212 at p below $p \approx 0.2$. Because the relation $n_H = p$ extends to the lowest levels of doping (see Fig. 19), two scenarios must be considered for these nodal states: one is related to the AF order and the other to the Mott insulator.

In the first scenario, the AF order, dominating in YBCO at a doping level below $p = 0.05$, reconstructs the large Fermi surface into four small hole nodal pockets, with p carriers in their total volume, whence $n_H = p$ (see Fig. 19). In electron-doped cuprates, the AF QCP is assumed to be the cause of the

sharp drop in the carrier density discovered in measurements of the Hall coefficient in the normal state of the sample [348].

In the second scenario, the pseudogap phase is a consequence of strong correlations associated with Mott physics. Numerical solutions of the Hubbard model have shown the existence of nodal Fermi arcs at a low level of doping and intermediate temperatures [349]. It was claimed that, as $T \to 0$, the Fermi surface must consist of four hole pockets [48, 350], whose total volume contains p carriers. These pockets/arcs develop even if translation symmetry is not broken. The question is whether the pseudogap based on Mott physics can appear at doping as high as $p = 0.19$.

Thus, according to the authors of [269], the pseudogap and CDW order are separate phenomena in YBCO, while the pseudogap and the AF Mott insulator are related. In view of this claim, we must now discuss recent paper [326] devoted to the behavior of the electron heat capacity in cuprates in the vicinity of a QCP.

3.7.4 Heat capacity in the vicinity of a QCP. The electron heat capacity is a fundamental property that provides thermodynamic evidence of the presence of a gap in the normal state of HTSCs. But interpreting the results of its measurements is complicated, because, at high temperatures that allow the normal-state gap to be seen, the phonon contribution to the specific heat capacity of a typical cuprate is 100 times greater than the contribution of charge carriers. Still, a sensitive differential technique has allowed exactly measuring the electron heat capacity contribution in several cuprates at temperatures corresponding to the pseudogap region [272].

The thermodynamic signature of a QCP is the divergence of the electron mass. For example, it is expected that, for the AF QCP in the two-dimensional case, the mass scales as $m^* \propto \log(1/|x - x^*|)$, and the heat capacity C, as $C/T \propto \log(1/|x - x^*|)$ when the system evolves toward the QCP x^* under variation of some tuning parameter x, such as pressure or concentration [323]. Just that was observed for the iron-based superconductor $BaFe_2(As_{1-x}P_x)$ [337] in its AF QCP as the concentration p was varied both for the carrier mass m^*, measured by quantum oscillations, and for the electron heat capacity, evaluated from the jump in T_c [324, 351]. At $x = x^*$, a logarithmic divergence $C/T \propto \log(1/T)$ should be expected, as was observed in the heavy-fermion metal $CeCu_{6-x}Au_x$ at its AF QCP tuned by varying the concentration of Au [323, 352]. Such a logarithmic divergence of C/T as $T \to 0$ is a true signature of the energy scale that turns to zero at x^*.

In studying quantum oscillations in YBCO [220], m^* was observed to increase as the doping level approached the critical value $p^* \approx 0.19$ in the pseudogap region in the phase diagram; it was hypothesized that p^* can be a QCP. The measured small value of m^* at $p = 0.10$–0.12 is consistent with the data on specific heat capacity [353], and its increase with increasing p corresponds to the abrupt increase in the heat capacity jump $\Delta C/T_c$ at T_c [354], with a maximum reached at p^*. But the conclusion on the presence of quantum criticality at that point can be arrived at only as a result of direct measurements of the specific heat capacity in normal-state YBCO as $T \to 0$ through p^*, which was indeed the subject of [326].

In [326], the $C(T)$ dependences were measured in kindred materials $La_{1.8-x}Eu_{0.2}Sr_xCuO_4$ (Eu-LSCO) and $La_{1.6-x}Nd_{0.4}Sr_xCuO_4$ (Nd-LSCO). Because of the low values of their T_c (< 20 K), superconductivity could be suppressed in a magnetic field of about 15 T. These systems have the same crystal structures and phase diagrams with very similar boundaries of the pseudogap and superconducting phases, $T^*(p)$ and $T_c(p)$. In Nd-LSCO, measurements of the specific resistance and the Hall effect yielded $p^* = 0.23 \pm 0.01$ [327]. At $p = 0.24$, the resistance $\rho(T)$ is linear as $T \to 0$, which is a signature of quantum criticality in electric transport. A very similar behavior was also observed in Eu-LSCO.

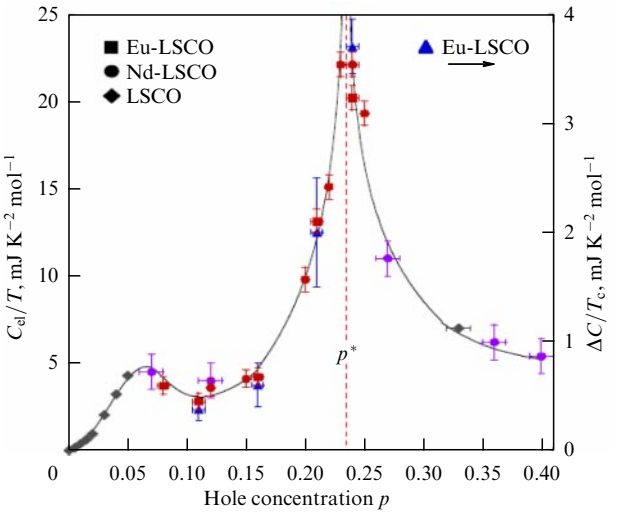

Figure 20. (Color online.) Dependences of the electron heat capacity C_{el}/T on the doping level p in the normal state for five Eu-LSCO crystals (squares) and seven Nd-LSCO crystals (red dots) at $T = 0.5$ K [326]. Also shown are values of γ for polycrystalline Nd-LSCO samples (magenta dots, $p = 0.07$, 0.12, 0.27, 0.36, and 0.40) and nonsuperconducting LSCO samples (diamonds for $p < 0.06$ [355] and $p = 0.33$ [312]), obtained by extrapolating $C/T = \gamma + \beta T^2$ to $T = 0$ from data at $T < 10$ K. Magnitudes of heat capacity jumps $\Delta C/T_c$ at T_c (right-hand axis) measured in Eu-LSCO (blue triangles) are shown for comparison. We can see that $\Delta C/T_c$ and C_{el}/T scale well. Dashed line shows the pseudogap critical point p^* in Nd-LSCO. Solid curves are drawn by eye.

Because the magnetic and nuclear contributions are negligibly small at low temperatures, the measured heat capacity is the sum of the electron and phonon contributions: $C = C_{el} + C_{ph} = \gamma T + \beta T^3$. The linear term γ is an electron, and the second term is a phonon one.

In Fig. 20, we show the dependences of the electron heat capacity C_{el}/T on the doping level p for five Eu-LSCO crystals and seven Nd-LSCO crystals. Also shown are the extrapolated values of γ for five polycrystalline Nd-LSCO samples ($p = 0.07$, 0.12, 0.27, 0.36, and 0.40) and an LSCO crystal with $p = 0.33$ [312]. The huge peak in the C_{el}/T dependence on p is similar to the observed peak in the iron-based superconductor $BaFe_2(As_{1-x}P_x)$ [337] at its AF QCP, where $C/T \propto \log(1/|x - x^*|)$ [351]. Thus, the dependences of C_{el}/T on p and T provide convincing proof of a QCP present in Eu-LSCO and Nd-LSCO.

In the opinion of the authors, the marked similarity of the Nd-LSCO and Eu-LSCO data with the data of other cuprates indicates that the characteristic signatures of a QCP described here are likely to be a general property of hole-doped cuprates. The authors compared the measured values of C_{el}/T in Eu-LSCO and Nd-LSCO at 10 K with those of γ in LSCO obtained by fitting the expression $C/T = \gamma + \beta T^2$ at temperatures between 4 K and 8 K, where C was measured in LSCO powders that were nonsuperconducting due to the addition of a large amount of Zn impurities [356]. A peak was

clearly observed in the dependence of γ on p, as in the case of Nd-LSCO, although at a somewhat lower level of doping, which agreed with the lower p^* in that material. Thus, the pseudogap phase of cuprates terminates at the QCP, and the fluctuations associated with it apparently participate in d-wave pairing and anomalous scattering of charge carriers. This was the main conclusion in [326].

4. High-temperature electron-doped superconducting materials

Although HTSCs are mainly hole-doped compounds, a small number of materials doped with electrons exists (to avoid confusion, in this section we call them p-type and n-type cuprates, respectively). Most of these materials have the chemical formula $R_{2-x}M_x\mathrm{CuO_4}$, where R is the rare-earth element Pr, Nd, Sm, or Eu and M is Ce or Th [105, 106]. n-type cuprates are understood less than their p-type analogues, but experiments with them are of great value in condensed matter physics, because they allow investigating the electron–hole symmetry in the HTSC phase diagram (see review [37] and the references therein). Currently, only an approximate symmetry with respect to the zero doping level exists between the p and n types, because the AF phase is much more stable in n-type materials. They exhibit superconductivity in a doping range that is one fifth as wide. In addition, the two ground states, antiferromagnetism and superconductivity, are much closer to each other and can even coincide, in contrast to those in p-type materials. In p-type cuprates, a small number ($\sim 2\%$) of carriers destroys the AF ordering and induces superconductivity, whereas, in n-type cuprates, antiferromagnetism is preserved as the doping level varies up to the optimum value ($\sim 15\%$). There are some other differences, including a T^2 dependence of the specific resistance near the optimum doping level, and lower values of T_c and of the critical magnetic field.

Despite the incomparable sizes of the AF and superconducting phases and the existence of a pseudogap in p-type systems, the cause of superconductivity and the nature of the strange metallic normal state are probably the same for both systems. This is so simply because both properties are determined by the interactions of electrons in the $\mathrm{CuO_2}$ planes, which is a universal property of all cuprates due to their anisotropic two-dimensional structure, which greatly weakens the interplane coupling.

4.1 Superconducting gap in electron-doped cuprates

It has been firmly established that the superconducting gap in p-type cuprates has the d-wave symmetry, reflecting the fact that electrons are strongly correlated and tend to avoid double occupation [357]. As regards n-type cuprates, the results of numerous previous studies also confirm the existence of the d-wave symmetry of the superconducting gap in them. In particular, the results of optical experiments [358] and ARPES experiments [359] have revealed the dependence of the superconducting gap on the momentum with a maximum near 'hot spots' (HSs) where the Fermi surface intersects the boundary of the AF BZ. In Fig. 21, we show the position of HSs on the Fermi surface in the n-type cuprate $\mathrm{Nd_{2-x}Ce_xCuO_4}$ (NCCO).

The maximum of the superconducting gap in NCCO, unlike that in p-type cuprates, is located closer to the nodes than to the BZ boundary. Away from the diagonal nodal directions, the gap rapidly opens and rapidly reaches the maximum value $4.4k_BT_c$ at the HSs at the intersection of the Fermi surface and the AF BZ [358]. The increase in the gap in the immediate vicinity of HSs underlines the important role that AF fluctuations play in superconductivity of n-type cuprates.

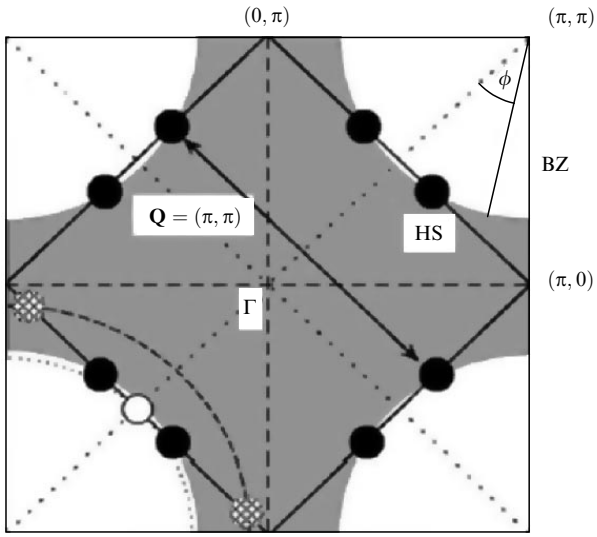

Figure 21. Fermi surface of electron-doped $\mathrm{Nd_{2-x}Ce_xCuO_4}$ (NCCO) [360]. Dark region shows the populated electron states. The AF Brillouin zone with half-filling is shown as a square rotated through 45°. AF fluctuations enhance interactions between electrons around hot spots (black dots). Parts of the Fermi surface are connected by the vector $\mathbf{Q} = (\pi, \pi)$ [361]. Positions of the hot spots strongly depend on the doping level. As electron doping increases further, the Fermi surface shrinks to the disappearance of the overlap with the AF BZ (dashed curve and circle in the lower left quadrant). p-type cuprates have a large Fermi surface with the hot spots shifted to the vicinity of $(\pi, 0)$ and equivalent points (dashed line and shaded dots in the lower left quadrant) [116, 362].

Thus, a conjecture has been put forward that the AF spin fluctuations make a large contribution to superconductivity, although the intrinsic dependence of the superconducting gap on momentum remains elusive, because its coexistence with the AF order does affect the superconducting gap [363].

4.2 Pseudogap in electron-doped cuprates

In the original studies of n-type cuprates with the help of optical measurements [364, 365] and STM [366], a 'pseudogap' was revealed, described as a suppression of the spectral weight at temperatures below a characteristic value T^* [367]. In the region of AF correlations, the one-particle gap $\Delta_{AF} \approx 9k_BT^*$ was observed, which occurred at the energy and momentum coordinated with the (π, π) direction on the BZ boundary [368, 369]. ARPES experiments showed that the pseudogap, as in p-type cuprates, opens around the HSs [359, 360, 369, 370].

But while the energy scales associated with the pseudogap and superconducting states can be very similar in p-type compounds with a low doping level, it was shown in [37] that these two scales differ by more than an order of magnitude in $\mathrm{Nd_{1.85}Ce_{0.15}CuO_4}$. In this case, the formation of a pseudogap in n-type cuprates may be related to a strong temperature dependence of the evolution of AF correlations.

However, the phase diagram of n-type cuprates was not finally clarified and remains vague. Debates about the phase

diagram can be explained by controversial experimental results due to the annealing of sample, which is necessary for the appearance of superconductivity in them. Annealing changes the oxygen content and strongly affects the physical properties of n-type materials. This dependence of the physical properties on the annealing conditions raises a fundamental question on the validity and justifiability of the phase diagram constructed as a function of Ce content (see, e.g., Fig. 2a).

The effects of annealing in n-type cuprates have not yet been satisfactorily understood at a microscopic level. In [109], the 'protect annealing' method [36] [371] was used for single crystals of the widely studied n-type cuprate $Pr_{1.3-x}La_{0.7}Ce_xCuO_4$ (PLCCO) with $x = 0.10$. Although PLCCO samples with such a low concentration of Ce had not been superconducting previously, their T_c values reached 27.0 K after the protect annealing. In the ARPES experiments in [109], the authors found a sharp quasiparticle peak on the entire Fermi surface, without indications of either AF fluctuations or the AF pseudogap, which had been observed in previous studies for all the other electron HTSCs. This was evidence of an abrupt reduction in the AF correlation length and/or magnetic moments. In the annealed sample, no scattering of quasiparticles on AF correlations at an HS near E_F was observed, but, similarly to p-type cuprates, enhanced scattering was observed in the antinodal region compared with the nodal region. This suggests the existence of common scattering mechanisms in p- and n-type cuprates. The results in [109] essentially challenge the old picture of the electronic structure in n-type systems.

In subsequent study [40], ARPES experiments were used to investigate the methods of annealing for the same PLCCO cuprate. The results showed that the optimum annealing condition to produce high-T_c samples depends not only on the Ce content x but also on the number of electrons n. The latter was estimated from the experimentally obtained volume of the Fermi surface. The authors proposed a new PLCCO phase diagram as a function of n, which is shown in Fig. 22. We can see from the figure that the T_c data have a dome-like shape (SC). The transition from a nonsuperconducting state to the superconducting one occurs between $n = 0.045$ and 0.08. After that, T_c gradually increases to 25 K at $n = 0.15$ and then decreases as n increases. In the previous phase diagrams of n-type cuprates, depending on the concentration x, T_c reached a maximum at $x \sim 0.10$ [372, 373]. Of interest is the fact that the superconducting dome extends from $n = 0.05$ to 0.25, as is the case with a similar p-type LSCO [374]. This result seems to indicate the possible absence of a discrepancy between phase diagrams of p- and n-type cuprates.

Based on their ARPES data, the authors of [40] concluded that, at $n > 0.045$, the short-range AF order disappears as the doping level increases. As superconductivity emerges at small values of n, the AF correlation length undergoes a sharp decrease, followed by a gradual transition to a moderate decrease at the optimum and higher doping levels. This phase of the short-range AF order with the mean correlation length in the range of small n can explain why some measurements showed an overlap of the AF and superconducting phases [372, 375, 376].

[36] Protecting annealing is done a milder way at a decreased oxygen pressure and for a longer time, which leads to fewer differences between the bulk and surface properties.

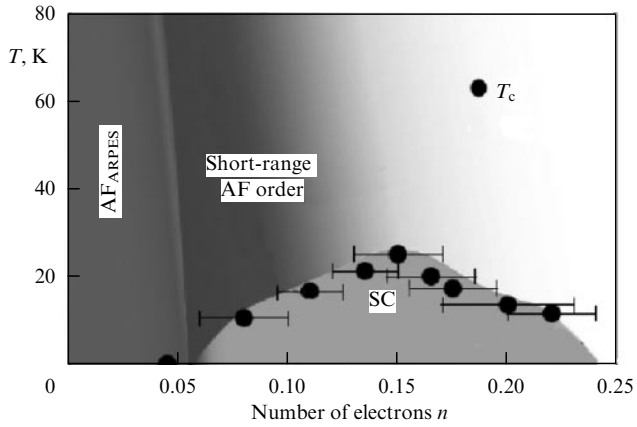

Figure 22. New phase diagram of the n-type cuprate $Pr_{1-x}LaCe_xCuO_{4-\delta}$ based on the number of electrons n. Values of T_c are shown by black dots. Values for the region of long-range AF order (AF_{ARPES}) and short-range AF order and/or AF-order fluctuations (short-range AF) are shown in accordance with ARPES data [40].

Answering the question of whether the pseudogap exists in n-type cuprates similarly to how it does in p-type cuprates is difficult because of the high ambiguity in its determination in p-type materials. Even in these compounds, the exact edge of the pseudogaps depends on the material of the system and the experimental method of its observation [37]. The complications related to determining the pseudogap edge are due in part to confusion in the literature between the notions of a "pseudogap in the density of states," which pertains to cuprates with a low level of doping and at fairly high temperatures, and of a "pseudogap in the spectrum of excitations," which is actually related to the increase in the density of states as a result of mass renormalization due to the bosonic resonance mode [270].

We note first of all that many pseudogap phenomena in n-type cuprates apparently must be related to antiferromagnetism and the relative stability of the AF phase in these materials. Optical conductance and ARPES studies of underdoped single crystals with $x = 0$–0.125 have shown the opening of a high-energy gap structure at temperatures much higher than the Néel temperature [367, 369]. This is the difference from p-type cuprates, in which the gap feature is not observed in the optical conductance in the *ab* plane and manifests itself only in the frequency-dependent scattering rate [32]. The gap in n-type cuprates gradually reduces with an increase in the doping level and disappears at concentrations $x = 0.15$–0.17 [367, 368], where superconductivity emerges. In [367], this gap was identified with an increase in AF correlations for the following reasons:

(a) in the range of a low doping level, a long-range AF order develops at the temperature T_N approximately equal to a half of T^*;

(b) the range of the AF exchange interaction coincides with the pseudogap width;

(c) the gap anisotropy discovered in ARPES experiments coincides with the one expected for two-dimensional AF correlations with the wave vector (π, π) [377].

The pseudogap in n-type cuprates can be similar to the one in p-type cuprates at high energies, although a number of differences exist: (1) the large pseudogap in p-type systems is maximal near $(\pi, 0)$, unlike the pseudogap in n-type cuprates, which is mainly concentrated around $(\pi/2, \pi/2)$; (2) as we have noted, the pseudogap feature itself is indistinguishable

in the optical conductance of the *ab* plane in p-type cuprates, possibly because it is weaker than in n-type compounds; (3) the ground state in an underdoped n-type system, where the formation of the pseudogap is well expressed, is antiferromagnetic, whereas in p-type cuprates, the superconducting phase is already present in underdoped samples.

Thus, although there are strong indications of the presence of a pseudogap in n-type compounds, it is unclear whether it is of the same nature as in p-type materials. A major part of pseudogap phenomena in n-type compounds seem to be related to AF correlations. Currently, there is no evidence that these systems have a number of phenomena that in p-type materials are related to pseudogap physics, such as the pseudogap in spin excitations [113], orbital currents [124], stripes [378], and violation of time-reversal symmetry [379]. These phenomena may be concealed by antiferromagnetism, or p- and n-type compounds may differ from each other as regards these effects [37].

We finally note experiments studying the dynamics of AF correlations in $La_{2-x}Ce_xCuO_{4\pm\delta}$ samples with low and optimal doping levels via spectroscopy with high temporal resolution [380]. The relaxation rate of AF correlations was measured in samples in the superconducting and normal states. Directly measured were the rate at which the reflectivity $\Delta R/R$ returned to equilibrium after optical laser pumping at a frequency of 1.55 eV (800 nm). In a similar previous study of the reflectivity of the n-type cuprate $Nd_{2-x}Ce_xCuO_{4+\delta}$ at the same frequency, a negative ratio $\Delta R/R$ was detected at $T > T_c$, as in p-type cuprates, and this feature was ascribed to either the pseudogap or AF correlations in the *ab* plane [381]. The authors of [380], who observed such a feature, believe that their data confirm the latter explanation.

To conclude this section, we discuss more recent results of phase diagram studies for n-type cuprates based on measurements of the Nernst effect. In [43], the Nernst effect was studied in $La_{2-x}Ce_xCuO_4$ (LCCO) superconducting films depending on the temperature and the magnetic field up to 14 T. For an optimally doped sample with $x = 0.11$, the temperature of the onset of superconducting fluctuations was found to be $T_{onset} = 39$ K, which turned out to be rather high compared with $T_c = 26$ K. As the doping level increased, T_{onset} decreased and tended to zero along with T_c at the end of the superconducting dome.

In Fig. 23, we present an LCCO phase diagram showing superconducting fluctuations in the Nernst-effect region. We can see that T_{onset} exactly follows the superconducting dome. At each level of doping, the diagram demonstrates the continuity of the region before which the Nernst signal due to superconducting fluctuations can be observed. The authors conclude that n-type cuprates must have a much simpler phase diagram than p-type cuprates.

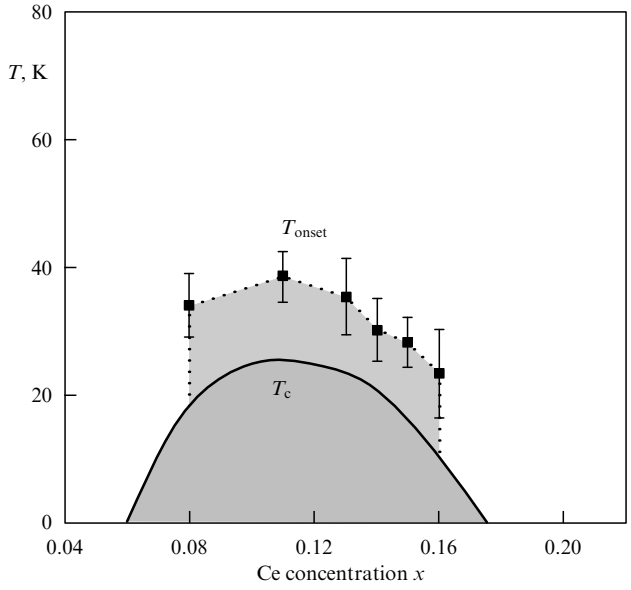

Figure 23. Phase diagram of $La_{2-x}Ce_xCuO_{4\pm\delta}$ showing superconducting fluctuations in the region of the Nernst effect at temperatures between T_{onset} and T_c for six samples with different doping levels [43].

5. Iron-based high-temperature superconducting systems

In concluding the discussion of the pseudogap problem in HTSC, it may be worth mentioning iron-based superconductors [37], which were discovered in 2006. Superconductivity in ferrous compounds, unlike that in cuprates, is not realized along the CuO_2 planes. This discovery soon resulted in the creation of a new class of HTSCs, so-called iron pnictides (FePn, where Pn is As or P) and iron chalcogenides (FeCh, where Ch is S, Se, or Te). More than 2000 papers on the subject appeared in the first three years [383]. Various Fe-containing superconducting systems with T_c up to 56 K demonstrate a complicated but often comparable behavior. Their Fermi surface can rapidly change with the doping level, and, as a result, the properties of normal and superconducting states are significantly different from the properties of normal superconductors. Most probably, superconductivity and magnetism or magnetic fluctuations are closely related in these systems, and even coexist in some of them. An opinion has been expressed that this coexistence can be responsible for the formation of superconducting pairs [383].

The question about the pseudogap in Fe-containing superconductors, just as that of the nature of superconductivity in them, remains open. There are several studies reporting the existence of a pseudogap, such as the ARPES experiments in [384–386], although the pseudogap is barely distinguishable in ARPES studies of Fe-based superconductors [387]. Optical studies of the $BaFe_2As_2$ (Ba122) system have even shown the existence of two pseudogaps, at lower and higher frequencies [388]. The formation of a high-energy pseudogap was attended by the transfer of the spectral weight from low to high frequencies. The IR characteristics of the low-energy pseudogap in Ba122 turned out to be close to those in the YBCO compound. In a recent study of the optical conductance of $Ca_{10}(Pt_4As_8)(Fe_2As_2)_5$ single crystals, some traces of the pseudogap were also detected [389]. However, these observations are not supported by the results of ARPES studies (see, e.g., [390–394]) exploring the effect of one-axis pressure in the *ab* plane on the specific resistance of several Fe-containing single crystals [395], nor by STM experiments [396, 397]. Obviously, more sensitive experiments are needed to support the existing views on the pseudogap in Fe-containing superconductors.

[37] Although iron had been believed to be detrimental to superconductivity in view of its strong local magnetic moment, a number of superconducting compounds containing Fe, which is nonmagnetic there, have been known for a long time (see, e.g., [382]). In fact, iron itself is a superconductor under pressure, with $T_c \sim 1.8$ K [382].

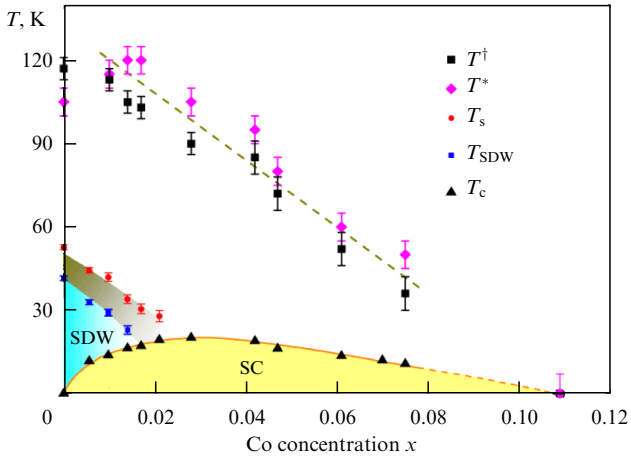

Figure 24. (Color online.) Phase diagram of $NaFe_{1-x}Co_xAs$ [398]. Temperatures T_c, T_{SDW}, and the structure transition temperature T_s are determined from the results of measurements of specific resistance, susceptibility, and heat capacity. Heat capacity of the original compound demonstrated a structural transition and an SDW transition without an anomaly at T_c, which is indicative of 'thread-like' superconductivity.

For clarity, in Fig. 24 we show the phase diagram of the $NaFe_{1-x}Co_xAs$ system and the dependence of temperatures $T^\dagger$ and T^* on the level of doping. The two characteristic temperatures agree well with each other, although they were derived by different methods. Both decrease as the Co concentration increases and tend to zero along with T_c. The temperature T^* is that at which the specific resistance and the cotangent of the Hall angle ($\cot\theta_H$) deviate from a power-law dependence on temperature. The temperature $T^\dagger$ was determined by deviations from the high-temperature power-law behavior of the specific resistance. In the phase diagram, T^* denotes a temperature similar to the pseudogap crossover temperature in cuprates. Overall, the phase diagram in Fig. 24 is very similar to the one of HTSC cuprates with a pseudogap. According to the authors, in discussing the results, they took special care to ensure that their data did not point to some particular gap-like behavior observed in cuprates, although they underline the similarity between T^* and the crossover temperature in cuprates.

More details on layered iron-based HTSCs can be found in review [399].

6. Conclusions

Recently, new experimental evidence has appeared suggesting the violation of some crystal symmetry in the pseudogap phase at temperatures below T^* [121, 123]. Violation of the time reversal symmetry in observations of magnetic moments (a new magnetic order) inside the elementary cell was also reported. Several other indications give grounds to assume that this phase must be a nematic phase that destroys the four-fold rotation symmetry of the copper–oxygen lattice [8, 400, 401]. In particular, new data on CDW and SDW orders in the superconducting and pseudogap regions of the phase diagram of cuprates have appeared [402–404]. Some of them are possibly one-directional and therefore have no four-fold rotation symmetry. Experimental data are also available indicating the fluctuational or short-range character of the CDW order in the pseudogap phase [403, 405, 406]. But we must note that, as soon as the CDW order sets in, violating the four-fold symmetry [407], no d-wave symmetry can be expected in the superconducting phase observed experimentally in a tetragonal crystal [408] such as Bi2212. Thus, the mechanism of the formation of these density waves and their relation to the superconducting and pseudogap phases are still not fully clarified and are of great interest.

We have noted that, in ARPES experiments, the pseudogap was observed near the boundary or in the antinodal region of two-dimensional BZ of cuprates. In addition, four disjoint segments (arcs) of the Fermi surface were found in the nodal region or at $|k_x| = |k_y| = \pi/2$. The length of these segments decreased to zero at the temperature extrapolated to zero [135, 245]. On the other hand, results are available indicating that they are insensitive to the temperature [160, 405], in which case this must be part of a small pocket [409]. The existence of a finite part of the Fermi surface agrees with measurements of the Knight shift [115], which have shown a finite density of states after the suppression of superconductivity. The full Fermi surface was reconstructed after the vanishing of the pseudogap, which occurred either at a temperature above T^* or when the doping level exceeded approximately 19%. At temperatures below T_c, the gap in the antinodal region merged with the superconducting gap and continued to exist simultaneously with it [59, 145].

Despite numerous theoretical proposals regarding the pseudogap state of cuprates, it is still difficult to understand the dependence of Fermi arcs on temperature and the level of doping, the existence of two gaps, and their manifest relation to the CDW order, as well as whether any of these is related to Mott physics or strong correlations [408]. Nevertheless, there are progressively more and more indications that the CDW order is not an order of the usual form, but can be an auxiliary order of a PDW.

It was assumed in some studies that the PDW state can be responsible for a number of observed exotic phenomena in the superconducting and pseudogap phases (see, e.g., [410–412]). In many studies, phenomenological models and weak-coupling approaches were used [5, 6, 413], but some numerical calculations based on microscopic models, such as the Hubbard model and its low-energy modification in the limit of strong Coulomb repulsion, the t–J model, have thoroughly substantiated the existence of such a state or states. Actually, there are many different types of PDW states, which can be unidirectional [414] or bidirectional, like a checkerboard [6, 415]. For a unidirectional PDW state interweaved with CDW and SDW orders, a stripe order forms. Ordering the stripes is attended by the Fermi surface reconstruction.

Currently, it is commonly accepted [281] that the phase diagram of cuprates has presented three new physical phenomena: two new normal states (a strange metal and a pseudogap with Fermi arcs) and a high-temperature d-wave superconducting phase. The pseudogap arises below the phase transition at $T^*(p)$ as a function of the level of doping, terminating at the QCP $p = p^*$. The strange-metal region is located on the other side of the $T^*(p)$ region and terminates upon a gradual transition to the Fermi-liquid phase. The Fermi-liquid normal phase also supports the existence of a QCP. Superconductivity arises in the region of p around the QCP.

Explaining the complicated structure of the phase diagram of cuprates can eventually pave the way toward the ultimate understanding of the physics of high-temperature superconductivity and therefore the way toward the creation

of materials with even higher superconducting transition temperatures.

References

1. Bednorz J G, Müller K A *Z. Phys. B* **64** 189 (1986)
2. Wu M K et al. *Phys. Rev. Lett.* **58** 908 (1987)
3. Keimer B et al. *Nature* **518** 179 (2015)
4. Hücker M et al. *Phys. Rev. B* **90** 054514 (2014)
5. Efetov K B, Meier H, Pépin C *Nat. Phys.* **9** 442 (2013)
6. Wang Y, Agterberg D F, Chubukov A *Phys. Rev. Lett.* **114** 197001 (2015)
7. Fradkin E, Kivelson S A, Tranquada J M *Rev. Mod. Phys.* **87** 457 (2015)
8. Comin R et al. *Science* **347** 1335 (2015)
9. Balédent V et al. *Phys. Rev. B* **83** 104504 (2011)
10. Varma C M *J. Phys. Condens. Matter* **26** 505701 (2014)
11. Cyr-Choinière O et al. *Phys. Rev. B* **92** 224502 (2015)
12. Saini N L et al. *Europhys. Lett.* **63** 125 (2003)
13. Ovchinnikov S G, Shneyder E I, Korshunov M M *J. Phys. Condens. Matter* **23** 045701 (2011)
14. Wulin D et al. *Phys. Rev. B* **80** 134504 (2009)
15. Uykur E et al. *Phys. Rev. Lett.* **112** 127003 (2014)
16. Ye M, Chubukov A V *Phys. Rev. B* **100** 035135 (2019)
17. Varma C M *Phys. Rev. B* **55** 14554 (1997)
18. Kivelson S A, Fradkin E, Emery V J *Nature* **393** 550 (1998)
19. Fernandes R M et al. *Phys. Rev. B* **85** 024534 (2012)
20. Schmalian J, Pines D, Stojković B *Phys. Rev. B* **60** 667 (1999)
21. Kuchinskii É Z, Sadovskii M V *J. Exp. Theor. Phys.* **88** 968 (1999); *Zh. Eksp. Teor. Fiz.* **115** 1765 (1999)
22. Abanov Ar, Chubukov A V, Schmalian J *Adv. Phys.* **52** 119 (2003)
23. Sedrakyan T A, Chubukov A V *Phys. Rev. B* **81** 174536 (2010)
24. Norman M R et al. *Phys. Rev. B* **57** R11093 (1998)
25. Franz M, Millis A J *Phys. Rev. B* **58** 14572 (1998)
26. Berg E, Altman E *Phys. Rev. Lett.* **99** 247001 (2007)
27. Wu Y-M et al. *Phys. Rev. B* **99** 144512 (2019)
28. Robinson N J et al. *Rep. Prog. Phys.* **82** 126501 (2019)
29. Proust C, Taillefer L *Annu. Rev. Condens. Matter Phys.* **10** 409 (2019)
30. Timusk T, Tanner D B, in *Physical Properties of High Temperature Superconductors I* (Ed. D M Ginsberg) (Singapore: World Scientific, 1989) p. 339
31. Timusk T, Statt B *Rep. Prog. Phys.* **62** 61 (1999)
32. Puchkov A V, Basov D N, Timusk T *J. Phys. Condens. Matter* **8** 10049 (1996)
33. Basov D N et al. *Rev. Mod. Phys.* **83** 471 (2011)
34. Shibauchi T, Carrington A, Matsuda Y, arXiv:1304.6387
35. Michon B et al., arXiv:1804.08502
36. Hüfner S et al. *Rep. Prog. Phys.* **71** 062501 (2008)
37. Armitage N P, Fournier P, Greene R L *Rev. Mod. Phys.* **82** 2421 (2010)
38. Greene R L et al. *Annu. Rev. Condens. Matter Phys.* **11** 213 (2020)
39. Dai P *Rev. Mod. Phys.* **87** 855 (2015)
40. Song D et al. *Phys. Rev. Lett.* **118** 137001 (2017)
41. Adachi T et al. *J. Phys. Soc. Jpn.* **85** 114716 (2016)
42. Horio M et al. *Phys. Rev. B* **98** 020505 (2018)
43. Mandal P R et al. *Phys. Rev. B* **97** 014522 (2018)
44. Horio M et al. *Phys. Rev. B* **100** 054517 (2019)
45. Lee P A, Nagaosa N, Wen X-G *Rev. Mod. Phys.* **78** 17 (2006)
46. Kordyuk A A *Low Temp. Phys.* **41** 319 (2015); *Fiz. Niz. Temp.* **41** 417 (2015)
47. Norman M R, Pines D, Kallin C *Adv. Phys.* **54** 715 (2005)
48. Rice T M, Yang K-Y, Zhang F C *Rep. Prog. Phys.* **75** 016502 (2012)
49. Vojta M *Adv. Phys.* **58** 699 (2009)
50. Eder R *Phys. Rev. B* **100** 085133 (2019)
51. Varma C M *Phys. Rev. B* **99** 224516 (2019)
52. Kuchinskii E Z, Nekrasov I A, Sadovskii M V *Phys. Usp.* **55** 325 (2012); *Usp. Fiz. Nauk* **182** 345 (2012)
53. Hussey N E, Takenaka K, Takagi H *Phil. Mag.* **84** 2847 (2004)
54. Sebastian S E, Harrison N H, Lonzarich G G *Rep. Prog. Phys.* **75** 102501 (2012)
55. Vedeneev S I et al. *JETP Lett.* **47** 194 (1988); *Pis'ma Zh. Eksp. Teor. Fiz.* **47** 159 (1988)
56. Xu Z A et al. *Nature* **406** 486 (2000)
57. Emery V J, Kivelson S A, Zachar O *Phys. Rev. B* **56** 6120 (1997)
58. Fischer Ø et al. *Rev. Mod. Phys* **79** 353 (2007)
59. Hashimoto M et al. *Nat. Phys.* **10** 483 (2014)
60. Vedeneev S I et al. *JETP Lett.* **47** 367 (1988); *Pis'ma Zh. Eksp. Teor. Fiz.* **47** 306 (1988)
61. Bulaevskii L N et al. *Supercond. Sci. Technol.* **1** 205 (1988)
62. Miyakawa N et al. *J. Phys. Soc. Jpn.* **59** 2473 (1990)
63. Wolf E L et al. *J. Supercond.* **7** 355 (1994)
64. Chen Q, Ng K-W *Phys. Rev. B* **45** 2569 (1992)
65. Vedeneev S I et al. *Physica C* **198** 47 (1992)
66. Ponomarev Ya G et al. *J. Alloys Compd.* **195** 551 (1993)
67. Zhang Z, Charles C M *Phys. Rev. B* **47** 3423 (1993)
68. Ichimura K, Nomura K *J. Phys. Soc. Jpn.* **62** 3661 (1993)
69. Shen Z-X et al. *Phys. Rev. Lett.* **70** 1553 (1993)
70. Vedeneev S I et al. *Phys. Rev. B* **49** 9823 (1994)
71. Kirtley J R et al. *Phys. Rev. B* **35** 8846 (1987)
72. Hoevers H F C et al. *Physica C* **152** 105 (1988)
73. Benhabib S et al. *Phys. Rev. Lett.* **114** 147001 (2015)
74. Miller T G, McElfresh M, Reifenberger R *Phys. Rev. B* **48** 7499 (1993)
75. Nantoh M et al. *J. Supercond.* **7** 349 (1994)
76. Tanaka S, Ueda E, Sato M *Physica C* **224** 126 (1994)
77. Renner Ch et al. *Phys. Rev. Lett.* **80** 149 (1998)
78. Miyakawa N et al. *Phys. Rev. Lett.* **80** 157 (1998)
79. Ding H et al. *Nature* **382** 51 (1996)
80. Sutherland M et al. *Phys. Rev. B* **67** 174520 (2003)
81. Moler K A et al. *Phys. Rev. B* **55** 3954 (1997)
82. Wen H-H et al. *Phys. Rev. B* **70** 214505 (2004)
83. Fong H F et al. *Nature* **398** 588 (1999)
84. Dai P, Mook H A, Doğan F *Phys. Rev. Lett.* **80** 1738 (1998)
85. Sacuto A et al. *Europhys. Lett.* **39** 207 (1997)
86. Renner Ch, Fischer Ø *Phys. Rev. B* **51** 9208 (1995)
87. Kirtley J R et al. *Nature* **373** 225 (1995)
88. Pan S H et al. *Nature* **413** 282 (2001)
89. Hoffman J E et al. *Science* **297** 1148 (2002)
90. Zou C et al. *Phys. Rev. Lett.* **124** 047003 (2020)
91. Stasio M D, Müller K A, Pietronero L *Phys. Rev. Lett.* **64** 2827 (1990)
92. Kotegawa H et al. *Phys. Rev. B* **64** 064515 (2001)
93. Vedeneev S I, Jansen A G M, Wyder P *Phys. Rev. B* **67** 052202 (2003)
94. Okamoto S, Maier T A *Phys. Rev. Lett.* **101** 156401 (2008)
95. Chakravarty S, Kee H-Y, Völker K *Nature* **428** 53 (2004)
96. Ideta S et al. *Phys. Rev. Lett.* **104** 227001 (2010)
97. Kunisada S et al. *Phys. Rev. Lett.* **119** 217001 (2017)
98. Slezak J A et al. *Proc. Natl. Acad. Sci. USA* **105** 3203 (2008)
99. Vedeneev S I, Stepanov V A *JETP Lett.* **73** 141 (2001); *Pis'ma Zh. Eksp. Teor. Fiz.* **73** 159 (2001)
100. Sekine R et al. *Phys. Procedia* **58** 82 (2014)
101. Vedeneev S I, Maude D K *Phys. Rev. B* **72** 144519 (2005)
102. Mott N F *Rev. Mod. Phys.* **40** 677 (1968)
103. Harris J M et al. *Phys. Rev. B* **54** R15665 (1996)
104. Eisaki H et al. *Phys. Rev. B* **69** 064512 (2004)
105. Armitage N P, Fournier, Greene R L, arXiv:0906.2931
106. Dalichaouch Y, de Andrade M C, Maple M B *Physica C* **218** 309 (1993)
107. Varma C *Nature* **468** 184 (2010)
108. Emery V J, Kivelson S A *Nature* **374** 434 (1995)
109. Horio M et al. *Nat. Commun.* **7** 10567 (2016)
110. Sterpetti E et al. *Nat. Commun.* **8** 2060 (2017)
111. Alloul H, Ohno T, Mendels P *Phys. Rev. Lett.* **63** 1700 (1989)
112. Berthier C et al. *J. Phys. I France* **6** 2205 (1996)
113. Curro N J et al. *Phys. Rev. B* **56** 877 (1997)
114. Ginzberg D M *Physical Properties of High Temperature Superconductors* (Singapore: World Scientific, 1989)
115. Kawasaki S et al. *Phys. Rev. Lett.* **105** 137002 (2010)
116. Norman M R et al. *Nature* **392** 157 (1998)
117. Wang Y, Li L, Ong N P *Phys. Rev. B* **73** 024510 (2006)
118. Fauqué B et al. *Phys. Rev. Lett.* **96** 197001 (2006)
119. Mook H A et al. *Phys. Rev. B* **78** 020506 (2008)
120. Mangin-Thro L et al. *Nat. Commun.* **6** 7705 (2015)
121. Shekhter A et al. *Nature* **498** 75 (2013)
122. Lubashevsky Y et al. *Phys. Rev. Lett.* **112** 147001 (2014)

123. Zhao L et al. *Nat. Phys.* **13** 250 (2017)
124. Li Y et al. *Nature* **455** 372 (2008)
125. Hotta T, Mayr M, Dagotto E *Phys. Rev. B* **60** 13085 (1999)
126. Maly J, Jankó B, Levin K *Phys. Rev. B* **59** 1354 (1999)
127. Engelbrecht J R et al. *Phys. Rev. B* **57** 13406 (1998)
128. Dubroka A et al. *Phys. Rev. Lett.* **106** 047006 (2011)
129. Corson J et al. *Nature* **398** 221 (1999)
130. Kokanović I et al. *Phys. Rev. B* **88** 060505 (2013)
131. Lee P A *Phys. Rev. X* **4** 031017 (2014)
132. Larkin A I, Ovchinnikov Yu N *Sov. Phys. JETP* **20** 762 (1965); *Zh. Eksp. Teor. Fiz.* **47** 1136 (1964)
133. Fulde P, Ferrell R A *Phys. Rev.* **135** A550 (1964)
134. Shi M et al. *Phys. Rev. Lett.* **101** 047002 (2008)
135. Nakayama K et al. *Phys. Rev. Lett.* **102** 227006 (2009)
136. Meng J et al. *Phys. Rev. B* **79** 024514 (2009)
137. Chatterjee U et al. *Nat. Phys.* **6** 99 (2010)
138. Yoshida T et al. *Phys. Rev. Lett.* **103** 037004 (2009)
139. Wang Y et al. *Phys. Rev. Lett.* **88** 257003 (2002)
140. Wang Y et al. *Science* **299** 86 (2003)
141. Ussishkin I, Sondhi S L, Huse D A *Phys. Rev. Lett.* **89** 287001 (2002)
142. Li L et al. *Phys. Rev. B* **81** 054510 (2010)
143. Chang J et al. *Nat. Phys.* **8** 751 (2012)
144. Vedeneev S I, Maude D K *Phys. Rev. B* **72** 214514 (2005)
145. He R-H et al. *Science* **331** 1579 (2011)
146. Boyer M C et al. *Nat. Phys.* **3** 802 (2007)
147. Kohsaka Y et al. *Nature* **454** 1072 (2008)
148. Storey J G et al. *Phys. Rev. B* **76** 060502 (2007)
149. Lee J et al. *Science* **325** 1099 (2009)
150. Ma J-H et al. *Phys. Rev. Lett.* **101** 207002 (2008)
151. Kondo T et al. *Nature* **457** 296 (2009)
152. Kondo T et al. *Nat. Phys.* **7** 21 (2011)
153. Kimura T et al. *Phys. Rev. B* **53** 8733 (1996)
154. Yan Y F et al. *Phys. Rev. B* **52** R751 (1995)
155. Vedeneev S I et al. *Phys. Rev. B* **75** 064512 (2007)
156. Renner Ch et al. *Phys. Rev. Lett.* **80** 3606 (1998)
157. Matsuda A, Sugita S, Watanabe T *Phys. Rev. B* **60** 1377 (1999)
158. Oda M et al. *Physica C* **281** 135 (1997)
159. Miyakawa N et al. *Phys. Rev. Lett.* **83** 1018 (1999)
160. Loeser A G et al. *Science* **273** 325 (1996)
161. Kugler M et al. *Phys. Rev. Lett.* **86** 4911 (2001)
162. Vedeneev S I et al. *Phys. Rev. B* **60** 12467 (1999)
163. Gorina J I et al. *Solid State Commun.* **108** 275 (1998)
164. Kleiner R et al. *Phys. Rev. Lett.* **68** 2394 (1992)
165. Yurgens A et al. *Phys. Rev. B* **53** R8887 (1996)
166. Yurgens A et al. *Phys. Rev. Lett.* **79** 5122 (1997)
167. Suzuki M, Watanabe T, Matsuda A *Phys. Rev. Lett.* **82** 5361 (1999)
168. Krasnov V M et al. *Phys. Rev. Lett.* **84** 5860 (2000)
169. Suzuki M, Watanabe T *Phys. Rev. Lett.* **85** 4787 (2000)
170. Krasnov V M et al. *Phys. Rev. Lett.* **86** 2657 (2001)
171. Yamada Y, Suzuki M *Phys. Rev. B* **66** 132507 (2002)
172. Sadovskii M V *Phys. Usp.* **44** 515 (2001); *Usp. Fiz. Nauk* **171** 539 (2001)
173. Yasuda T, Tonouchi M, Takano S *Physica C* **289** 109 (1997)
174. Yurgens A et al. *Phys. Rev. Lett.* **90** 147005 (2003)
175. Zavaritsky V N *Phys. Rev. Lett.* **92** 259701 (2004)
176. Zavaritsky V N *Phys. Rev. B* **72** 094503 (2005)
177. Zhu X B et al. *Phys. Rev. B* **73** 224501 (2006)
178. Bae M-H et al. *Phys. Rev. B* **77** 094519 (2008)
179. Anagawa˜ et al. *Appl. Phys. Lett.* **83** 2381 (2003)
180. Anagawa K, Watanabe T, Suzuki M *Phys. Rev. B* **73** 184512 (2006)
181. Suzuki M et al. *Phys. Rev. B* **85** 214529 (2012)
182. Yurgens A et al. *Phys. Rev. Lett.* **92** 259702 (2004)
183. Krasnov V M, Sandberg M, Zogaj I *Phys. Rev. Lett.* **94** 077003 (2005)
184. Krasnov V M *Phys. Rev. Lett.* **97** 257003 (2006)
185. Katterwe S O, Rydh A, Krasnov V M *Phys. Rev. Lett.* **101** 087003 (2008)
186. Zhao S P, Zhu X B, Tang H *Eur. Phys. J. B* **71** 195 (2009)
187. Kurter C et al. *Phys. Rev. B* **81** 224518 (2010)
188. Ren J K et al. *Phys. Rev. B* **86** 014520 (2012)
189. Ren J K et al. *Sci. Rep.* **2** 248 (2012)
190. Nakayama K et al. *Phys. Rev. B* **83** 224509 (2011)
191. Wen H-H et al. *Phys. Rev. Lett.* **103** 067002 (2009)
192. Zheng G et al. *Phys. Rev. Lett.* **94** 047006 (2005)
193. Vedeneev S I *JETP Lett.* **68** 230 (1998); *Pis'ma Zh. Eksp. Teor. Fiz.* **68** 217 (1998)
194. Jacobs Th, Katterwe S O, Krasnov V M *Phys. Rev. B* **94** 220501 (2016)
195. Bergeal N et al. *Nat. Phys.* **4** 608 (2008)
196. Benseman T M, Cooper J R, Balakrishnan G *Phys. Rev. B* **98** 014507 (2018)
197. Larkin A, Varlamov A *Theory of Fluctuations in Superconductors* (Oxford: Clarendon Press, 2005)
198. Zasadzinski J F et al. *Phys. Rev. Lett.* **87** 067005 (2001)
199. Johnson P D et al. *Phys. Rev. Lett.* **87** 177007 (2001)
200. Cuk T et al. *Phys. Rev. Lett.* **93** 117003 (2004)
201. Hwang J, Timusk T, Gu G D *Nature* **427** 714 (2004)
202. Vishik I M et al. *Proc. Natl. Acad. Sci. USA* **109** 18332 (2012)
203. Kondo T et al. *Nat. Commun.* **6** 7699 (2015)
204. Reber T J et al., arXiv:1509.01556
205. Storey J G *New J. Phys.* **19** 073026 (2017)
206. Reber T J et al. *Phys. Rev. B* **87** 060506 (2013)
207. Kohsaka Y et al. *Nat. Phys.* **8** 534 (2012)
208. Bilbro L S et al. *Nat. Phys.* **7** 298 (2011)
209. Wolf E L *Principles of Electron Tunnelling Spectroscopy* (Oxford: Oxford Univ. Press, 1989)
210. Dynes R C, Narayanamurti V, Garno J P *Phys. Rev. Lett.* **41** 1509 (1978)
211. Zasadzinski J F et al. *Phys. Rev. B* **68** 180504 (2003)
212. Zasadzinski J F et al. *Phys. Rev. Lett.* **96** 017004 (2006)
213. Ahmadi O et al. *Phys. Rev. Lett.* **106** 167005 (2011)
214. Vishik I M *Rep. Prog. Phys.* **81** 062501 (2018)
215. Kondo T et al. *Phys. Rev. Lett.* **98** 267004 (2007)
216. Lee W S et al. *Nature* **450** 81 (2007)
217. Yoshida T et al. *Phys. Rev. B* **93** 014513 (2016)
218. Hashimoto M et al. *Nat. Phys.* **6** 414 (2010)
219. Da Silva Neto E H et al. *Science* **343** 393 (2014)
220. Ramshaw B J et al. *Science* **348** 317 (2015)
221. Fujita K et al. *Science* **344** 612 (2014)
222. Tallon J L et al. *Phys. Rev. B* **68** 180501 (2003)
223. Laliberte F et al., arXiv:1606.04491
224. Božović I et al. *Nature* **536** 309 (2016)
225. Hossain M A et al. *Nat. Phys.* **4** 527 (2008)
226. Hashimoto M et al. *Nat. Mater.* **14** 37 (2015)
227. Kondo T et al. *Phys. Rev. Lett.* **111** 157003 (2013)
228. Mangin-Thro L et al. *Phys. Rev. B* **89** 094523 (2014)
229. Gomes K K et al. *Nature* **447** 569 (2007)
230. Zaki N et al. *Phys. Rev. B* **96** 195163 (2017)
231. Liang R, Bonn D A, Hardy W N *Phys. Rev. B* **73** 180505 (2006)
232. Zhao J et al. *Proc. Natl. Acad. Sci. USA* **110** 17774 (2013)
233. Presland M R et al. *Physica C* **176** 95 (1991)
234. Ando Y et al. *Phys. Rev. Lett.* **93** 267001 (2004)
235. Damascelli A, Hussain Z, Shen Z-X *Rev. Mod. Phys.* **75** 473 (2003)
236. Chakraborty D, Morice C, Pépin C *Phys. Rev. B* **97** 214501 (2018)
237. Shen K M et al. *Phys. Rev. B* **69** 054503 (2004)
238. Razzoli E et al. *Phys. Rev. Lett.* **110** 047004 (2013)
239. Drachuck G et al. *Nat. Commun.* **5** 3390 (2014)
240. Palczewski A D et al. *Phys. Rev. B* **81** 104521 (2010)
241. Chatterjee U et al. *Proc. Natl. Acad. Sci. USA* **108** 9346 (2011)
242. Alldredge J W et al. *Nat. Phys.* **4** 319 (2008)
243. Hashimoto M et al. *Phys. Rev. B* **77** 094516 (2008)
244. Oda M et al. *J. Phys. Soc. Jpn.* **69** 983 (2000)
245. Kanigel A et al. *Nat. Phys.* **2** 447 (2006)
246. Moore R G et al. *Phys. Rev. B* **81** 073102 (2010)
247. Chatterjee U et al. *Nat. Commun.* **6** 6313 (2015)
248. Ghiringhelli G et al. *Science* **337** 821 (2012)
249. Blanco-Canosa S et al. *Phys. Rev. B* **90** 054513 (2014)
250. Yang K-Y, Rice T M, Zhang F-C *Phys. Rev. B* **73** 174501 (2006)
251. Qi Y, Sachdev S *Phys. Rev. B* **81** 115129 (2010)
252. Freutel S et al. *Phys. Rev. B* **99** 081116 (2019)
253. Chakravarty S et al. *Phys. Rev. B* **68** 100504 (2003)
254. King P D C et al. *Phys. Rev. Lett.* **106** 127005 (2011)
255. Gerber S et al. *Science* **350** 949 (2015)
256. Wang Y et al. *Phys. Rev. B* **64** 224519 (2001)
257. Ong N P et al. *Ann. Physik* **13** 9 (2004)
258. Wang Z et al. *Phys. Rev. B* **72** 054509 (2005)

259. Otter F A (Jr.), Solomon P R *Phys. Rev. Lett.* **16** 681 (1966)
260. Anderson P W *Rev. Mod. Phys.* **38** 298 (1966)
261. Capan C et al. *Phys. Rev. Lett.* **88** 056601 (2002)
262. Wang Y et al. *Phys. Rev. Lett.* **95** 247002 (2005)
263. Cyr-Choinière O et al. *Phys. Rev. B* **97** 064502 (2018)
264. Vedeneev S I, Jansen A G M, Wyder P *Phys. Rev. B* **62** 5997 (2000)
265. Daou R et al. *Nature* **463** 519 (2010)
266. Rullier-Albenque F et al. *Phys. Rev. Lett.* **96** 067002 (2006)
267. Ito T, Takenaka K, Uchida S *Phys. Rev. Lett.* **70** 3995 (1993)
268. Rullier-Albenque F et al. *Europhys. Lett.* **81** 37008 (2008)
269. Badoux S et al. *Nature* **531** 210 (2016)
270. Basov D N, Timusk T *Rev. Mod. Phys.* **77** 721 (2005)
271. Puchkov A V et al. *Phys. Rev. Lett.* **77** 3212 (1996)
272. Timusk T, Statt B *Rep. Prog. Phys.* **62** 61 (1999)
273. Homes C C et al. *Phys. Rev. Lett.* **71** 1645 (1993)
274. Bernhard C et al. *Solid State Commun.* **121** 93 (2002)
275. Boris A V et al. *Phys. Rev. Lett.* **89** 277001 (2002)
276. Boris A V et al. *Science* **304** 708 (2004)
277. Kovaleva N N et al. *Phys. Rev. B* **69** 054511 (2004)
278. Mallett B P P et al. *Phys. Rev. B* **99** 054513 (2019)
279. Devereaux T P, Hackl R *Rev. Mod. Phys.* **79** 175 (2007)
280. Loret B et al. *Phys. Rev. B* **96** 094525 (2017)
281. Wu T et al. *Nature* **477** 191 (2011)
282. Chang J et al. *Nat. Phys.* **8** 871 (2012)
283. Doiron-Leyraud N et al. *Nature* **447** 565 (2007)
284. Chakravarty S *Science* **319** 735 (2008)
285. He Y et al. *Science* **344** 608 (2014)
286. Nie L et al. *Phys. Rev. B* **96** 085142 (2017)
287. Khaykovich B et al. *Phys. Rev. B* **71** 220508 (2005)
288. Chang J et al. *Phys. Rev. B* **78** 104525 (2008)
289. Kimura H et al. *Phys. Rev. Lett.* **91** 067002 (2003)
290. Panagopoulos C et al. *Phys. Rev. B* **69** 144510 (2004)
291. Wu T et al. *Nat. Commun.* **4** 2113 (2013)
292. Blanco-Canosa S et al. *Phys. Rev. Lett.* **110** 187001 (2013)
293. Grissonnanche G et al. *Nat. Commun.* **5** 3280 (2014)
294. Tranquada J M et al. *Nature* **375** 561 (1995)
295. Hoffman J E et al. *Science* **295** 466 (2002)
296. Howald C et al. *Proc. Natl. Acad. Sci. USA* **100** 9705 (2003)
297. LeBoeuf D et al. *Phys. Rev. B* **83** 054506 (2011)
298. Haug D et al. *New J. Phys.* **12** 105006 (2010)
299. Ando Y et al. *Phys. Rev. Lett.* **88** 137005 (2002)
300. Sidis Y, Bourges P *J. Phys. Conf. Ser.* **449** 012012 (2013)
301. Mangin-Thro L et al. *Phys. Rev. Lett.* **118** 097003 (2017)
302. Matt C E et al. *Phys. Rev. B* **92** 134524 (2015)
303. Okamoto S et al. *Phys. Rev. B* **82** 180511 (2010)
304. Auvray N et al. *Nat. Commun.* **10** 5209 (2019)
305. Murayama H et al. *Nat. Commun.* **10** 3282 (2019)
306. Bangura A F et al. *Phys. Rev. B* **82** 140501 (2010)
307. Vignolle B et al. *Nature* **455** 952 (2008)
308. Manako T, Kubo Y, Shimakawa Y *Phys. Rev. B* **46** 11019 (1992)
309. Mackenzie A P et al. *Phys. Rev. B* **53** 5848 (1996)
310. Proust C et al. *Phys. Rev. Lett.* **89** 147003 (2002)
311. Cooper R A et al. *Science* **323** 603 (2009)
312. Nakamae S et al. *Phys. Rev. B* **68** 100502 (2003)
313. Abdel-Jawad M et al. *Phys. Rev. Lett.* **99** 107002 (2007)
314. Jang H et al. *Phys. Rev. B* **97** 224513 (2018)
315. Hücker M et al. *Phys. Rev. B* **83** 104506 (2011)
316. Achkar A et al. *Science* **351** 576 (2016)
317. Wen J-J et al. *Nat. Commun.* **10** 3269 (2019)
318. Kofu M et al. *Phys. Rev. Lett.* **102** 047001 (2009)
319. Julien M-H *Physica B* **329–333** 693 (2003)
320. Badoux S et al. *Phys. Rev. X* **6** 021004 (2016)
321. Croft T P et al. *Phys. Rev. B* **89** 224513 (2014)
322. Monthoux P, Pines D, Lonzarich G G *Nature* **450** 1177 (2007)
323. Löhneysen H v et al. *Rev. Mod. Phys.* **79** 1015 (2007)
324. Shibauchi T, Carrington A, Matsuda Y *Annu. Rev. Condens. Matter Phys.* **5** 113 (2014)
325. Doiron-Leyraud N et al. *Phys. Rev. B* **80** 214531 (2009)
326. Michon B et al. *Nature* **567** 218 (2019)
327. Abanov A et al. *Phys. Rev. B* **99** 180506 (2019)
328. Fratino L et al. *Sci. Rep.* **6** 22715 (2016)
329. Fradkin E et al. *Annu. Rev. Condens. Matter Phys.* **1** 153 (2010)
330. Bok J M et al. *Sci. Adv.* **2** e1501329 (2016)
331. Varma C M *Phys. Rev. Lett.* **75** 898 (1995)
332. Hussey N *Nat. Phys.* **12** 290 (2016)
333. Yu Z-D et al. *Phys. Rev. B* **96** 045110 (2017)
334. Pan Z-H et al. *Phys. Rev. B* **79** 092507 (2009)
335. Brewer J H et al. *Phys. Rev. Lett.* **60** 1073 (1988)
336. Keimer B et al. *Phys. Rev. B* **46** 14034 (1992)
337. Collignon C et al. *Phys. Rev. B* **95** 224517 (2017)
338. Kaminski A et al. *Phys. Rev. B* **73** 174511 (2006)
339. Wu W et al. *Phys. Rev. X* **8** 021048 (2018)
340. Yoshida T et al. *Phys. Rev. B* **74** 224510 (2006)
341. Doiron-Leyraud N et al. *Nat. Commun.* **8** 2044 (2017)
342. Braganca H et al. *Phys. Rev. Lett.* **120** 067002 (2018)
343. Hussey N E *J. Phys. Condens. Matter* **20** 123201 (2008)
344. Ando Y et al. *Phys. Rev. Lett.* **92** 197001 (2004)
345. Segawa K, Ando Y *Phys. Rev. B* **69** 104521 (2004)
346. Tallon J L, Loram J W *Physica C* **349** 53 (2001)
347. Fournier D et al. *Nat. Phys.* **6** 905 (2010)
348. Dagan Y et al. *Phys. Rev. Lett.* **92** 167001 (2004)
349. Ferrero M et al. *Phys. Rev. B* **80** 064501 (2009)
350. Chowdhury D, Sachdev S *Phys. Rev. B* **90** 245136 (2014)
351. Walmsley P et al. *Phys. Rev. Lett.* **110** 257002 (2013)
352. Löhneysen H v et al. *Phys. Rev. Lett.* **72** 3262 (1994)
353. Kačmarčík J et al. *Phys. Rev. Lett.* **121** 167002 (2018)
354. Loram J W et al. *J. Phys. Chem. Solids* **59** 2091 (1998)
355. Komiya S, Tsukada I *J. Phys. Conf. Ser.* **150** 052118 (2009)
356. Momono N et al. *Physica C* **233** 395 (1994)
357. Scalapino D J *Rev. Mod. Phys.* **84** 1383 (2012)
358. Blumberg G et al. *Phys. Rev. Lett.* **88** 107002 (2002)
359. Matsui H et al. *Phys. Rev. Lett.* **95** 017003 (2005)
360. Armitage N P et al. *Phys. Rev. Lett.* **87** 147003 (2001)
361. Hlubina R, Rice T M *Phys. Rev. B* **51** 9253 (1995)
362. Shen Z-X, Schrieffer J R *Phys. Rev. Lett.* **78** 1771 (1997)
363. Yuan Q, Yuan F, Ting C S *Phys. Rev. B* **73** 054501 (2006)
364. Onose Y et al. *Phys. Rev. Lett.* **87** 217001 (2001)
365. Wang N L et al. *Phys. Rev. B* **73** 184502 (2006)
366. Zimmers A et al. *Phys. Rev. B* **76** 132505 (2007)
367. Onose Y et al. *Phys. Rev. B* **69** 024504 (2004)
368. Zimmers A et al. *Europhys. Lett.* **70** 225 (2005)
369. Matsui H et al. *Phys. Rev. Lett.* **94** 047005 (2005)
370. Sadovskii M V et al. *Phys. Rev. B* **72** 155105 (2005)
371. Adachi T et al. *J. Phys. Soc. Jpn.* **82** 063713 (2013)
372. Fujita M et al. *Phys. Rev. B* **67** 014514 (2003)
373. Fujita M et al. *Phys. Rev. Lett.* **101** 107003 (2008)
374. Takagi H et al. *Phys. Rev. B* **40** 2254 (1989)
375. Mang P K et al. *Phys. Rev. Lett.* **93** 027002 (2004)
376. Jin K et al. *Phys. Rev. B* **80** 012501 (2009)
377. Armitage N P et al. *Phys. Rev. Lett.* **88** 257001 (2002)
378. Mook H A, Dai P, Doğan F *Phys. Rev. Lett.* **88** 097004 (2002)
379. Xia J et al. *Phys. Rev. Lett.* **100** 127002 (2008)
380. Vishik I M et al. *Phys. Rev. B* **95** 115125 (2017)
381. Hinton J P et al. *Phys. Rev. Lett.* **110** 217002 (2013)
382. Shimizu K et al. *Nature* **412** 316 (2001)
383. Stewart G R *Rev. Mod. Phys.* **83** 1589 (2011)
384. Sato T et al. *J. Phys. Soc. Jpn.* **77** 063708 (2008)
385. Ishida Y et al. *J. Phys. Soc. Jpn.* **77** 61 (2008)
386. Xu Y-M et al. *Nat. Commun.* **2** 392 (2011)
387. Kordyuk A A *Low Temp. Phys.* **38** 888 (2012); *Fiz. Niz. Temp.* **38** 1119 (2012)
388. Moon S J et al. *Phys. Rev. B* **90** 014503 (2014)
389. Seo Y I et al. *Sci. Rep.* **9** 3987 (2019)
390. Evtushinsky D V et al. *Phys. Rev. B* **79** 054517 (2009)
391. Richard P et al. *Phys. Rev. Lett.* **102** 047003 (2009)
392. Shimojima T et al. *Science* **332** 564 (2011)
393. Zhang Y et al. *Nat. Phys.* **8** 371 (2012)
394. Evtushinsky V et al. *Phys. Rev. B* **89** 064514 (2014)
395. Gu Y et al. *Phys. Rev. Lett.* **119** 157001 (2017)
396. Yin Y et al. *Physica C* **469** 535 (2009)
397. Massee F et al. *Europhys. Lett.* **92** 57012 (2010)
398. Wang A F et al. *New J. Phys.* **15** 043048 (2013)
399. Sadovskii M V *Phys. Usp.* **51** 1201 (2008); *Usp. Fiz. Nauk* **178** 1243 (2008)
400. Sato Y et al. *Nat. Phys.* **13** 1074 (2017)
401. Wu J et al. *Nature* **547** 432 (2017)

402. Comin R, Damascelli A *Annu. Rev. Condens. Matter Phys.* **7** 369 (2016)
403. Comin R et al. *Nat. Mater.* **14** 796 (2015)
404. Yazdani A, da Silva Neto E H, Aynajian P *Annu. Rev. Condens. Matter Phys.* **7** 11 (2016)
405. Comin R et al. *Science* **343** 390 (2014)
406. Torchinsky D H et al. *Nat. Mater.* **12** 387 (2013)
407. Kohsaka Y et al. *Science* **315** 1380 (2007)
408. Tu W-L, Lee T-K *Sci. Rep.* **9** 1719 (2019)
409. Bangura A F et al. *Phys. Rev. Lett.* **100** 047004 (2008)
410. Berg E, Fradkin E, Kivelson S A *Phys. Rev. B* **79** 064515 (2009)
411. Berg E et al. *New J. Phys.* **11** 115004 (2009)
412. Berg E, Fradkin E, Kivelson S *Nat. Phys.* **5** 830 (2009)
413. Sachdev S, La Placa R *Phys. Rev. Lett.* **111** 027202 (2013)
414. Wang Y, Chubukov A *Phys. Rev. B* **90** 035149 (2014)
415. Hirsch J E et al. *Phys. Rev. B* **26** 5033 (1982)